Master Thesis, Department of Geosciences

3D structure and formation of hydrothermal vent complexes in the Møre Basin

Sigurd Kjoberg

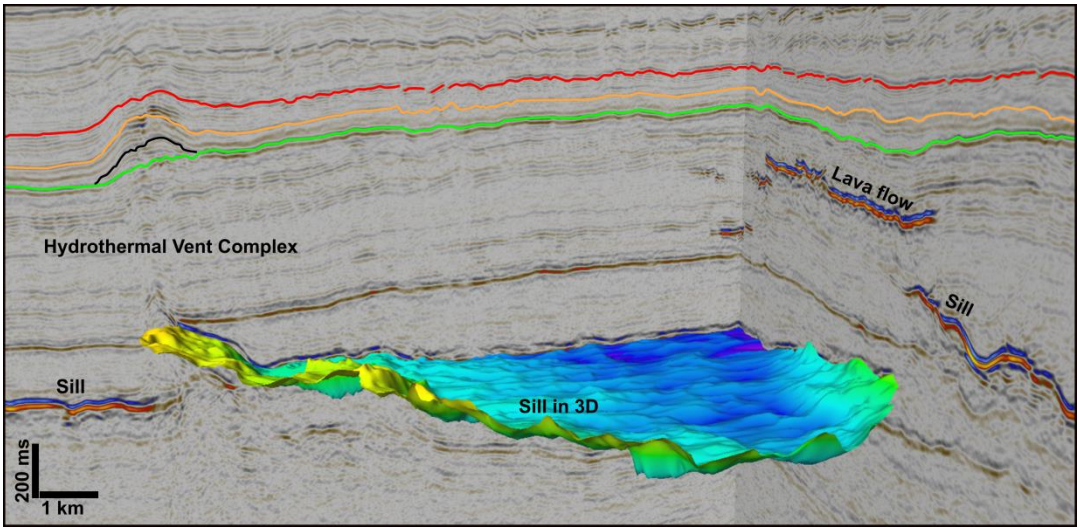

UNIVERSITETET I OSLO
DET MATEMATISK-NATURVITENSKAPELIGE FAKULTET

3D structure and formation of hydrothermal vent complexes in the Møre Basin

Sigurd Kjoberg

Master Thesis in Geosciences

Discipline: Geology

Department of Geoscience

Faculty of Mathematics and Natural science

University of OSLO

June 2016

Acknowledgements

First of all I want to thank my main supervisor, Sverre Planke for all the inspiring conversations and good guidance during this thesis. Thanks to my co-supervisors Henrik Svensen and Olivier Galland for giving constructive feedback throughout the project.

I would also like to thank NORSAR for the free academic use of the software during the modelling procedures, and especially Isabelle Lecomte for all the guidance.

To everyone at CEED, thank you for a great year.
The time spent writing this master thesis wold not have been the same without my fellow master student. Our discussions and breaks have been truly appreciated.

Lastly I want to thank my family and friends for always being there and cheering me on.

Abstract

This thesis presents a 3D seismic analysis of fluid and gas induced hydrothermal vent complexes in a 310 km^2 area at the Møre Basin, offshore Norway. The mid-Norwegian Møre Margin is regarded as a type example of a volcanic rifted margin, with its formation usually related to the influence of the Icelandic plume activity and the NE Atlantic break-up. The area is characterized by the presence of voluminous basaltic complexes such as extrusive lava sequences, intrusive sills and dikes, and hydrothermal vent complexes. Seismic data from the Tulipan prospect located in the western part of the Møre Basin have been used in this study. The investigation focusses on (1) the hydrothermal vent complex geometries, (2) the induced surface deformation patterns, (3) the relation to the intrusions (heat source), (4) the initiation depth of the hydrothermal vent complexes, as well as (5) the age of the hydrothermal vent complexes. To approach these questions, a detailed 3D seismic interpretation of the Tulipan seismic data cube together with quantitative sandbox experiments and simulated seismic modelling is implemented. Emplacement of hydrothermal vent complexes is accommodated by deformation of the host rock. The edges of igneous intrusions mobilize fluids by heat transfer into the sedimentary host rock (aureoles). Fluid expansion may lead to formation of piercing structures due to upward fluid migration. Hydrothermal vent complexes correspond to bending of overlying strata, leading to the formation of dome structures ("mounds") above the paleo-surface. Larger-scale dome structures are formed above sills ("forced folds"). These domes indicate the accommodation created for the intrusions by deformation of the overburden, and may form important structures in many volcanic margins. Both the morphological characteristics of the upper part and the underlying feeder-structure (conduit-zone) can be imaged and studied on 3D seismic data. The complexes formed during the initial Eocene, and are believed to be a key factor behind the rapid warming event called the Paleocene-Eocene thermal maximum (PETM). The newly derived understanding of age, eruptive deposits, and formation of hydrothermal vent complexes in the Møre Basin enables one to contribute to the general understanding of the igneous plumbing system in volcanic basins and their implications on the paleoenvironment at the time of their emplacement.

Contents

1. Introduction

At the mid-Norwegian Margin, the Paleocene-Eocene interval is considered to represent the time period of the early NE Atlantic rifting and continental break-up. Evidence of volcanic activity in sedimentary basins can be correlated along the entire European NE Atlantic margin (Bell and Butcher, 2002; Gibb and Kanaris-Sotiriou, 1988). Volcanic processes and deposits have resulted in structural impact and geodynamic development of the margins and associated sedimentary basins. The study area of Møre Basin is located beneath the outer shelf and slope region offshore mid Norway, and contains classical examples on how volcanic activity and igneous intrusions in the sedimentary strata may impact the basin history (Brekke, 2000; Skogseid et al., 1992). Identification of volcanic complexes is an important aspect to study, since these features may have a major impact on the basin evolution.

The aim of this thesis is to document and map out the distribution and nature of volcanically derived intrusions, and the associated hydrothermal vent complexes at the Møre Basin. The study present evidence of extensive hydrothermal activity associated with volcanic and sedimentary intrusions, expressed by conical and cylindrical structures piercing the overlaying strata and seafloor. Similar kilometre-scale piercement structures within sedimentary successions have been described in seismic data (e.g., Planke et al., 2005; Hansen et al., 2005) and in outcrops (e.g., Svensen et al., 2006). One of the main objectives is to obtain structural images and detailed mapping of morphological features related to the hydrothermal vent complexes. The present study is based on a 3D seismic survey acquired over the central Møre Basin, together with modelling procedures to establish a new understanding of the structures related to fluid and sediment remobilization.

1.1 Outline of the thesis

In this thesis, structural investigation and modelling reconstruction of the hydrothermal vent complexes at the Møre Basin is conducted. Three-dimensional (3D) seismic analysis, laboratory- and synthetic modelling are implemented to investigate how these structures may look in natural settings, how they developed and what effect these structures impose during emplacement. Additionally, the study will provide a regional investigation and seismic reconstruction of the main study area. The Møre Basin is ideal for studying the influence of the hydro thermal vent complexes, since extensive high-quality seismic reflection data and other geophysical data are currently available.

The thesis study begins with a literature summary of the geological framework and structural setting of the mid-Norwegian Margin. The chapter summarizes the development of the NE Atlantic system focusing on the main tectonic episodes, and followed by a closer insight into the study area and structural setting of the Møre Margin. Geological systems and models are also presented in this chapter to highlight important concepts. Chapter three ‘Theories of quantitative and simulated modeling’ is meant to propose an overview of modeling procedures and comparable work published in the literature.

Chapter four ‘Data’ is the first methodology chapter giving an overview of seismic data and well-tie correlations used in this study. Chapter five ‘Seismic interpretation methods’ outlines the different interpretation methods implemented, together with methods explaining the modelling procedures.

The results are divided into two parts, Chapter six ‘Well data and seismic results’ and Chapter seven ‘Modelling results’. Both chapters give a more detailed description on each of the workflows. The seismic interpretation part is based upon the structural and lithological history of the study area, whiles the modelling results present development and images of the experimental modelling.

Finally, Chapter eight ‘discussion’ provides a summary of the findings in this thesis. At the end of the thesis the appendix A.1 to A.3 provide tables and images of the hydrothermal complexes mapped out, a summary overview and biostratigraphical tables.

1.2 Main workflow of the thesis

In order to study the characteristics and development of the hydrothermal vent complexes together with basin development, a detailed workflow approach have been utilized in this thesis. Step by step layout is presented in Figure 1.1 below.

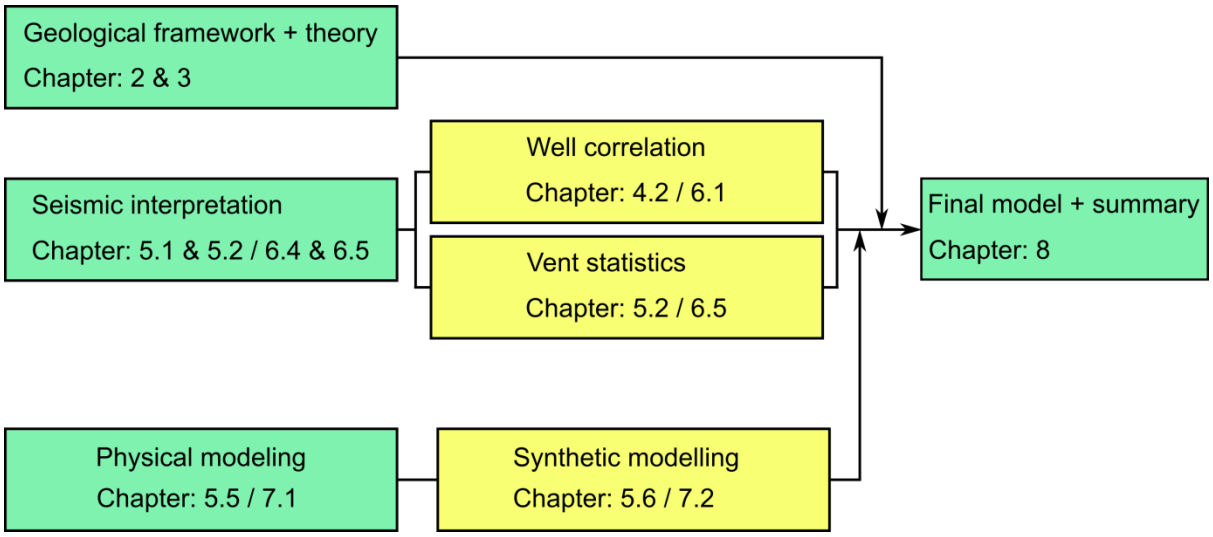

Figure 1.1: Diagram outlining the main workflow of the thesis.

Geological framework and theory

Geological framework, structural setting and background theory from previous published work at the mid-Norwegian Margin, is used to correlate the interpretations for confidence and greater understanding.

Seismic interpretation and well correlations

One 3D cube has been interpreted with emphasis on basin reconstruction and hydrothermal vent complex recognition. The seismic profiles within the cube have been correlated with different well log electrofacies as input for further analysis and interpretation.

Physical and synthetic modelling

The physical experiments consist of a sandbox experiment. The purpose is to recreate a vent structure and relating it with synthetic seismic imaging using NORSAR seismic modelling software **SeisRox** (See Table 1.1 for software). The main objective of the sandbox experiment is to make a piercement structure with known geometry and relate it to development and parameters involved. The resulting imaging of the piercement structure will be used as background model for the synthetic seismograms.

The final interpretation of the results, summary and conclusions is the last step of the main workflow.

Table 1.1: Software implemented in the thesis work

No.	Software program	Description / applied for
1	Microsoft office word	Used to write the thesis
2	Schlumberger PETREL 2015	Seismic interpretation, well-tie correlations
3	SeisRox	Synthetic seismic modelling
4	Geo Teric 2016	Attribute illustration of horizons
5	Inkscape	Vector based drawing software for various illustrations

2. Geological framework

2.1 Mid Norwegian Margin

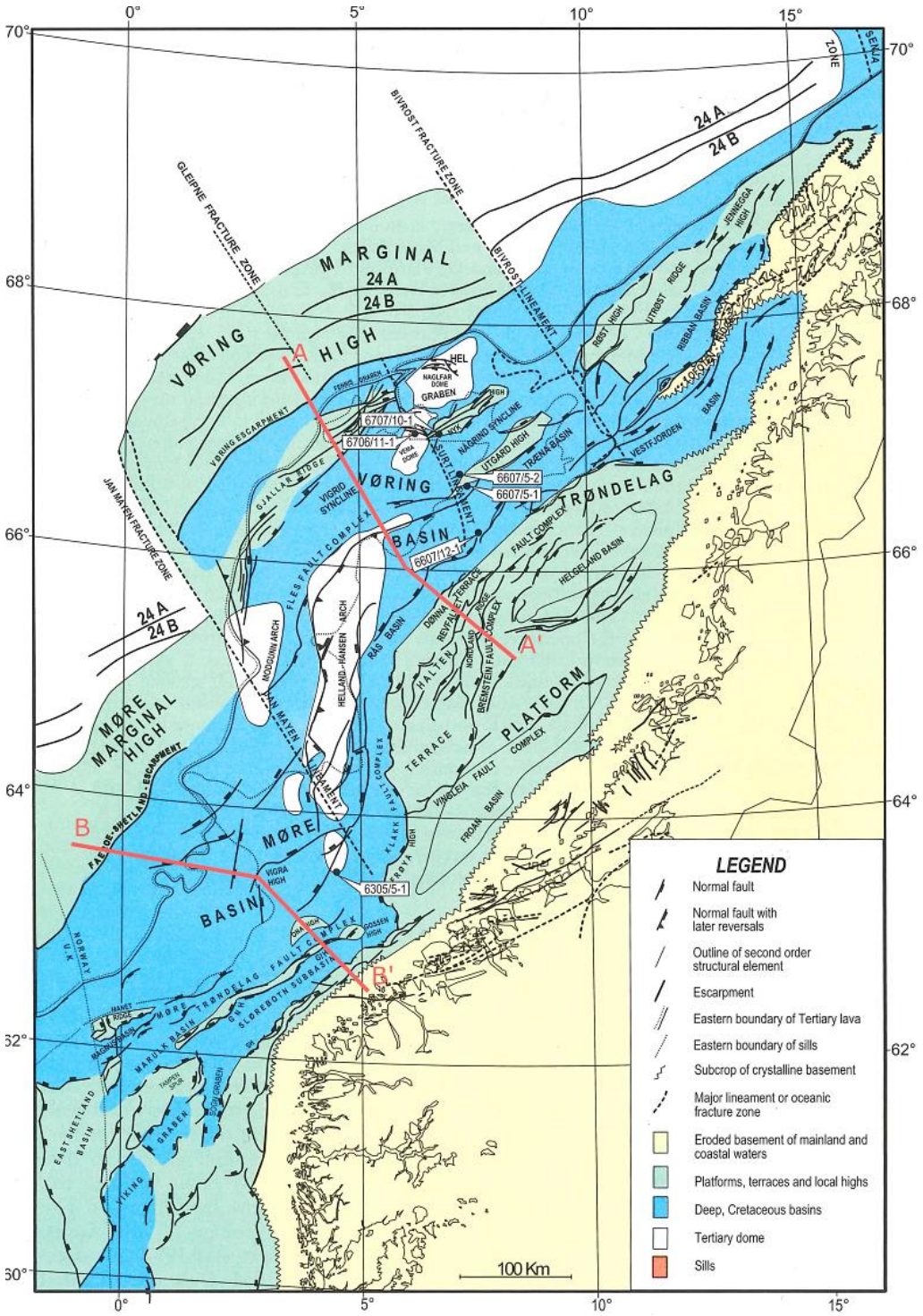

Figure 2.1: Simplified structural map of the Norwegian continental margin with line locations for Geoseismic section, A-A' and B-B'. Map modified after Brekke, (2000).

The mid-Norwegian Margins seen today is a result of the tectonically derived episodes forming the area during the Late Jurassic–Early Cretaceous rifting episodes. The basins are characterized by the infill of thick Cretaceous sedimentary accumulations, and can in places reach up to 13 km of deposited sediments, of which 8-9 km comprises of the Cretaceous succession (Figure 2.1) (Blystad et al., 1995; Brekke, 2000; Skogseid et al., 2000; Faleide et al., 2008). The geological profiles from Brekke, (2000) and Skogseid et al., (2000) are used as a first order approximation in order to give a geological framework of the continental margin.

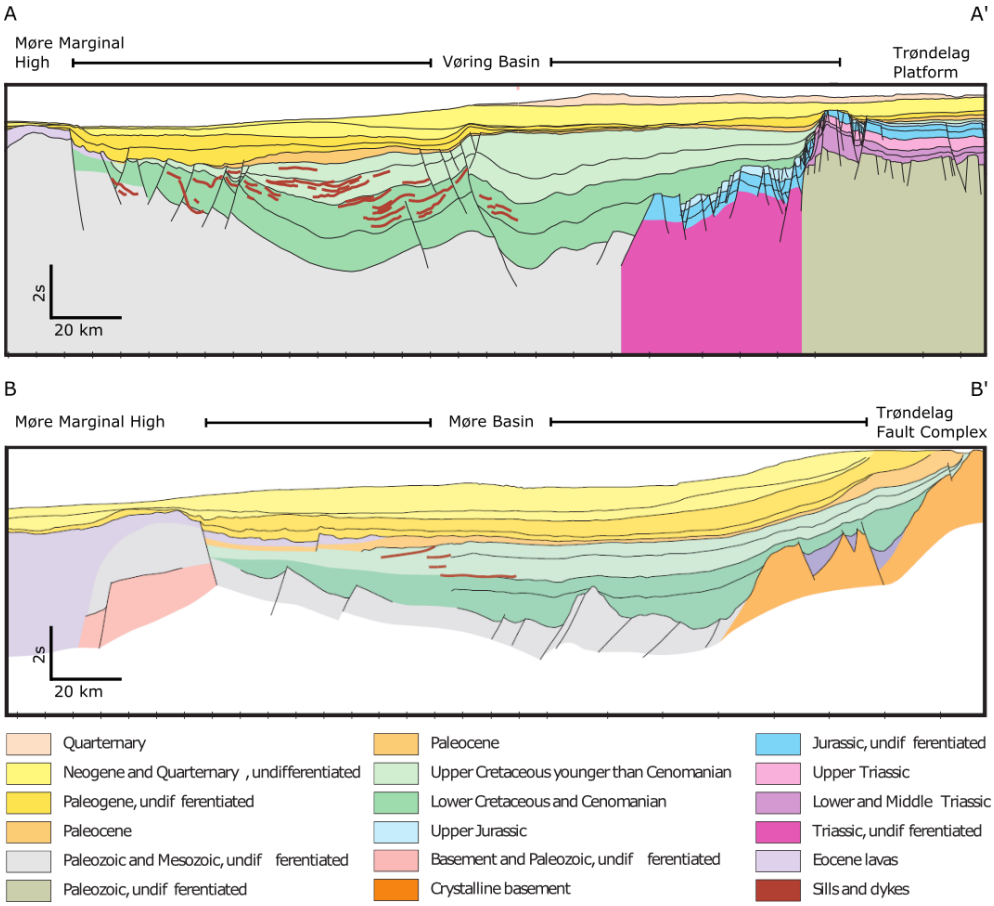

Figure 2.2: Interpreted geological profiles based on reflection/refraction. Figure slightly modified after Brekke, (2000). See Figure 2.1, for line locations.

The mid-Norwegian Margin between (62-70°N) is a rifted volcanic margin. The margin developed through a series of rift phases that culminated with the onset of oceanic crust at c. 56 Ma in the Norwegian Greenland Sea (Osmundsen *et al.*, 2002). The mid-Norwegian margin includes three main segments (Møre, Vøring and Lofoten-Vesterålen) each between 400-500 km long, and separated by the east Jan Mayen Fracture Zone and the Bivrost Lineament (Faleide et al., 2008) (See Figure. 2.1). Skogseid et al., (2000) described the Møre and Vøring basins formation primarily as a result of the Late Jurassic-Early Cretaceous rifting. However the thick sedimentary strata of Cretaceous origin make the seismic resolution of the Late Jurassic-Early Cretaceous faulting poor and difficult to interpret. Following the late- to post-Caledonian the successive rift event that occurred affected the NE Atlantic margin in Late Palaeozoic, Triassic, Jurassic and Cretaceous times (Osmundsen et al.,

2002). This event was followed by Late Cretaceous to early Eocene extension which led to the breakup and onset of seafloor spreading (Osmundsen et al., 2002).

The sills associated with the formation of hydrothermal vent complexes are linked to the breakup between Norway and Greenland, this resulted in large amounts of magmatism creating the 'North Atlantic Igneous Province' (Faleide et al., 2008; Saunders et al., 1997). Dating of two sills at approximately same depth as the study interval of this thesis concluded the age to be 55.6 ± 0.4 Ma and 56.3 ± 0.4 Ma using U-Pb ratio in zircon crystals (Svensen et al., 2010). The age derived coincide with the Paleocene-Eocene transition, which marks a period of major climatic changes involving a global temperature rise of about 5-10 degrees (e.g., Dickens et al., 1995).

2.2 Main Structural setting

Two separate rift segments are recognised at the mid-Norwegian Margin (See Figure. 2.1 and 2.3). The Vøring Margin in the north and the Møre Margin in the south. Booth segments share similar structural characteristics such as erosional escarpments, marginal highs and deep cretaceous basins.

The basins to the west are flanked by the Møre and Vøring Marginal Highs. The transition zone between the marginal high and the basin area is defined by the Vøring Escarpment to the north, and the Faeroe-Shetland Escarpment to the south. The Møre Basin is defined by the flanking of uplifted mainland to the east and the Vøring Basin by the Trøndelag platform.

In the northern part the deep Vøring basin is confined by the NW-SE bearing Bivrost Lineament, separating the basin from the narrow Lofoten ridge. The Jan Mayen lineament separates the Vøring basin to the north and the Møre Basin to the south. These lineaments continue onwards as the Bivrost and Jan Mayen fracture zone respectively, and may reflect an old structure in the crystalline basement (Brekke, 2000). The post Caledonian development at the continental margin off central Norway can be linked to these two lineaments as controlling features zones, dividing the margin into extension segment between Norway and Greenland (Brekke, 2000).

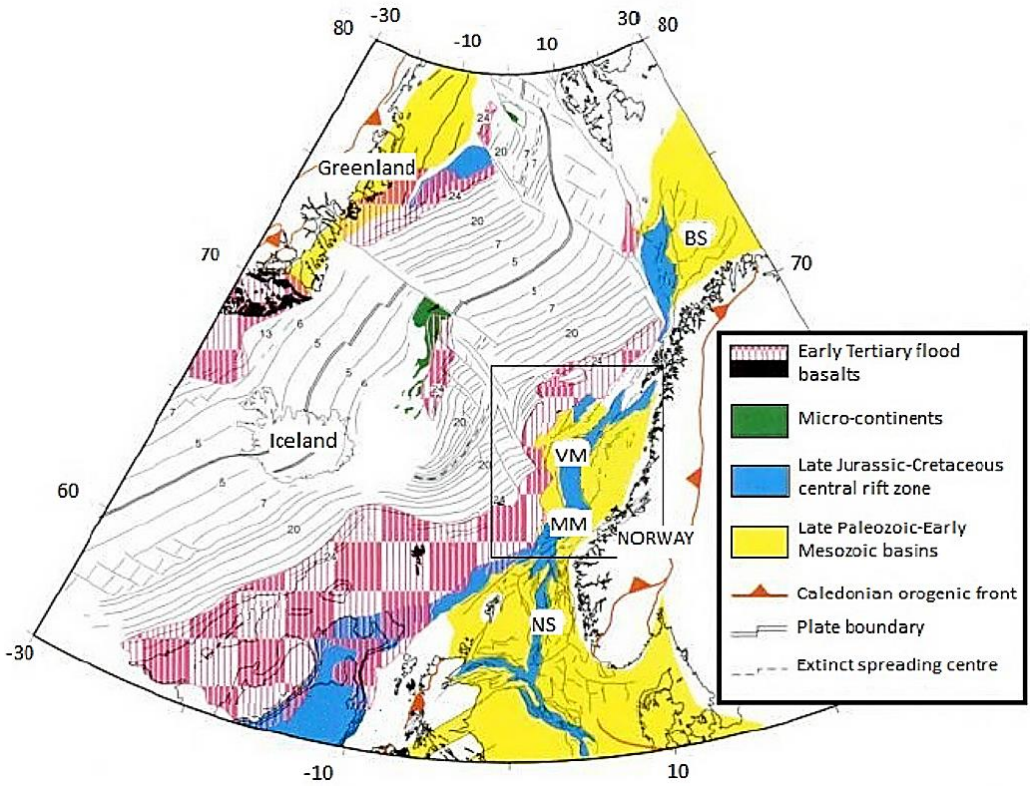

Figure 2.3: Location map of structural elements in the NE Atlantic region. Study area of the mid-Norwegian Margin outlined in the black square. BS, Barents Sea; VM, Vøring margin; MM, Møre margin; NS, North Sea. Numbered lines correspond to seafloor spreading anomalies. Modified after Skogseid et al., (2000).

2.3 The Møre Margin

The Møre margin is defined at the base level of the Cretaceous unconformity, and by a greatly expanded Cretaceous sequence (Blystad, 1995). The Basin area is bounded to the north by the Jan Mayen Lineament and to the southeast by the Møre-Trøndelag fault complex. The western part of the Møre Basin Area is bounded by the Faeroe-Shetland Escapement (Brekke, 2000). The Basin has an overall NE-SW trend, which also is reflected in the structuring of the unconformity at the base of the Cretaceous (Blystad, 1995). In contrast to the Vøring basin situated north of the Jan Mayen Lineament, the Møre Basin seems to have been tectonically quiet since the Mid Jurassic-Early Cretaceous rifting, which was the major tectonic episode in the Møre Basin (e.g., Blystad, 1995, Brekke, 2000) (Figure 2.1 and 2.3).
The Møre Basin is a result of Late Jurassic–Early Cretaceous crustal stretching and thinning, resulting in faulting, thermal cooling and subsidence. The eastern part of the basin area is characterized by deeper faulting down to the basin, which can indicate a high degree of crustal thinning (Blystad, 1995). The further expansion of the Upper Cretaceous sequence with basin-ward thickening could indicate that the Møre Basin responded to the further subsidence of the late cretaceous tectonic events taking place in the north and probably western parts (Blystad, 1995). Much of the western flanks of Møre Basin are hidden under the Eocene lavas. This results in difficulties when producing the maps of detailed cretaceous areas (Brekke, 2000). In areas where the lavas display reasonably transparent seismic imaging the data shows that the cretaceous sequence becomes thinner by onlap onto the

western basin flanks (Figure. 2.2) (Brekke, 2000) Close to the present Faeroe-Shetland Escapement the Cretaceous intervals is as thin as the upper parts of the eastern basin flank, on the edge of the Trøndelag Platform. This could imply that the Faeroe-Shetland Escapement probably is close to the cretaceous boundary between the Møre Basin and the western platform (Blystad, 1995, Brekke, 2000)

2.4 Volcanic basins

Volcanic basins are sedimentary basins influenced by major components of primary emplaced intrusive and extrusive volcanic rocks (e.g., Planke et al., 2014. These magmas are mostly composed of basaltic composition, and associates with formation of Large Igneous Provinces (**LIP's**). When the magma rises through the sedimentary strata, and reaches the surface it can create kilometre thick piles of lava, referred to as flood-basalt. Below the surface, the igneous intrusions are emplaced as both sub-horizontal (sills) and sub-vertical (dikes). Figure 2.4 Show a sketch of a possible subvolcanic complex, within a volcanic basin.

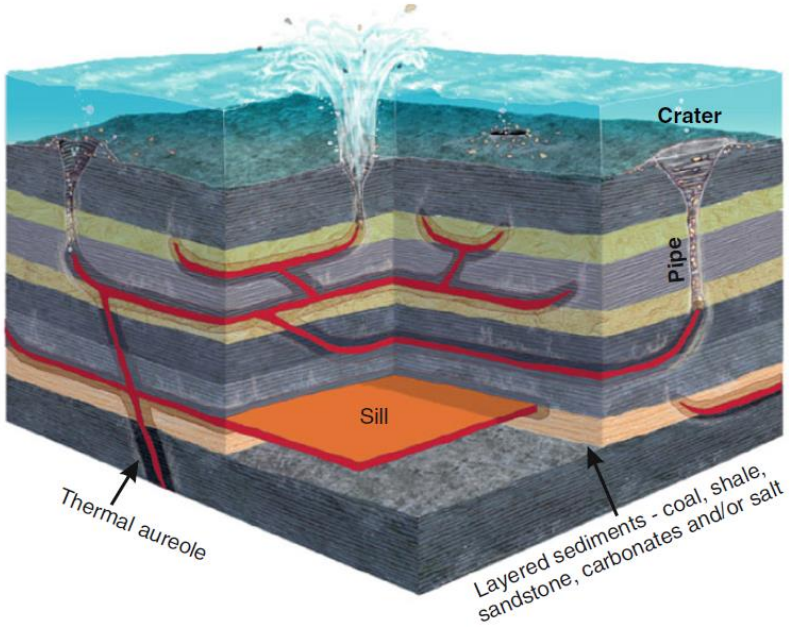

Figure 2.4: Sketch showing sill complex (red colour), thermal aureoles and associated hydrothermal vent complexes within a volcanically influenced sedimentary basin. The Figure shows typically located vent complexes situated above the tip of the transgressed sills. Figure after Planke et al., (2014).

Sedimentary basins represent one of the largest accumulation reservoirs for carbon on Earth (Falkowski et al., 2000). The potential for release of carbon gasses, such as CH_4 and CO_2 due to contact metamorphism between sediments and sills can be very large (Aarnes et al., 2015; Svensen et al., 2004). In 2004 Svensen et al., suggested a possible link between volcanic basins and the well-established environmental change recorded at ~ 56 Ma (The Paleocene Eocene thermal Maximum; **PETM**). This discovery was based upon detailed seismic survey and borehole analyses at the Møre and Vøring basins. The key factor determining the quantities and volumes of greenhouse gasses is based upon contact metamorphism at the thermal aureole. Together with hydrothermal vent complexes this can contribute to efficient pathways between the sill-sediments and the atmosphere.

By studying basins such as the ones in Karoo and the mid-Norwegian Margin, it may be possible to correlate climatic changes and influence by LIP's on a global scale.

2.5 The sill complex

Some of the largest short-lived magmatic events recorded, involve the emplacement of sill complexes into sedimentary basins (Walker, 1993). Processes prior to continental break-up and formation of new ocean basins contribute to voluminous sequences of basaltic lavas erupted into the rifted continental crust (Bell and Butcher, 2002). Magma that cools and solidifies in sedimentary basins before reaching the surface, leads to igneous intrusions and formation of igneous provinces within the strata.

Igneous intrusions are common and present in tectonically exposed basins worldwide. These basins are associated with processes such as continental and volcanic rifted margins, resulting in LIP's. Our understanding of sill emplacement relies to a large extent upon field observation done, for example the Karoo basin in South Africa (e.g., Chevallier and Woodford, 1999) and seismic surveys, for example the mid-Norwegian Margin (e.g., Planke et al., 2014). These field observations enable discussions regarding geometric structure and related processes creating sill emplacement.

Sill geometry shows a typically planar sheet like feature, composed by fine to coarse-grained igneous rock. Individual sheets of the sill complex can achieve thicknesses of several tens of meters, and in some exceptional cases several hundreds of meters (STOSE and LEWIS, 1916). The sheet or leaf structure is commonly the result of one single magma-pulse, although multiple intrusions are also recognized (Bell and Butcher, 2002). Accumulated thicknesses of sills within sedimentary sequences can in some cases be in excess of thousand meters, with an estimated volume of $2 \times 10^5 km^3$ (Du Toit, 1920). Smaller volumes of igneous introductions are also present above sedimentary sequences, and the oceanic lithosphere.

Sills as geological features has been studied and described in geological literature since the beginning of the 20th century. Transgressive sills (sills that cut the stratigraphy) have been described as far back as (Rogers et al., 1905) and (STOSE and LEWIS, 1916). Since these times, a great variety of sill complex geometries and the impactions they impose to the accommodation area has been mapped out. Especially the introduction of seismic surveys from the petroleum exploration has enhanced the accuracy of sill interpretations and study.

2.6 Hydrothermal vent complexes (HTVC)

Sills intruding sedimentary basin causes heating and thus boiling of pore-water and rapid maturation of organic material in the aureole zone within the sedimentary strata (Jamtveit et al., 2004).This introduced heat-source can under certain conditions cause pressure build up quicker than the pressure relaxation, and might lead to phreatic volcanic activity by fracturing the pore space and localize the flow through the overlaying sediments.

The resulting piercement structures of hydrothermal vent complexes (**HTVC**) are today seen as pipe-like structures evident of localized flow in seismic profiles. Raising fluids in the fractured pore space initiate formation of cylindrical conduits formed by rapid transport of water and hydrothermal derived fluids onto the paleosurface (Svensen et al., 2006). The HTVC thereby represent a pathway for gasses and fluids generated by the heat transfer from sill bodies to the country rocks surrounding the igneous intrusions. A schematic overview of the HTVC and the geological setting is represented in Figure 2.5.

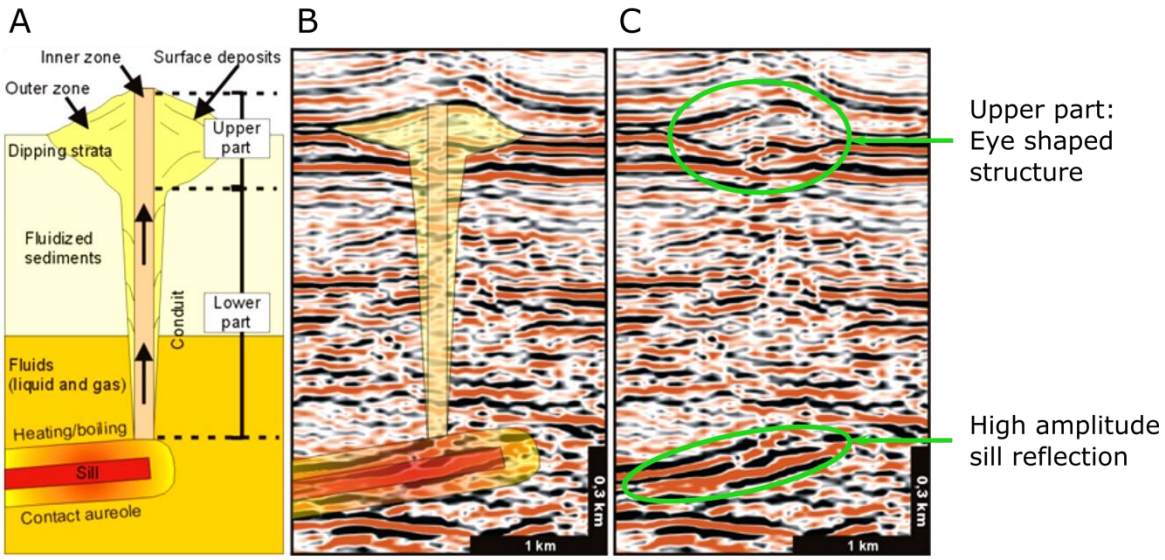

Figure 2.5: A) Represents a Sketch sowing the development of a HTVC, based on an idealized cross-section, in association with volcanic intrusions. B) and C) are seismic imaging illustrating the morphological details of the HTVC. The high amplitude inclined reflector is interpreted as a sill intrusion. Disrupted zone between the sill and the upper part (Eye shaped structure) is the conduit zone, characterising the piercement structure of the vent system. Schematic interpretation modified after Planke et al., (2005).

Measurements of the organic amount and maturation (indicated as vitrinite reflectivity, %Ro) at contact aureoles have been performed (e.g., Brekke, 2000). They found that vast amounts of organic material lacked compared to the surrounding sediments. If reactions in the contact aureole release greenhouse-gasses such as H_2O, CO_2, and CH_4 quickly, it could potentially initiate global climate changes (Svensen et al., 2004).

Two- and three dimensional seismic data have suggested a correlation between sills emplaced in porous sedimentary-rocks and in loosely consolidated sediments. The fluidization of initially consolidated sediments near sill contacts and the subsequent expulsion of large volumes of pore water toward the surface, are possesses initiating a hydrothermal system (Grapes et al., 1974; Jamtveit et al., 2004; Krynauw et al., 1988). Generally the

HTVC's are defined as channels for conveying fluids and gasses, represented by a conduit zone as large as 8 Km long with the origin at the contact aureoles around the sill intrusion. The upper part of the vent complexes comprise of eyes, crates and mounds (Figure 2.6) with structural extent of up to 10 Km in diameter (Planke et al., 2005; Svensen et al., 2006).

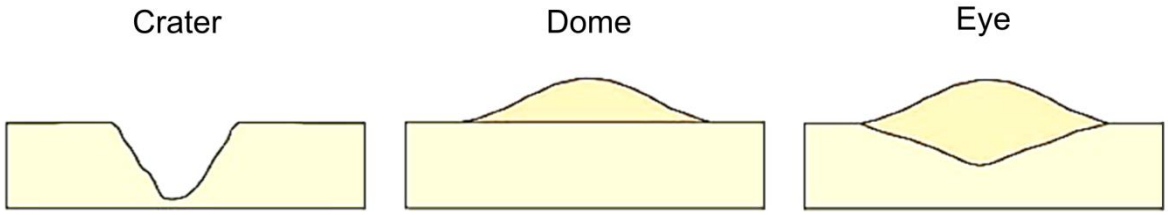

Figure 2.6: Illustrations of upper vent combinations: Eyes, crates and mounds. Figure modified after Planke et al., (2005).

2.7 HTVC in the field

Areas such as the Karoo-Lesotho province, Siberian Traps and the North Atlantic are characterized by an extensive network consisting of sills and dykes imbedded in the sedimentary strata (Bell and Butcher, 2002; Brekke, 2000; Chevallier and Woodford, 1999; Jamtveit et al., 2004; Svensen et al., 2006; Svensen et al., 2009; Svensen et al., 2015). Vents and conduit structures associated with these networks have been identified during field studies, and the spatial relationship between igneous intrusions and HTVC have been established. Detailed mappings of the HTVC's, focusing on the structural extents and sedimentary units from tectonically derived processes have been carried out in different areas, Jamtveit *et al.*, (2004) and Svensen *et al.*, (2006) among others.

The Karoo basin in the centeral south Africa is a typical exmple of an sedimentary basin influenced by LIPs. The basin experienced an extencive volcanic activity in the early Jurassic period (Duncan et al., 1997). this resulted in a 1.4 km sequence of basaltic lava capping the clastic sediment column (Johnson et al., 1997). Sill and dyke intrusions are present througout the basin sucression, and can locally form up to 70% of the sedimentary terrain (Rowsell and De Swardt, 1976). A direct consequence of the Karoo LIPs is the prominent and numerous HTVC structures identified during field studies.

The vents themselves are highly variable in composition, ranging from dominantly fractured sandstone, to those consisting of metamorphic shale. Studies concentrating on the structural behaviour have found that HTVC's are surrounded by inward dipping strata. The vents are composed of sedimentary breccia as well as massive sandstone. Intersection of sandstone dykes, pipes and Zeolite mineralization with corresponding lack of igneous material, indicate hydrothermal derived process to the system in contrast to an magmatic (Svensen et al., 2007). Cylindrical structures (breccia pipes) are also encountered, but much deeper in the stratigraphy.

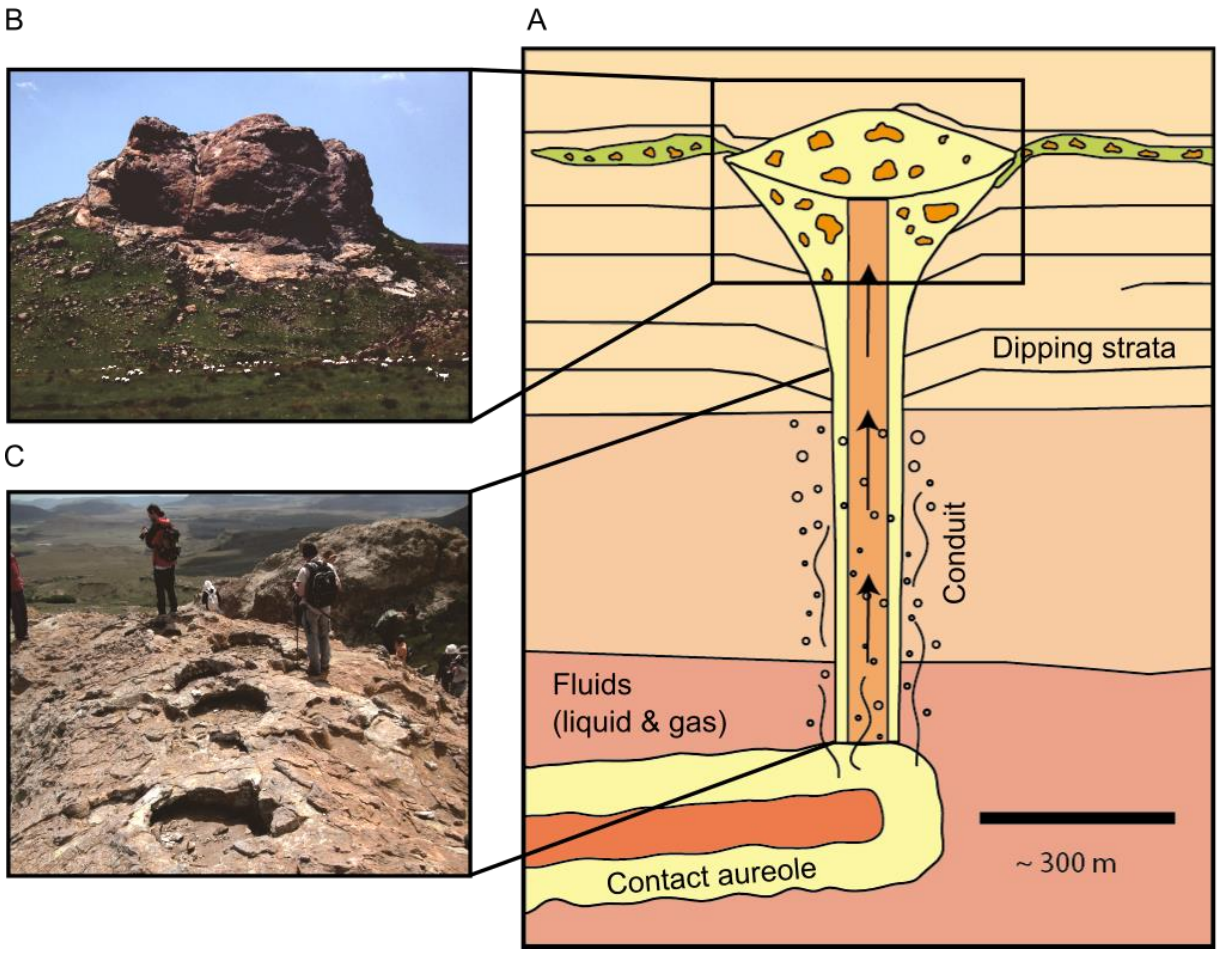

Figure 2.7: A) Sketch showing the development of a hydrothermal vent complex, based on an idealized cross-section and seismic interpretation from the Karoo Basin and the Norwegian Sea. The assembly of the vent complex is divided into a lower and upper part, and an inner and an outer zone (Jamtveit et al., 2004; Planke et al., 2005). Boiling of pore fluid and gas formation (degassing of magma, metamorphic reactions) cause fluid-pressure to build-up, and formation of explosive cone-shaped hydrothermal vent complex occur. Upper part of the hydrothermal system is defined by subsequently, large (several meters across) pipe structures of fluidized sandstone cross-cutting the brecciated rock. Sketch modified after Svensen et al., (2006). B) Upper part and crater structure of HTVC in the Karoo Basin, representing a crater filled with sediment breccia and sandstone (Svensen et al., 2006). C) Sediment pipes/conduit zone outcrop from the Karoo Basin. The pipe is characterized as a sandstone pipe cutting the sedimentary breccia of the inner zone of the HTVC. The pipe has a thick internal deformation zone along the margin, defined by both vertical and horizontal deformation (Svensen et al., 2006).

3. Theories of quantitative and simulated modeling

One of the main challenges regarding the description and interpretations of geological structures is the ability of observing the development as they progress. This is also the case when studying the HTVC's. Although, similar structures occur in nature today (e.g., mud volcanos and black smokers), geologist must generally turn to experimental or remote sensing techniques in order to understand the evolution.

In this thesis an experimental study of piercement structures in granular and unconsolidated media was performed. The experimental part consists of a qualitative sandbox experiments and subsequent implementation of synthetic seismic, to give a better understanding of the structural development and dynamics of the piercement structures.

3.1 Modelling sedimentary features and structures

Qualitative modelling such as sandbox experiments is a useful tool to study geological processes which are not easily obtained during numerical modelling or collection of field data alone. Experimental geophysics lab equipment is used to study the Earths dynamical processes and structures related to it. One example is the generation of piercement structures related to the development of HTVC's.

Experimental sandbox models of piercement structures are based on establishing a set of physical parameters that are relevant for the process. This qualitative modelling enables one to simulate the geological features and obtain new understanding of the parameters that governs the geophysical processes. The system of which this experiment focuses on, correspond to the rapid venting due to a sudden pressure build-up in magma intruded host rocks generating rapid degassing and volatilization of fluids. In both experiments and in nature the geometrical parameters are the depth (h) of the volcanic intrusion and overburden sediments, the pressure (P) at the vent source which might correspond to size and thickness of the sill intrusion and aureole in the country rock. The experiment setting is related to unconsolidated sediments, where the rock property is given as density (ρ), and mechanically properties as angle of internal friction (ϕ). The initial state in terms of infill-height and pre-determent pressure supply, defines the state of the experiment and the values which goes into the model of venting and piercement structures.

Previous studies have performed quantitative modelling of sedimentary basins aimed at explaining structural and physical processes. For instance, the study of fragmentation and fluidization of sediments as geological implications, have shown a correlation between the fluid pressure build up at contact aureoles and the formation of vent structures such as HTVC's, mud volcanos and kimberlites (Galland et al., 2014; Haug et al., 2013; Nermoen et al., 2010; Ross et al., 2011). The experimental modelling conducted seams to better predict how the geometries of the piercement structures occur, although scaling needs to be performed in order to better constrain the critical parameters controlling the material transport.

3.2 Simulated seismic imaging

Descriptions of sedimentary basins and subsurface structures have usually been based upon seismic interpretation and well data information to provide parameters like thickness, extent and divisibility. The contribution of synthetic seismic in experimental modelling can improve mapping of faults, piercement structures and other markers related to seismic observations. Taking into account the petrophysical properties derived from well logs and core data a relation between in situ features and experimental setting can be established.

The synthetic seismic is a conceptual tool for testing case by case studies by acquiring software derived seismic images. Implementing synthetic modelling on real data cases or physical experimental results can be a key factor to retrieve information about Earths subsurface layers within a target zone. Valuable information from these images is not always provided in full extent due to issues like lack of illumination and limited resolution. When faced with interpretation issues, synthetic modelling provides a useful tool for theoretical testing of geological models as long as an appropriate method and input information is available. In the case of qualitative experimental modelling, the implementation of synthetic seismic can provide a link to better understand the scale and resolution in detail. Correlation of the simulated seismic imaging with structures visualized in actual seismic surveys can establish a more confident interpretation, and provide valuable information regarding data limitations.

Previous studies by (Botter et al., 2014; Lecomte et al., 2015; Lecomte et al., 2016) show the importance of synthetic seismic as a tool for studying geological features. By establishing an understanding regarding limitation of seismic analysis, it is possible to undertake a more precise and cost efficient evaluation of the geological framework in question. Examples of geological case studies that further illustrate illumination and resolution issues in seismic images can for instance be related to fault-zone modelling in reservoirs or digital outcrop mapping.

Fault interpretation is often simplified in reservoir models and poorly defined in seismic data. However, faults are three dimensional structures zones with material properties that differ from the host rock. Seismic modelling applied to numerical or laboratory models may improve characterization and understanding of reservoir fault zones and misleading results avoided if the structures are properly included (Botter et al., 2014).

Digital outcrop modelling utilizes state of the art methods to obtain quantitative and qualitative data by laser scanning (Buckley et al., 2013). The resulting 3D photogrammetry and topography models of the outcrop are a powerful way to obtain field data. This data can then be used as a basis for different studies, such as structural mapping and reservoir modelling. For synthetic seismic, models linked to digitalized outcrops can be created, and allows for detailed interpretation of geometry and structural relationship between field studies and seismic surveys offshore. In this way, the correlation between observed field data and seismic data can be combined to retrieve a better understanding of the overall framework.

4. Data

4.1 Seismic data and study area

The seismic data available for this thesis study comprises the upper 7 s two-way-travel time (TWT) of the Norwegian survey named Tulipan. The survey is situated in the western part of the Møre Basin, offshore mid-Norway in the area between 63° 31' 38" N and EW degrees: 2° 45' 51" E (See Figure 4.1 A). The project database is a part of a 3D seismic data set collected in connection with the PL251 licence by Statoil. The extent of the total data set covers approximately 2100 km^2, and the bin-size (in-line and cross-line) of the interpreted area is approximately 310 km^2 (See Figure 4.1 B). The data set is regarded as zero-phase, and displayed so that white/blue (depending on colour scheme of active seismic object) denotes downward positive acoustic impedance. The data are 3D migrated, and the overall quality is regarded as excellent.

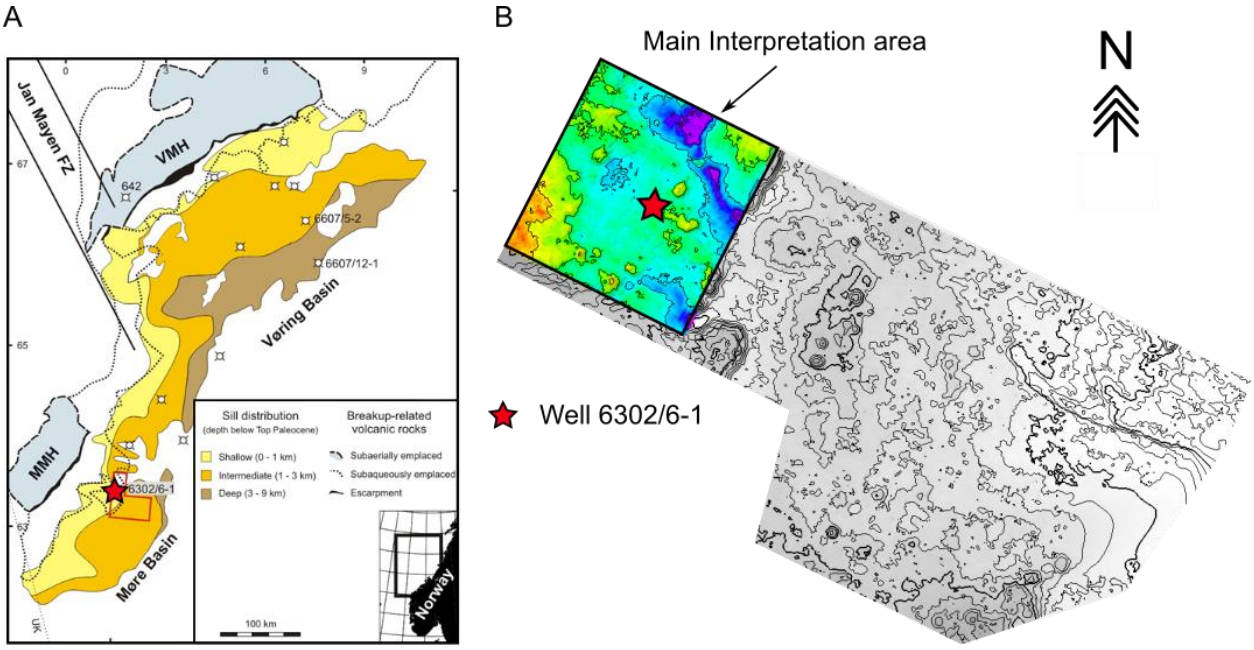

Figure 4.1: A) Simplified structural map of the mid-Norwegian Margin and the location of 3D seismic survey PL251 marked with a red box. The survey is situated at the western part of the Møre Basin. Modified after (Planke et al., 2007). B) Outline of the PL251 seismic survey and location of main interpretation area in this study. The main survey is approximately 2100 km2, and the bin-size of the interpretation area is approximately 310 km2.

The geophysical data interpreted in this study is based upon three data sets. One full 3D stacked seismic cube, one set of conventional borehole wireline and check-shot data (time, depth curve). Only the time-migrated cube was available for this study, and depth conversion has not been implemented. Subsurface velocities between intervals have been calculated from the average transit times provided by the sonic-log of well 6302/6-1. The velocities vary from about 2000 m/s at the top to about 3000 m/s at the base of the well succession. The main frequency spectrum of the data set is about 40-50 Hz. This implies a dominant wavelet order

of 30-50 m, corresponding to seismic resolution of about ~10 m ($\delta h = \lambda/4$: one quarter of the dominant wavelet).

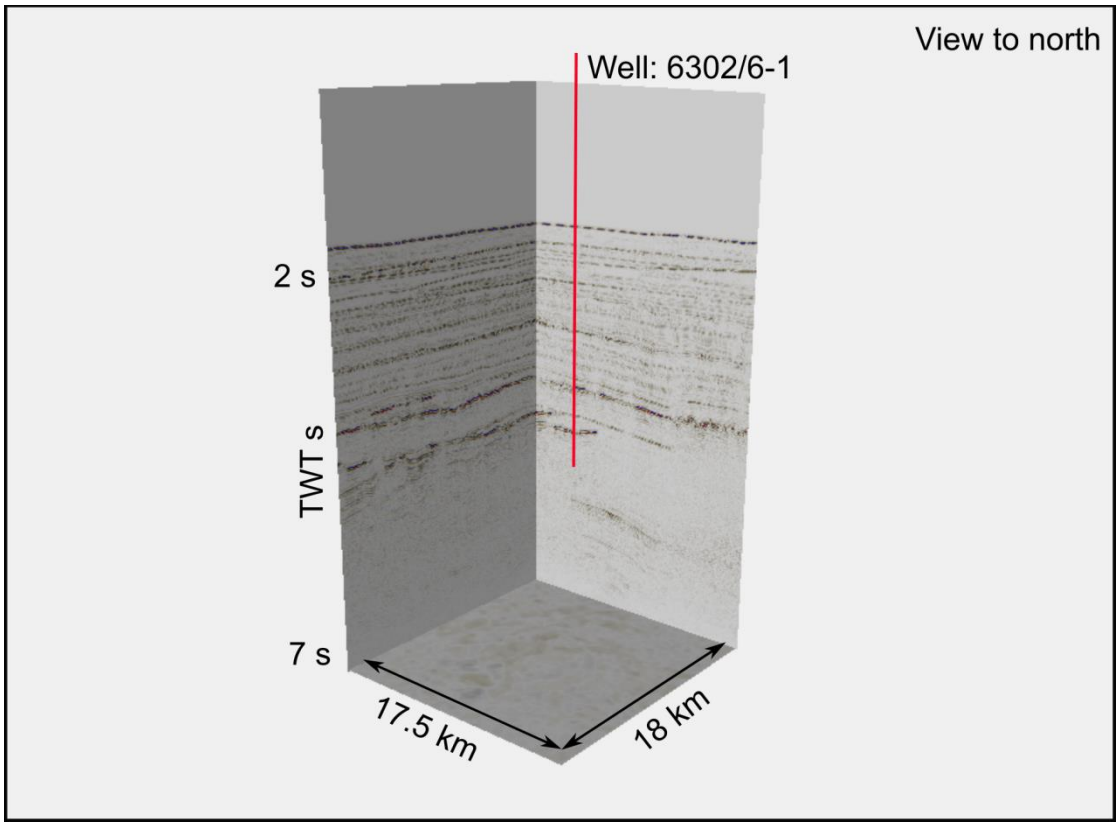

Figure 4.2: Project database and the cropped 3D cube. The area correlates to the location of main interpretation area in Figure 4.1, B. Overall sizes measured to be: c. 310 km^2 and 7s TWT.

4.2 Well data

Well 6302/6-1:

Table 4.1: General licence and well information (Statoil Tulipan discovery report (Planke et al., 2007), npd fact page well: 6302/6-1)

License Partners: Statoil (Op) 70%, BG Norge 20%, Norske Shell 10%,
Entered date: 24.06.2005
Completed date: 04.10.2005
Water depth [m]: 1261.0
Final vertical depth (TVD): 4234.0
Geodetic datum: ED50
NS degrees: 63° 31' 38.43" N
EW degrees: 2° 45' 51.56" E
NS UTM [m]: 7044540.65
EW UTM [m]: 488277.59
UTM zone: 31

Exploration well 6302/6-1 was the first well licence to be drilled after the general awarding in 2000. The well function at this stage was considered as a play opener in case of hydrocarbon discovery at the Tulipan block (See table 4.1 for general licence information). The main objective of the exploration of well 6302/6-1 was to test the prospects and quality of rocs of Early Tertiary age, as well as defining primary reservoir target for hydrocarbons in sandstone of Danian age (Paleocene) (Planke et al., 2007).The drilling of well 6302/6-1 was performed by the semi-submergible drilling facility Erik Raude in 2005, at a total recorded wellbore-depth exceeding 4200 m (loggers depth). Oldest penetrating formation is the Springar formation of Late cretaceous age with surface top at c. 4080m.

Three cores were cut during the exploration, with a total of 15.7 m recovered in the interval between 3903-3942 m in the Danian sandstone of the Rogaland group. Cutting samples are available from top depth 1975m and bottom depth 4230 m.

The well was permanently abandoned on the 4 October 2005, as a gas discovery. The pressure data from the well suggests that only a relative small (17m) column of gas is present. The overall quality was generally poor due to the carbonate cementation of the sandstone and the lowering of the porosity at the reservoir. For a discovery to have a commercial value the column would have to be significantly larger. The discovery where therefore classified as non–commercial. Gamma-ray (GR), sonic (DT), density (RHOB) and some composite logs are available from the well 6302/6-1.

5. Seismic interpretation methods

5.1 Stratigraphic horizons and surfaces

The horizon interpretation involves digitizing of horizon surfaces by generating a discrete set of samples within the three-dimensional survey volume. Horizon surfaces are surfaces that are selected to correspond with reflections in the volume represented by the seismic survey.

The first conventional method implemented is the guided auto-tracker. In this approach, a planar '2D slice' from the seismic volume is displayed. These lines are in most cases orthogonally lines, represented by inline, crossline and time-slices (X, Y, and Z respectively in the Cartesian coordinate system). The interpretation is done by selecting 'seed' points within a reflector of a given horizon. Based on the computer algorithm and neighbouring seed-points, the resulting surface is generated by interpolation of the chosen amplitude event (Dorn, 1999). This method of interpretation is the favourable approach considering the accuracy of the final result due to the removal of human error involved in pick-digitizing. However, the guided auto-tracker has its limitations. To successfully interpolate between seed-points, the horizon surface has to remain connected; faults, discontinuity and other reflection splitting events, presents interference in the seismic volume.

To overcome instances of seismic discontinuity the method of manual picking is implemented. This process is based upon judgment of the seismic signals themselves. While manual picking can be quite accurate, the sheer volume of the 3D data survey prohibits this approach, due to the time-consuming selection.

During the horizon interpretations the picking intervals between the inline and crossline is set to be between 5–25 increments (steps) depending upon the continuity of the reflectors. The gridded surface is then 3D auto-tracked from the seed -points and outward, completing the horizon volume for detailed amplitude and structural study.

5.2 Hydrothermal vent complexes

The description of Vent complexes and seismic imaging will be compared to former interpretation done at the mid-Norwegian Margin by Planke et al., (2005) and the seismic interpretation of the Møre Basin area. The hydrothermal vent systems interpreted at the mid-Norwegian Margin are based on three main horizons within the Intra-Paleogene stratigraphic Colum. This reference datum is based on the seismic characteristics, and well-defined geometry of the vent systems. The emphasis is on the top vent horizon as the key structure (See Figure 5.1). The top vent/mound horizon is characterized by a series of vertical convex structures which can be seen as mounded highs terminating at a given consistent stratigraphic layer. These mounded highs can be seen in the seismic imaging as structures located above the upper part of the hydrothermal vent system. To determinate the extent of these structures the top mound horizon was picked at a well-defined, high amplitude and continuous stratigraphic boundary, defined by the presence of the uppermost part of the convex reflections. These picks are done manually by selecting the greatest positive relief of the mounds. The top mound horizon of the seismic cube from the Møre Basin is distinct

throughout the whole project database and is defined by the relative high-amplitude and continuous reflector.

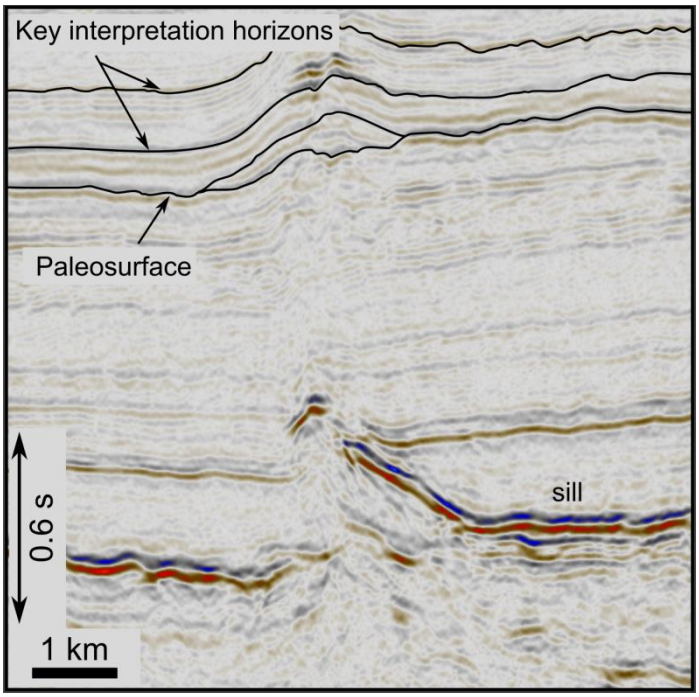

Figure 5.1: Figure summarizing the features taking into account when interpreting the HTVC's in seismic sections.

The seismic characteristics emphasized in the interpretations of the HTVC

- The geometry and overall size of the upper part of the vent complex (eye, crater or dome shaped morphology of the surface deposit upper part);
- The behaviour and nature of the overlaying reflectors (mounded key surfaces, high amplitude surfaces and disrupted seismic lines);
- The behaviour and nature of the underlying reflectors (dipping reflectors: inward- and outward events around the chimney/conduit. High amplitude events, and disrupted seismic lines);
- The presence and interference of vent systems with underlying sill complexes.

5.3 Measurement criteria for HTVC's

Measurements of the upper and lower part are based on 2D projection profiles from the seismic data implemented in Petrel for calculation. The procedure is done manually by interpreting individual HTVC's, and assigning them their unit sizes. Measurement criteria of the upper part are defined by the down lapping dome structure on the paleosurface. Since the dome structure in 3D show an ellipsoid geometry, both minor and maximal widths have been mapped (Figure 5.2). The conduit height is defined by the depth between underlying Feeder sill and paleosurface (Figure 5.2). The origin is not always clear because a single vent may be formed by fluid discharge from two or more sills. During the mapping procedure it was considered important not to double count the HTVC's for the quantitative analysis, so each vent was assigned one sill. All HTVC's within the studied area have been assigned sizes based on what could be observed in the seismic imaging, in total 13 HTVC values.

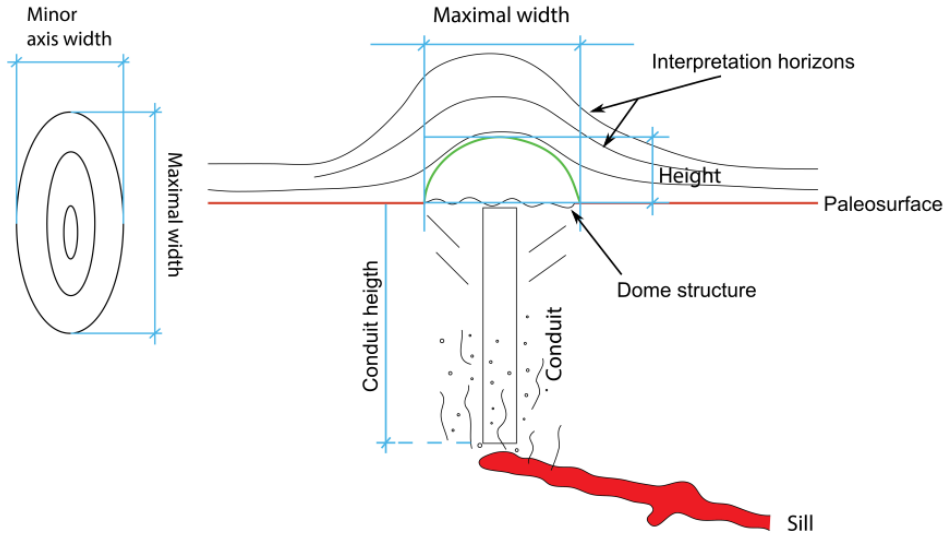

Figure 5.2 schematic drawing, showing the measurement criteria for height/width and conduit zone of the HTVC.

5.4 Well tie

By identifying stacking patterns of different beds and correlating with well log signature it is possible to identify surfaces within the subsurface. Stacking patterns and well log electro facies provides a solvable approach for interpretations of physical processes that have affected the various depositional environments and the material deposited trough time.
The approach of well log data and core comparison has been in use for a number of years, and still remain the most efficient way to investigate the structural and lithological units at the subsurface.

To relate the stratigraphy and to give an age correlation at the interested area of the seismic section one well at the Møre Basin has been tied for interpretation purpose. The well was cored in three sections at one certain interval, and logged continuous with an array of conventional electric and nuclear logging-tools. This provides control of the upper Cretaceous to percent day Pliocene seismic reflectors and well log-data.

In this study, the focus is directed at the regional boundaries surrounding the piercement structures related to the HTVC. The area is defined by the transition between Eocene and Paleocene, and show distinct seismic characteristics and main unconformities together with internal reflectors. The approach utilized to determine age and stratigraphy is a combination of seismic interpretation of Chrono-surfaces, well log electrofacies and biostratigraphical data. The obtained data will be compared to each other, and will be a basis for the final interpretation of the lithological sequence, together with an interpretation of the HTVC timing.

5.4.1 Biostratigraphical evaluation in well 6302/6-1, Tulipan Prospect

This section will present palynology and micropaleontology from the wellsite, based upon analyses undertaken for Statoil on the exploration well 6302/6-1, Tulipan prospect, Norwegian North Sea. The reports used emphasized on resolving the questions regarding the source of argillaceous sediments in the Paleocene-Eocene interval, age correlations, zone depth and a discussion of the main biological marker events (Jolley, 2006; Mahdi and Ayress, 2006). The underlying data are based on cutting samples analysed over the interval 1980 m – 4230 m, and Three cores recovered in the interval between 3903 m – 3942 m in the Danian sandstone reservoir.

Work undertaken of the collected data include quantitative palynological study, together with palynological and micropalaeontological analyses.

5.4.2 Method for stratigraphical breakdown and palynological counting

The Biostratigraphical zones are defined on premises based on downhole occurrence of key marker taxa together with influxes and changes in assemblage composition (Mahdi and Ayress, 2006). The recognition of benthic and planktonic microfossil evolution-events can be used to divide the lithological record into biozones, and thereby towards a stratigraphical age and environment correlation. The biostratigraphical zonation of the well-trace and resulting formation scheme, has been developed using a combination of both micropaleontology and palynology. (Biostratigraphical zonation scheme from early Paleocene to early Oligocene can be viewed in Appendix A.3).

Palynological counting was carried out by identifying 100 palynomorphs, wherever possible, then giving an estimate of the dinocyst present in the assemblage (Dinocyst% of assemblage). This method of counting continued until a total of 100 dinocysts were reached, and the process repeated throughout the well section (Mahdi and Ayress, 2006).

5.5 Piercement structures in the laboratory

This part aims to establish an approximation of the processes thought to have initiated the distribution and morphology of HTVC. The experiments are divided into a two part sequence. The first part is a laboratory experiment meant to develop a qualitative experiment of the physical processes as a function through time. The setup and approach of the sandbox experiment is based on similar procedures as used by Nermoen et al., (2010) and Haug et al., (2013) within the physics department at the University of Oslo. The same physical setup is used.

The second part focuses on building a complete SeisRox model, defining the geometry and properties of the HTVC structures. The model building is based on implementing synthetic seismic on the resulting pictures, which was generated during the sandbox experiment. The complete model and dataset will be discussed in terms of observations and comparison of the actual seismic interpretation of the HTVC at the Møre Basin.

5.5.1 Physical experimental setup

The experiment was done using a vertical orientated cell consisting of two parallel Plexiglas plates positioned 0.7 cm apart. The plated cell measures 60x60 cm and are sealed at the bottom and the vertical sides, whiles the top part of the box is open (See Figure 5.3). The fixed air inlet positioned at the bottom of the cell was raised 5 cm into the cell, to prevent airflow to focus along the lowermost part of the cell and its walls. Compressed air was used to induce the fluid pressure into the bedded material, which consists of alternating layers of olivine-sand and **aluminium-silicate** (See 5.5.2 Experimental materials, for composition). Each experiment conducted, was prepared by slowly poring the sand through a funnel, from the top of the fixed cell to a chosen height (h). The height (h) varied from 9 – 21 cm measured from a fixed datum positioned at the lowermost part of the 60 cm Plexiglas plate. By using the procedure of funnel filling, a better control of the filling height, material distribution and bedding with a horizontal and planar surface was obtained. This approach also enables a consistent and similar initial packing of the material for each experiment.

The flow velocities in this experiment are regarded as constant, since the air supply is induced at a uniform pressure throughout the experiments. Digital images during the experiment were captured at 7 frames per second using a high resolution DSLR (digital single lens reflex camera) Olympus E-3 setup. Due to the importance of capturing the structures with best possible detail resolution the camera was set to high contrast imaging.

In the experiment study two quantitative parameters varied from one configuration to another: The injection pressure (pressure from air supply/tank gauge) p, ranging from 0.15 to 0.3 Mpa, and the depth (h) of the olivine-sand/aluminium-silicate layering, ranging from 9 to 21 cm.

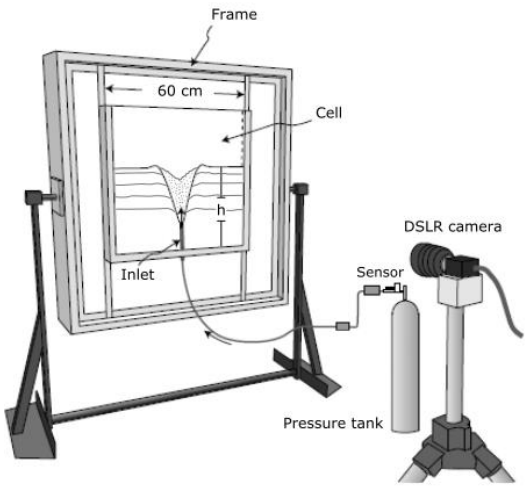

Figure 5.3: Sketch of the experimental setup, cell filled with olivine-sand and aluminium-silicate. Compressed air is injected through an inlet within the unconsolidated material from a pressure tank. Figure modified after Haug et al., (2013).

5.5.2 Experiment material

Two types of material were used in the experiments, olivine-sand and aluminum-silicate. The name aluminum-silicate is used as a collective description of the quarts and aluminum-oxide composition. Both materials have a close to spherical shape with an angular outer margin of the grains (See Figure 5.4). The olivine was measured to a diameter d_{OL}=150–300 µm and density ρ_{OL}=1.80 g/cm^3, and the aluminum-silicate with a diameter d_{AL}=200-600 µm and density ρ_{AL}=2.80 g/cm^3. The densities of the different of materials were measured out by weight and volume ratio in the lab (ρ=Mass/Volume), and the size were determined using a sediment grain size chart.

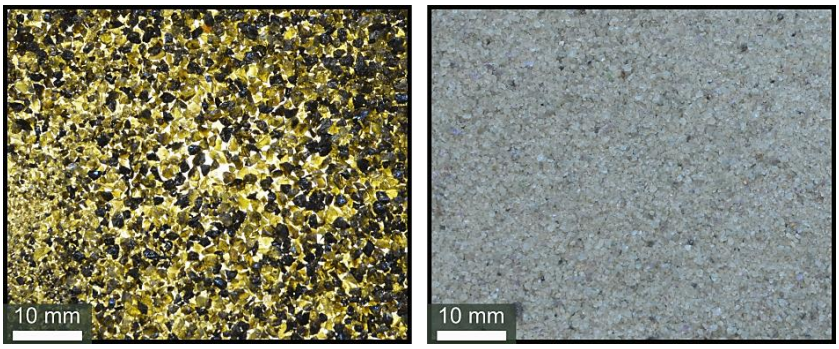

Figure 5.4: Pictures illustrating materials used to perform the venting experiment. To the right: Olivine sand, to the left: aluminium silicate.

5.6 Synthetic seismic model

Synthetic seismic modelling can be a useful tool in validating the seismic interpretation and understanding of the structural features in seismic imaging. Ray-based approach can provide rapid modelling results, taking into account the complexities of the geological features in

question (Lecomte et al., 2015). For this study, the sandbox experiment provided a 2D projection image of the piercement structure and associated HTVC (See Chapter 7, Vent modelling).

5.6.1 From sandbox model to seismic model

The most representative picture obtained during the sandbox experiment, will serve as input to define the target (zone to image) for the synthetic modelling. This picture will be implemented into a vector based drawing program (Inkscape) to define zones which is later assigned to specific elastic properties. By establishing these zones it is possible to take into account the seismic wave propagation effects from the survey geometry, source wavelet and overburden.

The background picture in this study was implemented as a 1D layer model. This implies that property variations only takes place in one direction (z-direction, depth). The alternating light and dark coloured sand used in the sandbox experiment makes up the basic geometry of the model. It is defined by the 15 different layers related to sedimentary sequences and coherent change in elastic values (Vp- and Vs- velocities). Since well data is available for the specific study area, an effort was made to apply borehole data that could represent how the piercement structures actually looks like in real stratigraphy.

The following assumptions and well data were implemented**:**

- The horizontal and vertical sizes of the background picture are defined as 1800 m and 850 m respectively based on dimension analysis done during seismic interpretation.
- Elastic values available from borehole data at the HTVC depth ranges from Vp ~ 2.0-2.5 km/s and Vs ~ 1.1-1.8 km/s, increasing with depth (km).
- Two sets of elastic properties (Vp and Vs) were implemented to create the impedance/reflectivity model. These values range between: Vp ~ 2.0-2.3 km/s and Vs ~ 1.2-1.3 km/s.
- Density in the model varies from 2.0-2.2 g/cm^3.
- The seismic properties within one zone are homogeneous and identical throughout the sequence, no internal reflections.

5.6.2 PSF-based, pre-stack depth migration (PSDM) algorithm

The method used for obtaining synthetic seismic profiles relies on a proprietary 'pre-stack depth migration' (**PSDM**) simulation (Lecomte and Kaschwich, 2008). The PSDM simulator creates a seismic image based upon the elastic properties defined as reflectivity grids in target zone. This approach accounts for illumination and resolution according to a given survey geometry and overburden model (Lecomte et al., 2003).

A key element of this modelling process is the calculation of so-called illumination-vector at a given reference point in the target (e.g. the centre). This vector is based on the difference between two slowness vectors P_S and P_R, at that reference point.

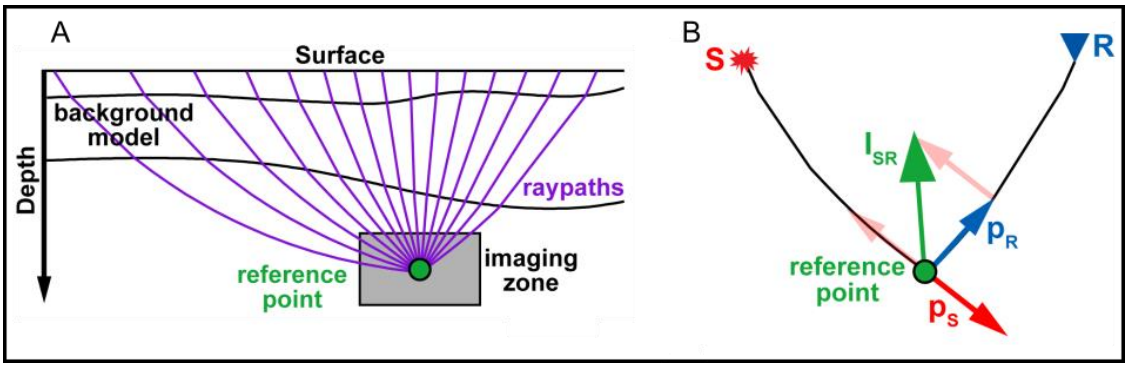

Figure 5.5: A) Ray paths towards a reference point. B) Illustration of the illumination vector ISR, resulting from the two slowness vectors PS and PR. Modified after Lecomte et al., (2016).

- For a given velocity model at a given reference point, the illumination vector is defined as: $\mathbf{I_{SR}} = \mathbf{P_R} - \mathbf{P_S}$ (See Figure 5.5 B).

The slowness vector-pairs from a shot (P_S) and receiver (P_R) is obtained by ray-tracing in the background model down to a reference point. I_{SR} is characterized as a function of local velocity, frequency spectrum and opening angle between P_S and P_R. The resulting vector-length and its orientation are the key factors in controlling illumination quality and resolution of PSDM imaging.

Different sets of (P_S and P_R) pairs corresponding to a given survey will provide different geometry of the I_{SR} vector, based upon incident angle at the reference point (See Figure 5.5 A for ray paths towards a reference point). The information from all shot-receiver pair combined with a source pulse is implemented into a so-called PSDM filter in the wavenumber domain. This filter represents the total illumination, resolution and wave propagation down to the reference point. A Fourier transformation converting the wavenumber domain to space domain generates a spatial resolution function, or **Point Spread Function** (PSF). When applied to an input reflectivity model of the target, the PSDM filter simulates PSDM imaging on that structure. The simulation is incident-angle dependent and based on the elastic properties implemented in the target model (Lecomte et al., 2016). Figure 5.6 B illustrates a frequency-dependent illumination vector (I_{SR}) mapped with dip limitation of ±45° and 0-90°.

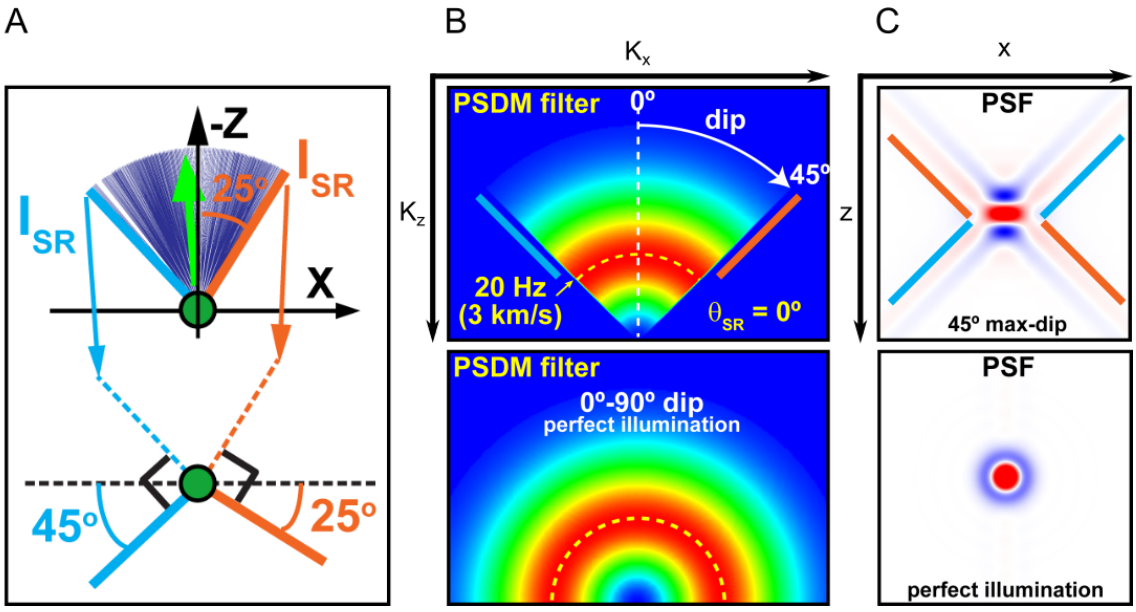

Figure 5.6: A) Span of IRS illumination vector, corresponding to a specific dip range. Note that reflectors outside detection range (steeper than 45° to the left, and steeper than 25° to the right) will not be imaged. B) PSDM-filter showing illumination based on IRS vector and dip-limited span of ray traces. C) Corresponding PSF after Fourier-transformation of the PSDM. Note how total PSF resolution depends on the IRS illumination vector and dip related reflectors. Figures modified after Lecomte et al., (2016).

The approach of pre-stack image from the reflectivity boundaries is used as further constraint to interpret the experimental piercement-structures. This provides a cost efficient and timesaving method for interpretation of geological structures, and provides more reliable results than the 1D convolution method geologist tends to depend on when more advanced modelling is not affordable.

6. Well data and seismic results

6.1 Biostratigraphy

This part will present a summary of the biostratigraphical data from the PE-transition (Paleocene-Eocene) done of well 6302/6-1. The biostratigraphical results are based on extraction from Appendix 1 in Planke et al., (2007). This appendix presents a re-evaluation of the biostratigraphy data from the Eocene to Paleocene intervals. The interpretation is based on the report produced by Ichron Ltd. in January 2006, and an examination of the palynological slides that formed a basis for that report. Also two biostratigraphical consultation of well 6302/6-1 by Jolly et al., (2005) and Mahdi and Ayress, (2006) on the behalf of Statoil have been implemented to correlate the findings.

New resolution-chart of the palynological appearance and table for age of the key horizons has been produced in this thesis (Figure 6.1, to 6.3). The retrieved data will be presented as interval sequences ranging from c. 3100-3500 meters, covering the stratigraphic zonation of the HTVC event (See Figure 6.7 for complete seismic interpretation sequence).

- Summary of each interval is extracted from Appendix 1 in Planke et al., (2007).

INTERVAL: 3090 – 3120 m
Eocene-Oligocene transition
Zone: TP8A
Brygge Formation

The interval is based on the last occurrence of *Systematophora placacantha* at 3110m. The zone is regarded as a good interval for fossil markers, and implies an age corresponding of 42.8-45.0 Ma. *Systematophora placacantha* are relatively common, and displays a good taxa resolution from first occurrence at 2520 and last occurrence at 3110 meters. Key interpreted horizon in this interval is the Intra Brygge 2.

INTERVAL: 3200 - 3220m
Lower Eocene
Zone: TP6B
Tare Formation

Based on the abundance of *Globigerina linaperta* at 3270m, with its common, but short occurrence interval of 3200-3220 meters. The thickness of the taxa zone amounts to 70-90 m and correlation implies an age interval around 52.17 Ma. The key horizon is the mounded surface of the Top Tare reflector.

INTERVAL: 3260 m
Lower Eocene
Zone: TP5B3
Tare Formation

Based on the last occurrence of *Cerodinium wardenense* at 3260m. The depth corresponds to the Intra Tare horizon, and an age correlation estimated to be between 53.6-54.6 Ma.

INTERVAL: 3270-3350 m
Lower Eocene
Zone: TP5B2
Tare-Tang Formation transition

Based on the last occurrence of *Cerodinium wardenense* at 3260m, and the sporadic appearance to abrupt last occurrence of *Cerodinium dartmoorium* in the interval 3260-3250m. No horizon has been interpreted in this interval, but the age is determined to be between 54.8-54.9 Ma.

INTERVAL: 3335 m
Paleocene-Eocene transition
Zone: TP5B2
Tang Formation

Based on the last occurrence of *Apectodinium augustum*. This is the key interval defined by the Top Tang horizon, in which the upper part and dome feature of the HTVC's is lapping down onto. The depth interval between 3335-3340 m have a correlated age of 54.7-55.8Ma. The taxa resolution is quite good as it shifts from last occurrence of *Apectodinium augustum* to first occurrence of *Phelodinium*.

INTERVAL: 3350-3410 m
Upper Paleocene
Zone: TP5B1-B0
Tang Formation

This interval is to a large extent a continuation of the *Apectodinium augustum* interval above, but there are several observations of older Paleocene and Cretaceous taxa's such as the full range observation of *Spiniferites 'membranispina'*, and the first occurrence of *Glaphyrocysta ordinata 'granulata'*. There is also income of palynological Tang Formation markers which is somewhat confusing to interpret. This interval concludes the stratigraphic zonation of the HTVC event, and is defined by the underlying Intra Tang horizon. Age correlation is set to be between 54.8-55.9 Ma.

A

Age Ma	Depth (m)	Seismic horizon	Stage	Palyno zones	Key Taxa	symbol
42.8-45.0	3120	Intra Brygge 2	Eo-Olig transition	TP7-8	Systematophora placacantha	S.plac
52.17	3220	Top Tare		Tp6	Globigerina linaperta	G.lina
53.6-54.6	3260	Intra Tare	Eocene	Tp5	Cerodinium wardenense	C.war
54.8	3270-3330				Cerodinium dartmoorium	C.dart
54.9		Earliest Pal-Eo transition			Phelodinium	Phel
54.7-55.8	3335	Top Tang			Apectodinium augustum	A.aug
54.8-55.9	3410	Intra Tang	Late Paleocene	Tp4	Spiniferites 'membranispina' Glaphyrocysta ordinata 'granulata'	Spin G.ord

B

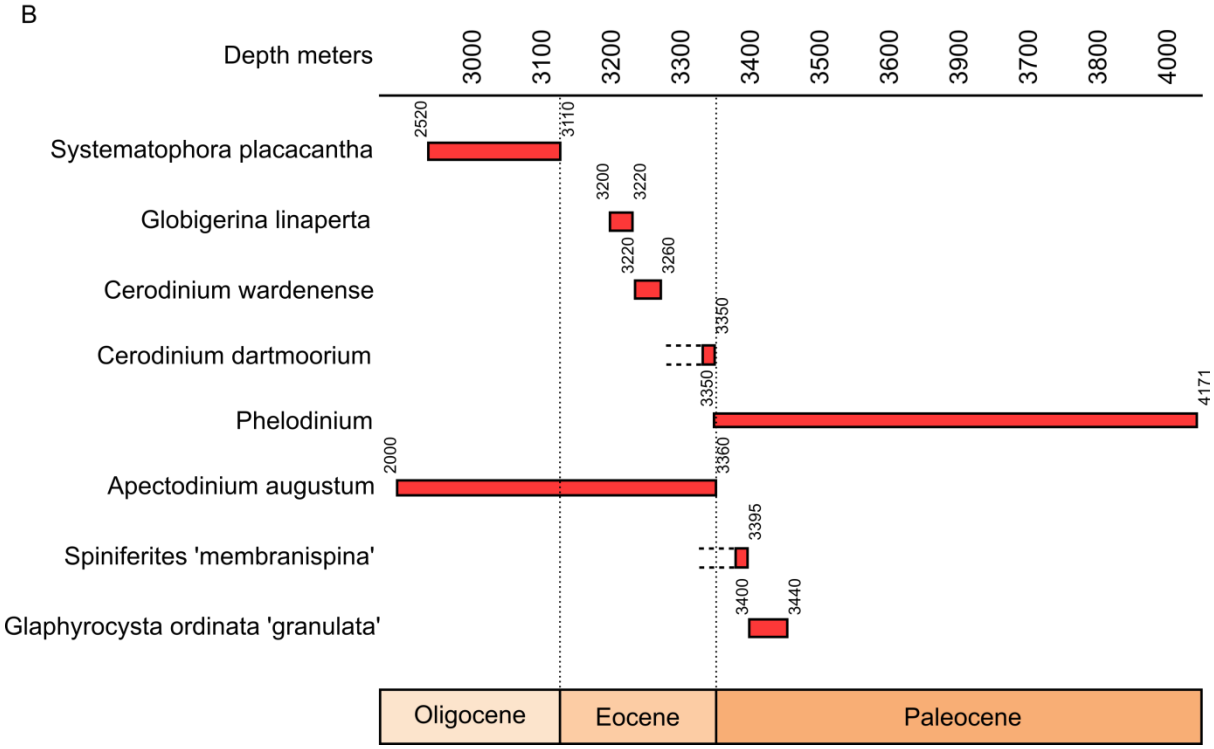

Figure 6.1: A) Table showing the key taxa distribution correlated with relative age and horizons interpreted at the HTVC interval. Palyno-zones correspond to taxa distribution at given time stages. Symbols in the left column act as notation for the seismic in Figure 6.2. Table is based on extracted from Appendix 1 in Planke et al., (2007), together with results from Jolly et al., (2005) and Mahdi, Ayress, (2006).
B) Taxa resolution of the key palynomorphs, based on first and last occurrence. The range of each bar is defined by palynomorphs counting and mapping done by Jolly et al., (2005), Mahdi and Ayress, (2006) and Planke et al., (2007).

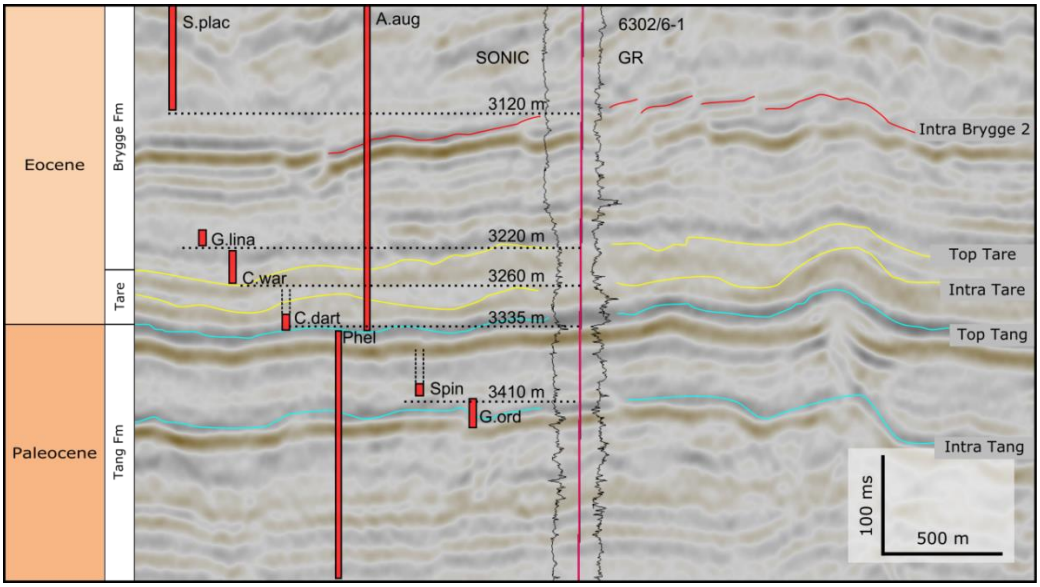

Figure 6.2: Seismic section and taxa resolution of the HTVC interval. Depth of seismic horizons is calibrated with check-shot data from well 6302/6-1. See Figure 6.7 for location in the overall seismic section.
Taxa resolution is based on mapping done by Jolly et al., (2005), Mahdi and Ayress (2006) and Planke et al., (2007).

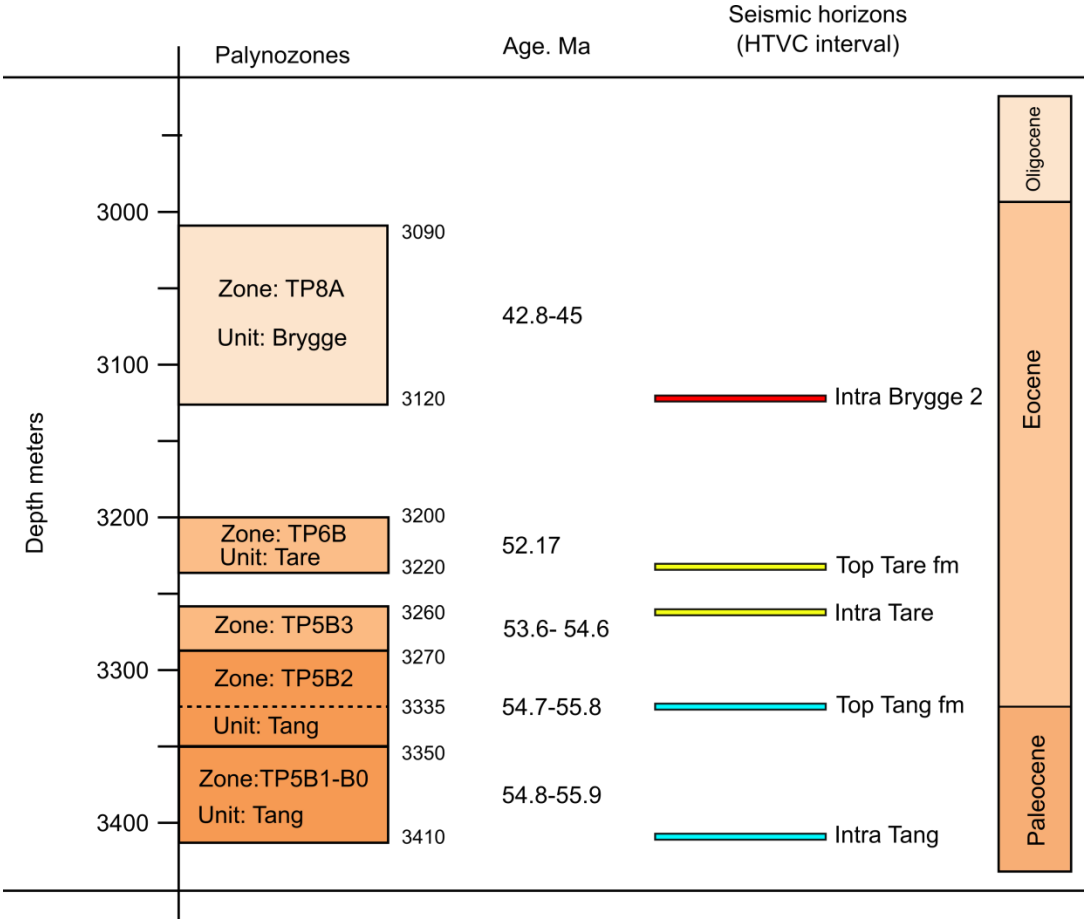

Figure 6.3: Overview of the Palynozones from the biostratigraphical summary in appendix 1 Planke et al., (2007). Depth is correlated to the check-shot log of well 6302/6-1, together with the main horizons at the HTVC interval. See Appendix A.3 for complete table.

6.2 Stratigraphy of the Møre Basin

To relate the stratigraphy at the area of interests the well 6302/6-1 has been tied for interpretation purpose. The well is cored in three sections at one certain interval, and logged continuous with an array of conventional electric and nuclear logging-tools.
The dataset used in this thesis study enables an excellent imaging of the Paleogene and Neogene (Cenozoic) successions. Sub-successions below 4.4-s TWT in the late Cretaceous provides limited imaging du to transition loss and impedance interference of the seismic signals.
In order to achieve a detailed description of the strata successions and relationship between the different boundaries, stratigraphy of well 6302/6-1, correlations with check-shots, and paleontological analysis of the sediments provided from drill-cuttings have been provided.

The stratigraphy interpretation will be divided into formation packages and described from the lowermost unit to percent. Correlation to previous work will be implemented, to ensure confident results regarding of the stratal succession.

At the study area the lowermost interpreted formation is the Springar formation, it consists of predominantly greyish-green claystones interbedded with stringers of carbonates and sandstone (Dalland et al., 1988). Limestone beds exceeding over ten meters in thickness interbedded with shale are encountered at an interval from 4076 – 4140 meters (Measured Depth - MD) (Figure 6.4 and 6.7). Such amounts of carbonate have not been established in this area before, and might lead to a slight revision on previous accepted depositional and geological history of the area (Helsem, 2006). The Springar Formation is overlain by the early Paleogene Tang Formation which is characterized by dark grey to brown claystone with minor sandstone and limestone (Dalland et al., 1988). The lithology of the lowermost part and transitional zone into the Springar formation is interpreted as the Danian derived sandstone reservoir in the Tulipan prospect. This sandstone section is typically 1-7 meters thick and interbedded with siltstone and claystone in the range between 3901 - 4000 (MD). The Tare Formation is defined by dark grey, green or brown claystones with some thin sandstone stringers which show a variable content of tuff. The tuff content is placed towards the basal section of the formation, with increasing volume at the lowermost Eocene stratigraphic column. The Tare Formation is overlain by the late Eocene to middle Miocene Brygge Formation, which is part of the Hordaland Group (Dalland et al., 1988; Deagan and Scull, 1977). The Brygge formation consists mainly of claystone, interbeds of sandstone and bio-siliceous ooze (Hjelstuen et al., 1997) . The two uppermost Formations in the study interval are the Lower Miocene to recent Nordland group which is sub divided into the Kai Formation, and the upper Pliocene Naust formation (Dalland et al., 1988). The Kai formation consists of alternating claystone, siltstone and sandstone with limestone interbedded, and the Naust formation mainly of claystone, siltstone.

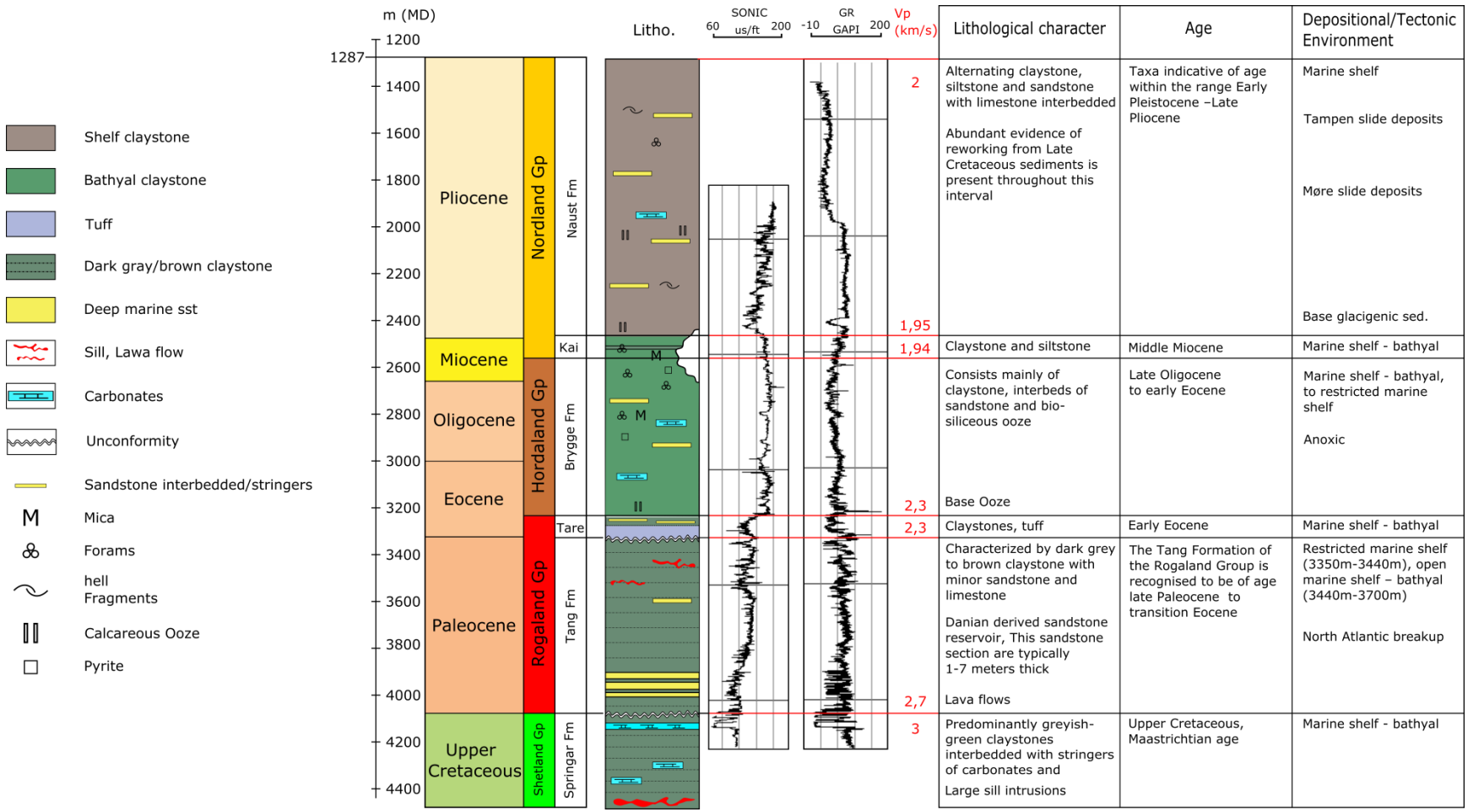

Figure 6.4: Lithological column based on the well log data provided. Lithology is correlated with sonic and gamma ray electrofacies. From left to right in figure: The first column is the total vertical depth from sea-level (subsea) in meters; the second is the stage of interpreted geological time; third is the lithological interpretation based on cuttings and geophysical response; forth column is the sonic, gamma and velocity logs respectively; fifth is an informational summary.

6.3 Well log electrofacies and velocity

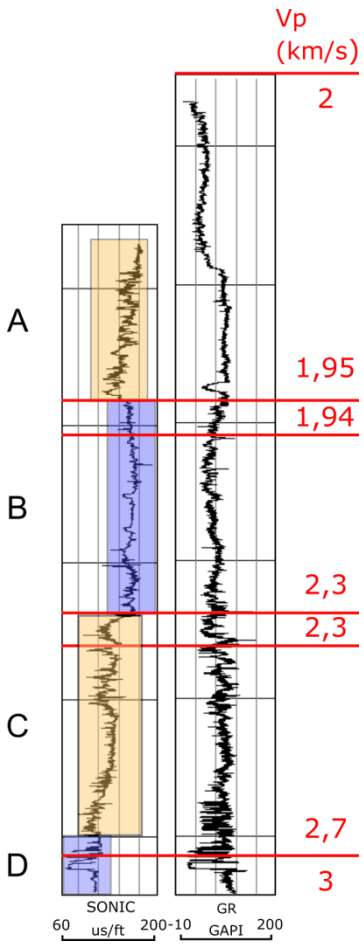

Figure 6.5: Log sections from well 6302/6-1. To the left: sonic log, to the right: gamma log. Interval velocities represented as red lines and numbers in the figure. Correlation to lithology, see Figure 6.4.

The results presented here are based upon the relationship between gamma ray and the transit time provided by the sonic log at key interval and transition zones (See Figure 6.4). The aim is to present a chemical and mechanical development of stratigraphical intervals which are regarded as important when studying the HTVC's in seismic sections. Knowledge of sediment trends provides essential relationships for basin modelling and analysis. The overall lithology through the well section is known, but there are still processes which are important to consider when interpreting the seismic section. The well log results are presented throughout the whole section, and divided from A-D as seen in Figure 6.5.

Relationship between gamma ray and p-wave velocity as a function of depth of well 6302/6-1 are presented within the context of the Pliocene to Upper Cretaceous seismic sequence. The silt and claystone sequence of the Naust formation (A in Figure 6.5) display increasing gamma and velocity (Vp) readings down to the transition Miocene and Kai formation. The section displays

some fluctuation with progressive burial depth. However, the overall trend is an increasing value in both gamma and sonic readings. This response is most likely due to the overpressure distribution and the rapid burial of the glaciogenic Naust sequence (Cicchino et al., 2015).

The upper Paleogene (Oligocene-Eocene) interval of the Brygge Formation (B in Figure 6.5) shows some fluctuation, but an overall continuous trend suggesting under compacted and relatively homogeneous claystone succession.

The lower Paleogene intervals (Eocene-Paleocene) of the Tare and Tang Formations (C in Figure 6.5) mainly comprise of clay and mudstone. This composition tends to reduce the permeability and result in an over pressured sequence (Cicchino et al., 2015). The likely cause of the lower Paleogene overpressure at the Møre Basin is disequilibrium compaction, resulting from the rapid sedimentation of the Naust Formation.

The lowermost unit D corresponds to the Upper Cretaceous sequence of the Springar Formation. The log section is defined by a strong shift, displaying the highest gamma ray and Velocity (Vp) readings in the entire log interval. These fluctuations correspond to the limestone beds exceeding ten meters in thickness.

6.4 Seismic structure of Tulipan prospect

This section will present the seismic interpretation done within the main project database at the central Møre Basin. The seismic interpretation undertaken in this study focuses on the interval between the seafloor-surface and down to 5s (TWT) (See Figure 6.6 and Figure 6.7). There are 14 fundamental horizons interpreted in order to obtain a detailed description of especially the Paleogene package which are of high interest when it comes to the general understanding and correlation with the sill- and vent-complex distribution. The HTVC interval has higher requirements in terms of geometrical mapping, and is reflected in the seismic interpretation. Only a few reflectors at the overburden have been mapped out in detail, whiles a more thorough interpretation was conducted at the interval of the HTVC.

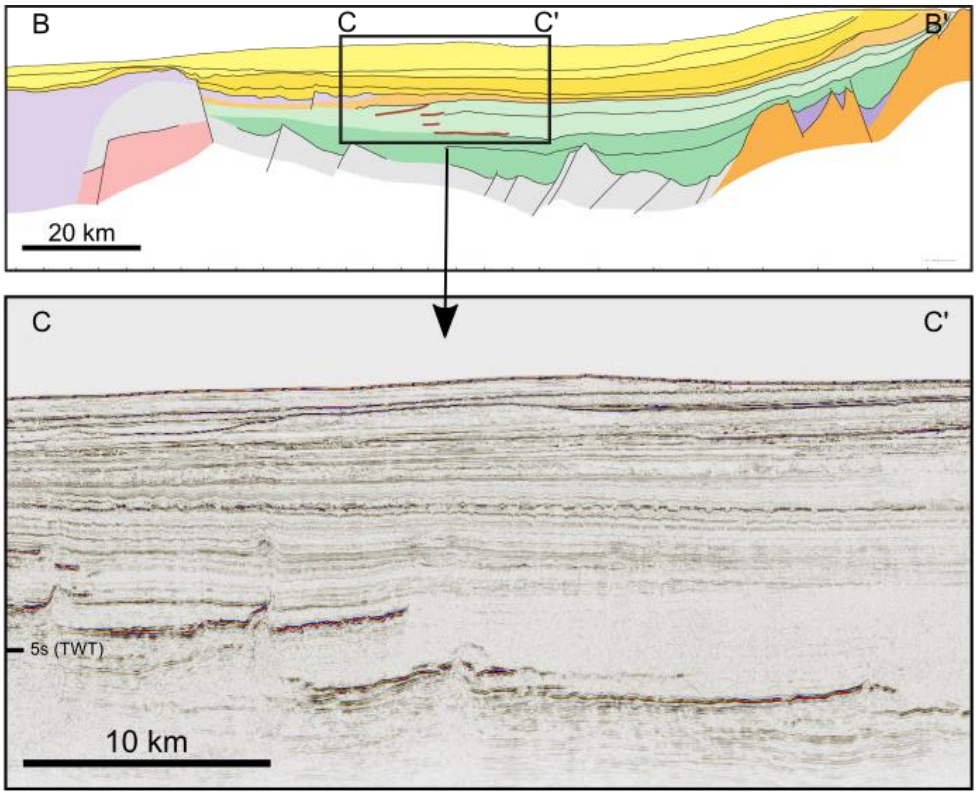

Figure 6.6: Time-migrated seismic sections from the PL25 seismic survey (Møre Basin). See Chapter 2, Figure 2.1 for Geoseismic line location B-B' and legend.

Previous interpretations of seismic data done at the Møre Basin is available, but very little is directed at this specific study area. However correlation to the geological setting and structural evolution of the mid-Norwegian Margin (Chapter 2 geological framework) provide useful information when proceeding to understand the local geological succession and context. The technique of seismic interpretation in this thesis is based on dividing the study area into well-defined and established horizon boundaries, and then correlates these units to borehole data.

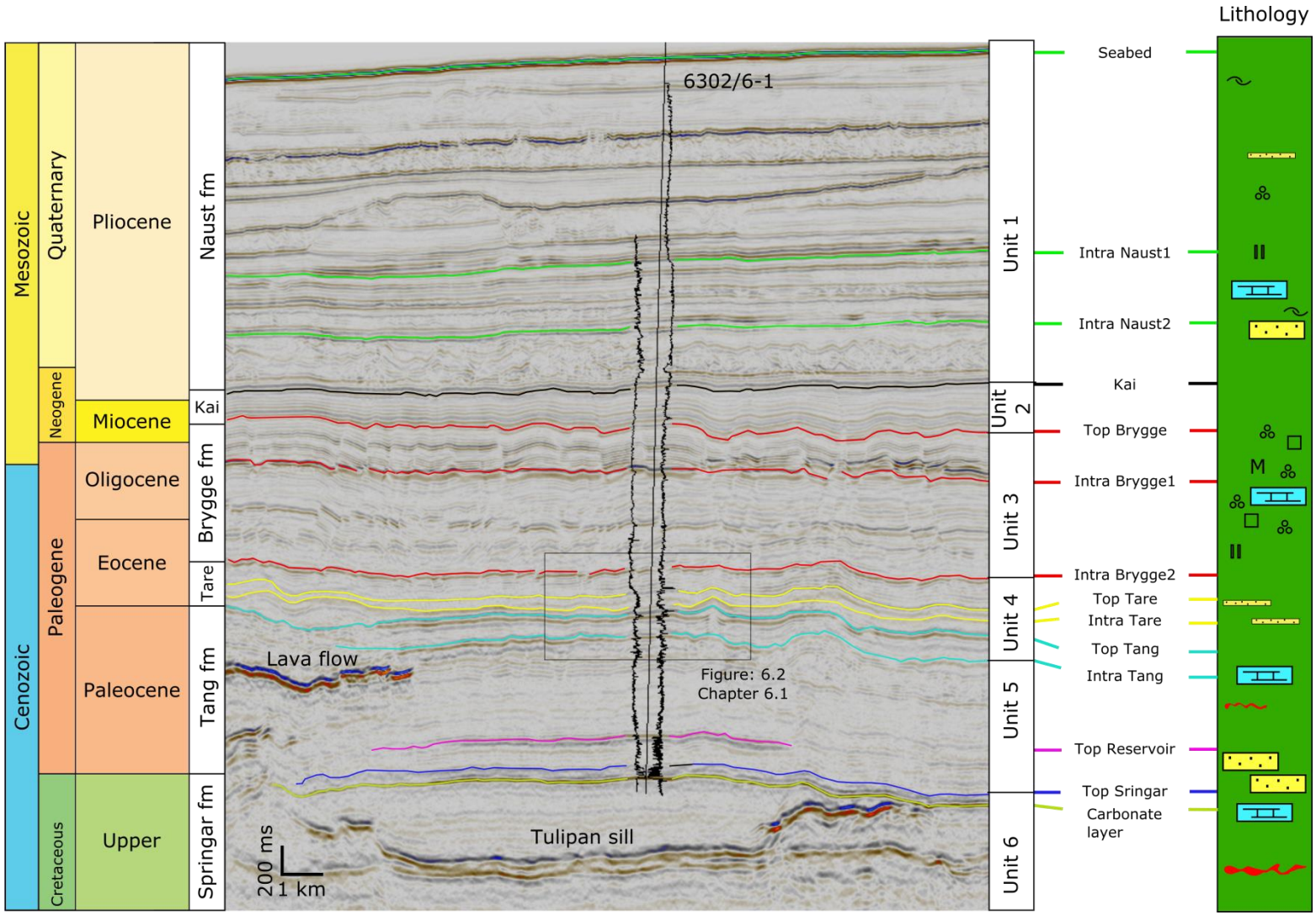

Figure 6.7: Illustration of the key interpreted horizons within the seismic dataset of this thesis. A simplified stratigraphic column of main lithology is given in the left of the figure. Colour scheme of horizons corresponds to surfaces within the same formation. Well 6302/6-1 with sonic log to the right and gamma to the left. Unit 1-6 in the left of the figure relates to description done of the seismic characteristics between main horizons.

6.4.1 Main horizons and surfaces in the Tulipan prospect

Interpretation of prominent reflectors down to transition Eocene-Oligocene was relatively straight forward in terms of horizon picking. Borehole data provided show decisive lithological changes that fit well with the strong continuous reflectors throughout the seismic cube. Figure 6.7 illustrates the interpretation done of what is regarded as the key horizons within the seismic cube. The stratigraphic column in Figure 6.4 shows a depth projection of the different geological formations that makes up the range of the survey section. The predicted stratigraphic column is based on borehole data, described in the stratigraphy chapter. The seismic dataset used in this thesis study enables an excellent imaging of the Paleogene and Neogene (Cenozoic) successions. Sub-successions below 4.4s (TWT) in the Upper Cretaceous provides limited imaging du to transition loss and impedance interference of the seismic signals.
In the following section, the interpretation will be presented as sequences from top (seabed) to bottom (carbonate layer).

The uppermost horizon is interpreted as the **seabed** surface. The horizon is defined as laterally consistent, without any seismic discontinuity. There are no major patterns defined in the amplitude map, and the horizon is overall flat and structureless.

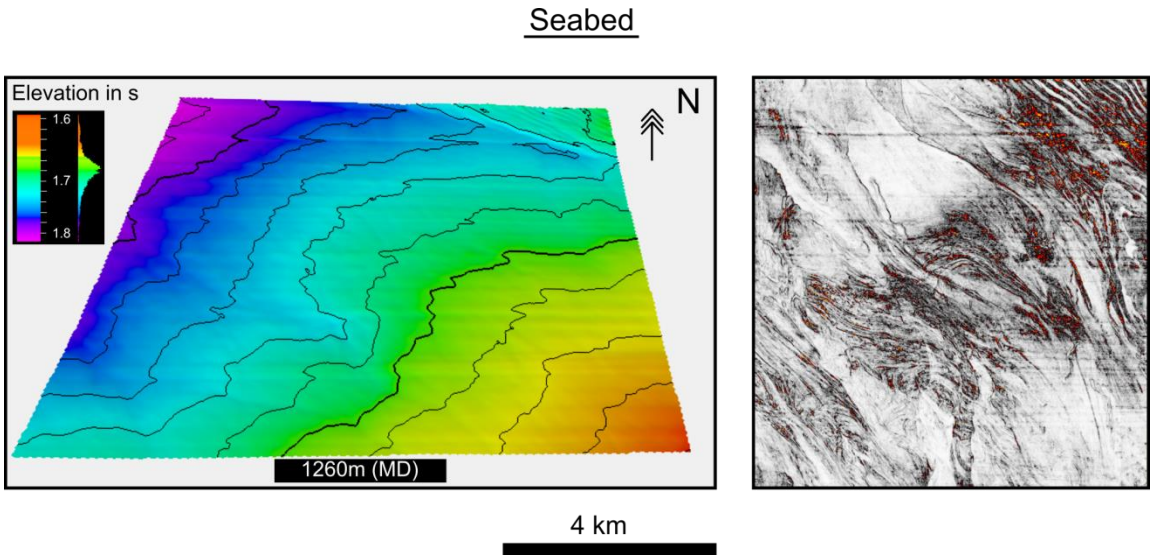

Figure 6.8: The uppermost 3D interpreted seafloor surface. The horizon is shown in elevation time at the right, and variance time-slice to the left. Purple colour is lower I the stratigraphy then the orange. This Implies that a larger elevation number in the figure corresponds to a deeper section on the surface.

Reflector below the seabed represents the **Intra Naust 1** reflector. The high reflection of the Intra Naust 1 has a gently dipping incline mimicking the seafloor, but no significant decrease in amplitude down-slope. The next strong negative reflection **Intra Naust 2** is interpreted as an overall continuous, strong and smooth amplitude event at the lower Pliocene interval. The reflection amplitude at the central parts of the horizon will at certain intervals be exposed to

abrupt decreases in amplitude strength, and thereby undergo manual picking in the discontinuity volumes. The horizon also display some dispersed topographic reliefs throughout the amplitude plane, in what seems to be a response to the tectonically derived structures in the basal lithology.

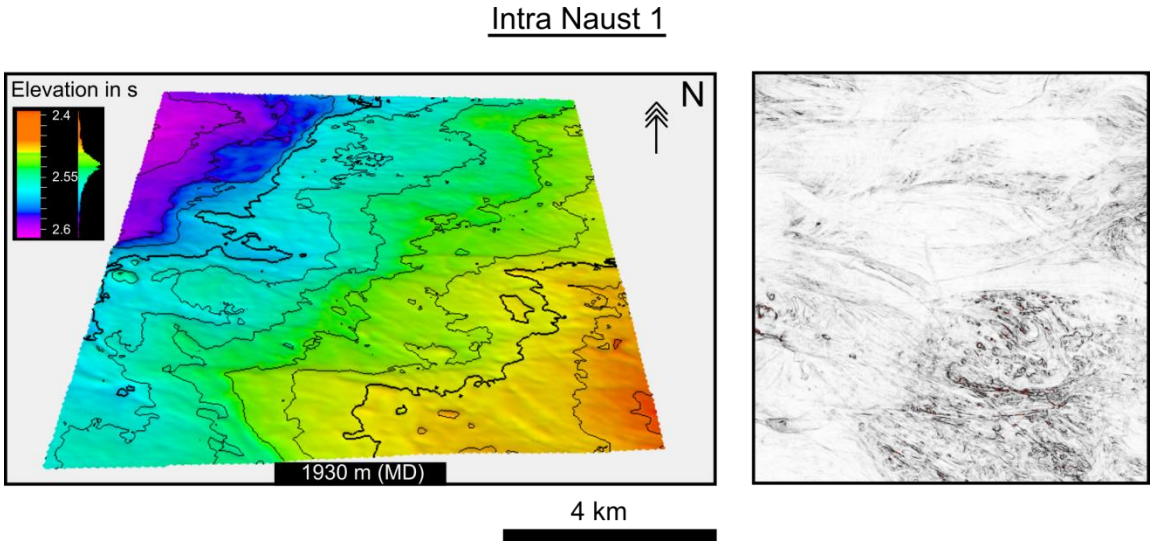

Figure 6.9: 3D interpreted Intra Naust 1 surface. The horizon is shown in elevation time at the right, and variance time-slice to the left. Total topographic elevation difference is 0.1 s.

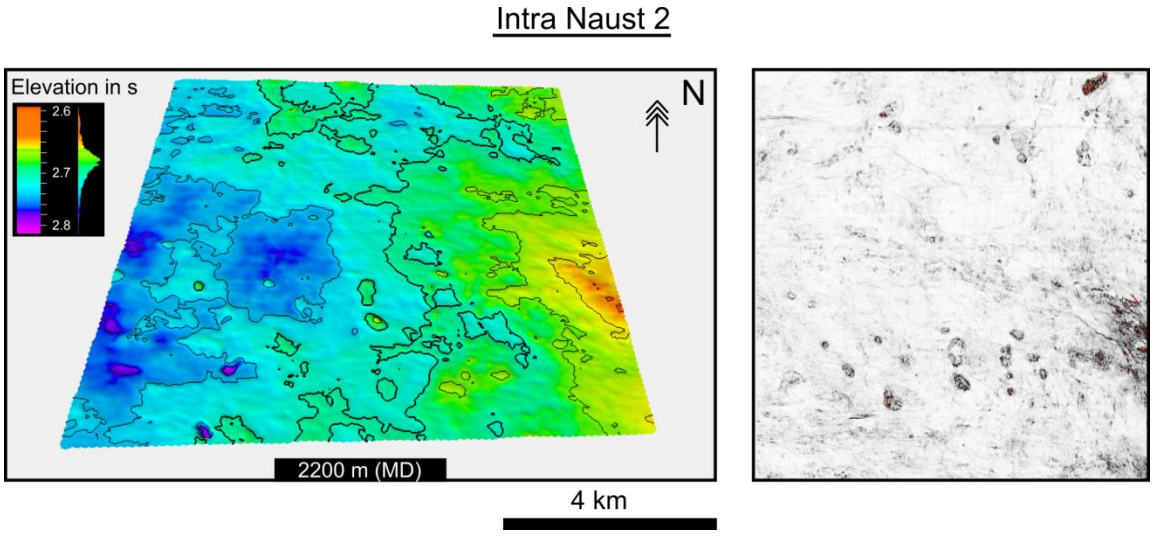

Figure 6.10: 3D interpreted Intra Naust 2 surface. The horizon is shown in elevation time at the right, and variance time-slice to the left. Total topographic elevation difference is 0.2 s.

The Miocene-Oligocene interval containing the three reflectors of the **Brygge Formation** (**Top, intra 1 and intra 2**) shows an internal reflection pattern that is characterized by a well-developed system of structural highs, major deep-seated faults and flexures. The fault pattern are classified as intraformational polygonal faults, that develop because of early burial and

dewatering of fine grained mudstones (Cartwright, 1994). The faults exhibit an uncommonly steep displacement gradient just above the Eocene-Oligocene boundary.

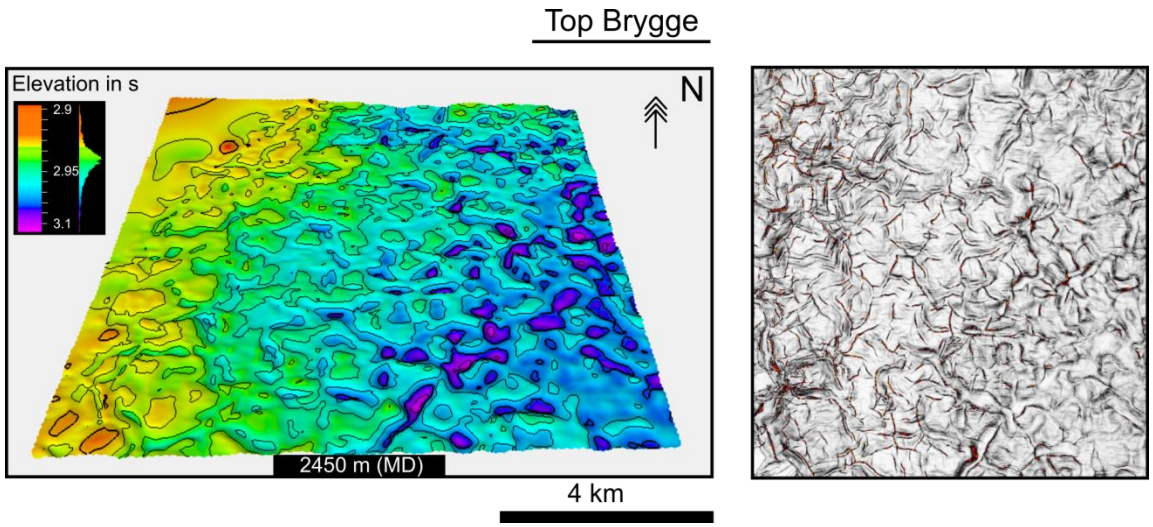

Figure 6.11: 3D interpreted Top Bygge. The horizon is shown in elevation time at the right, and variance time-slice to the left. Total topographic elevation difference is 0.2 s. Note the polygonal fault pattern in the variance slice.

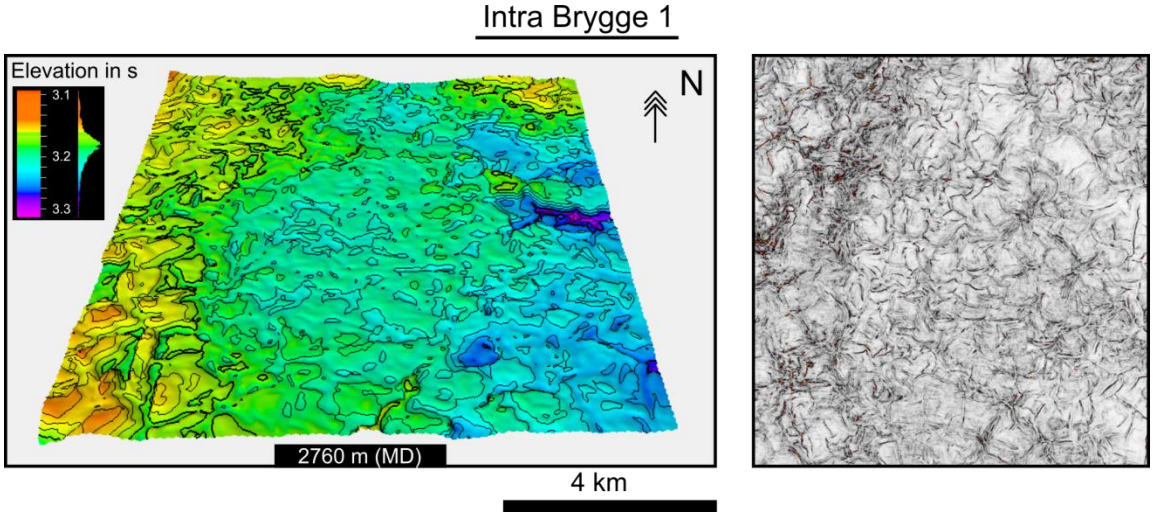

Figure 6.12: 3D interpreted Intra Brygge 1. The horizon is shown in elevation time at the right, and variance time-slice to the left. Total topographic elevation difference is 0.2 s. Note how the polygonal fault pattern develops through time.

The lowermost horizon of the Intra Brygge 2 is relatively undisturbed compared to the two uppermost horizons, although the faulting pattern prograde downward. The reflectors in the lowermost part have a tendency to lose their character, and transcend into more transparent zones.

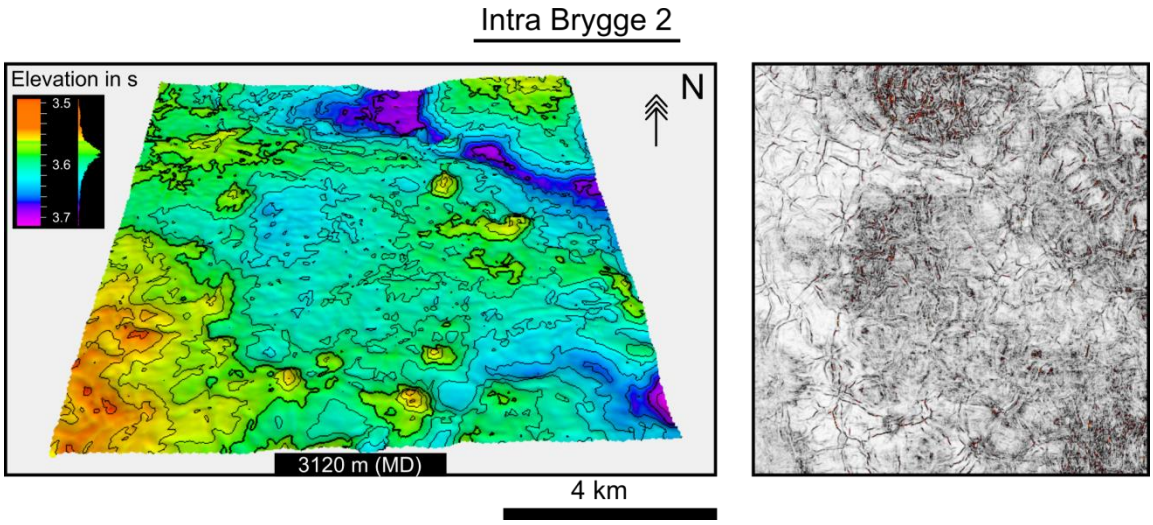

Figure 6.13: 3D interpreted Intra Brygge 2. The horizon is shown in elevation time at the right, and variance time-slice to the left. Total topographic elevation difference is 0.2 s. Note the polygonal fault pattern in the variance slice.

The **Top Tare horizon** is a smooth, high amplitude reflection defined by the interpretation level of the identified HTVC's. The horizon intersects at the depth of intra Tare level, and displays gradually shallowing to the west. The reflections at this interval are relatively continuous, except at the intersection towards the uppermost part of the HTVC structures. This area is often seen as discontinuous reflectors which terminate upwards at the mounded structures.
The underlying **Intra Tare** is interpreted and considered in the same way as the Top Tare reflection with no major differences in terms of seismic behaviour.

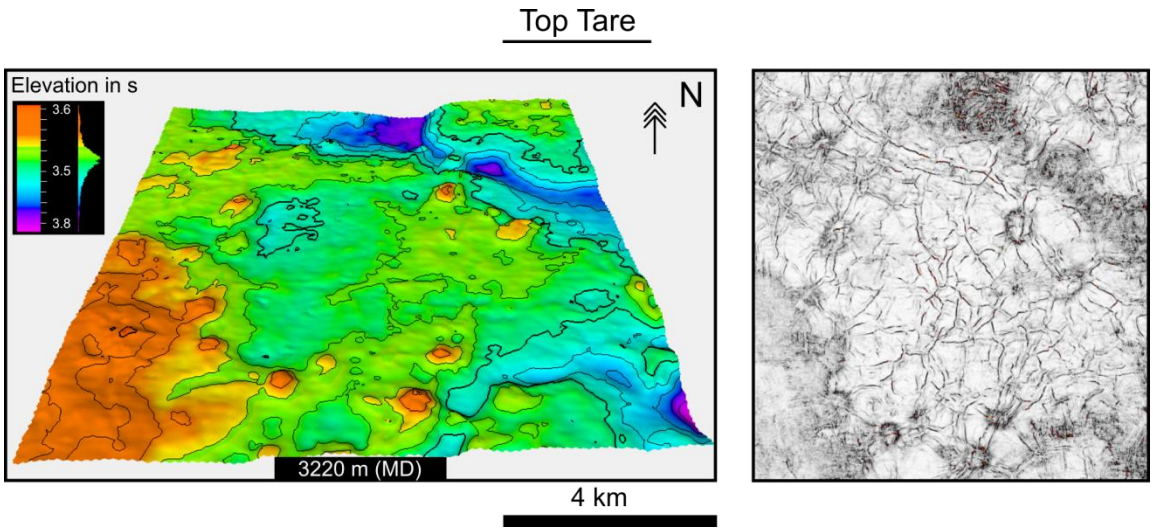

Figure 6.14: 3D interpreted Top Tare. The horizon is shown in elevation time at the right, and variance time-slice to the left. Total topographic elevation difference is 0.2 s. Note the mounded structures in the middle of the surface, and the radial faults at the rounded structures in the variance section.

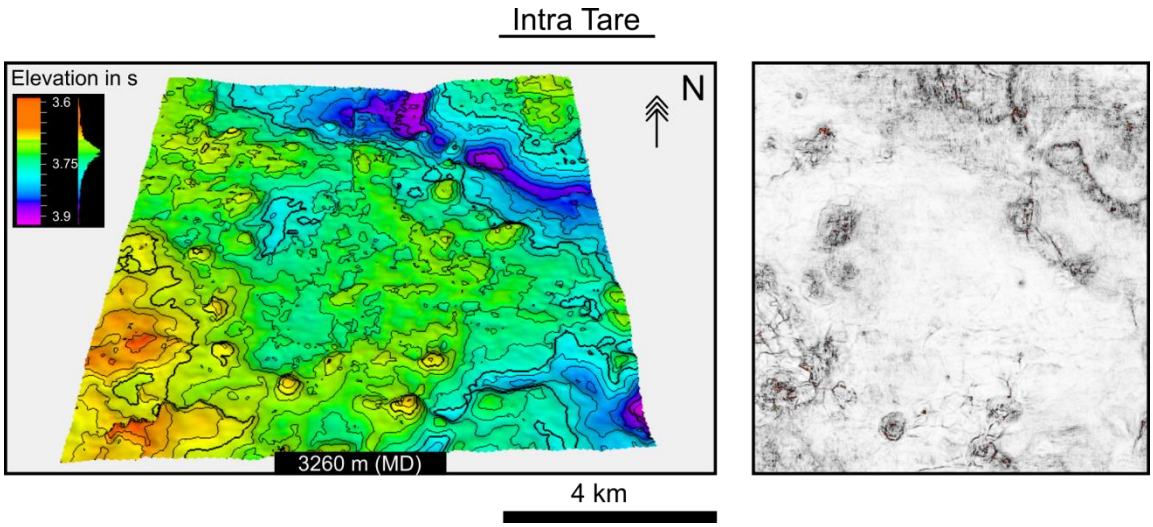

Figure 6.15: 3D interpreted Intra Tare. The horizon is shown in elevation time at the right, and variance time-slice to the left. Total topographic elevation difference is 0.3 s.

The horizon of **Top Tang** defines the deeper stratigraphy of the dome shaped vent complexes interval. These domes are seen in the seismic as down lapping structures on the paleosurface. However, correlation of the horizon itself throughout the cube is difficult, due to local discontinuity and partly disrupted reflections. These disruptions are caused by high-amplitude reflections, most likely representing basaltic lava flows emplaced on the seafloor during the time of HTVC formation. The boundary of this specific horizon is defined as the Tang level, and transition zone between Paleocene-Eocene.

Intra Tang reflection is partly disrupted by piercing HTVC's conduit zones. This leads to discontinuity of the reflector and horizon correlation throughout the cube.

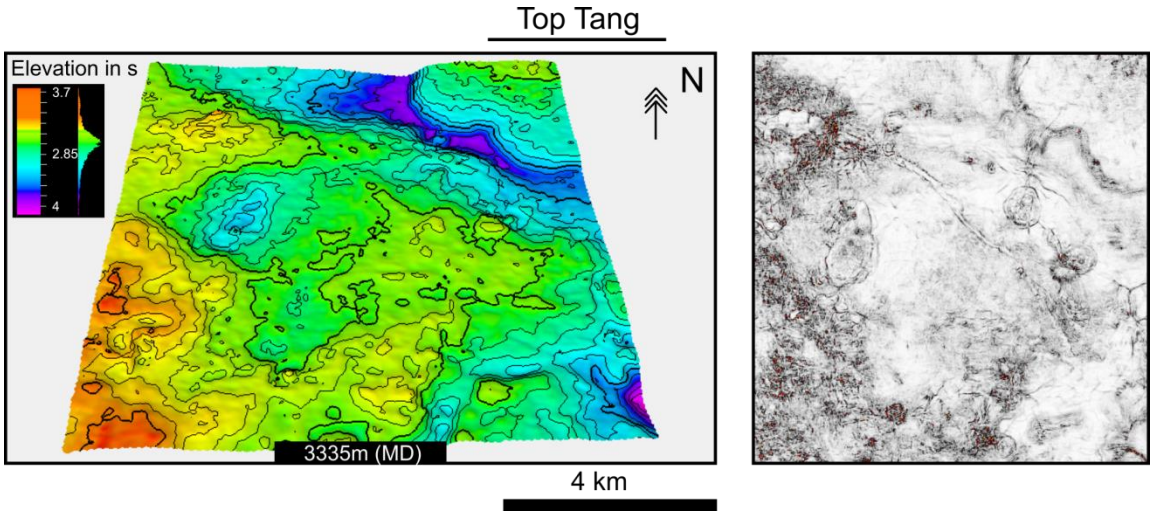

Figure 6.16: 3D interpreted Top Tang. The horizon is shown in elevation time at the right, and variance time-slice to the left. Total topographic elevation difference is 0.3 s. In the variance slice it is possible to see traces of the upper dome features of the HTVC's, and the radial faults on the paleosurface.

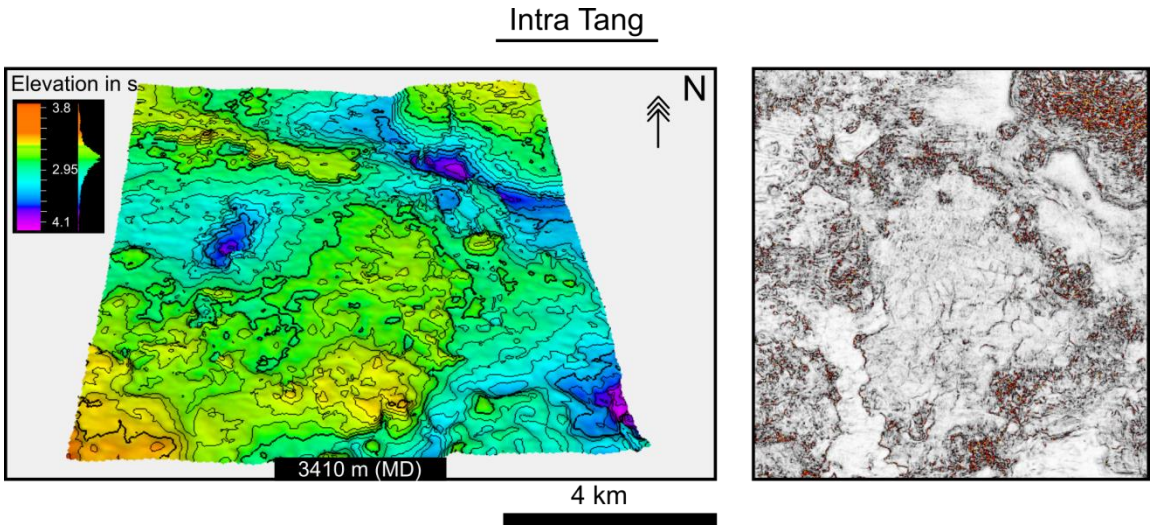

Figure 6.17: 3D interpreted Intra Tang. The horizon is shown in elevation time at the right, and variance time-slice to the left. Total topographic elevation difference is 0.2 s.

The horizon overlaying the Danian sandstone reservoir, named **Top Reservoir** is a smooth, high amplitude event located in the center part of the main study area. The horizon forms a well-defined dome with four-way dip closure. At the uppermost part of this sealing dome, high amplitudes revile bright spots interpreted to be gas-charged sand. The outer edge of the horizon is masked by the overlaying lava flows from the Top Tang horizon. This causes disruptions in the reflection and thereby gaps in the horizon images.

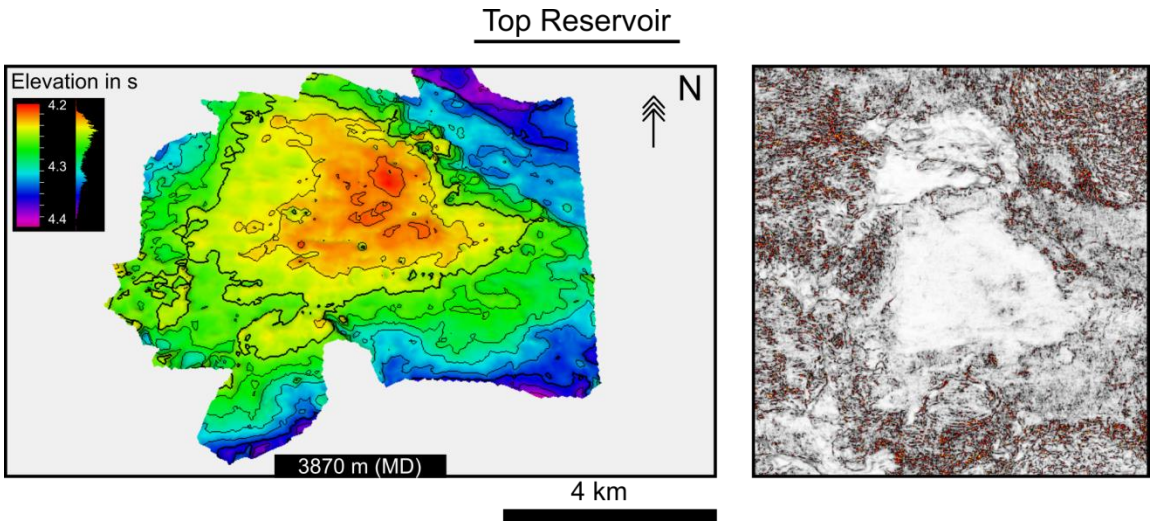

Figure 6.18: 3D interpreted Top Reservoir. The horizon is shown in elevation time at the right, and variance time-slice to the left. Total topographic elevation difference is 0.2 s. The outer edge of the horizon is masked by the overlaying lava flows from the Top Tang horizon, making the horizon somewhat incomplete. Note the white outlined structure in the variance surface, this correlates to the four-way dip closure of the reservoir fold.

Base of the Danian reservoir is bound by the underlying **Top Springar horizon**. Like the Top Reservoir, the Springar horizon is difficult to interpret throughout the 3D cube due to the overlaying lava flows.

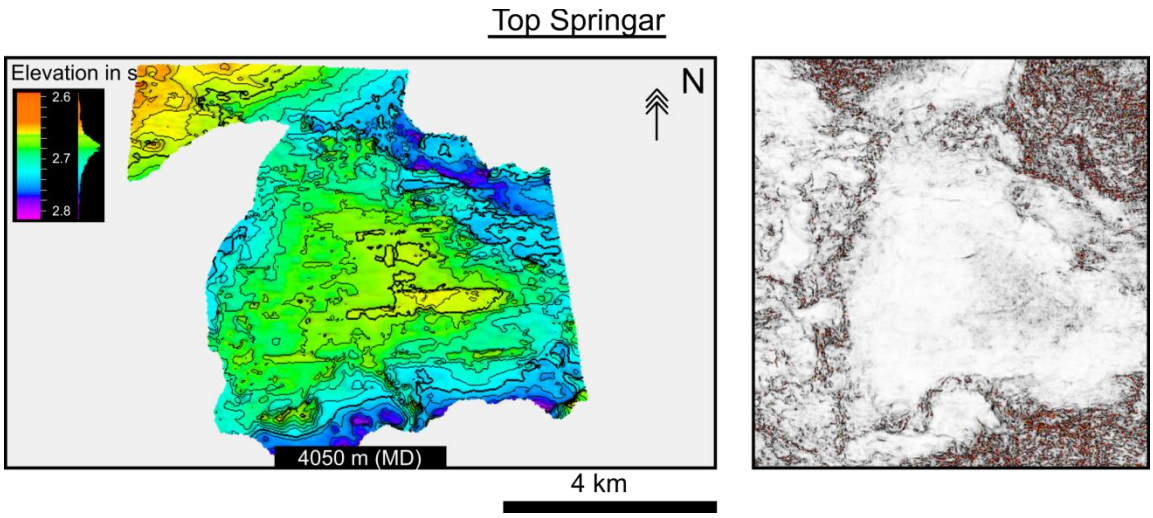

Figure 6.19: 3D interpreted Intra Tang. The horizon is shown in elevation time at the right, and variance time-slice to the left. Total topographic elevation difference is 0.2 s.

The lowermost section of the horizon mapping is marked by the strong character reflector corresponding to the **carbonate layer**. This smooth, high-amplitude event is possible to correlate over a large part of study interval, with some exceptions where the horizon is masked by the high amplitude regions of igneous intrusions.

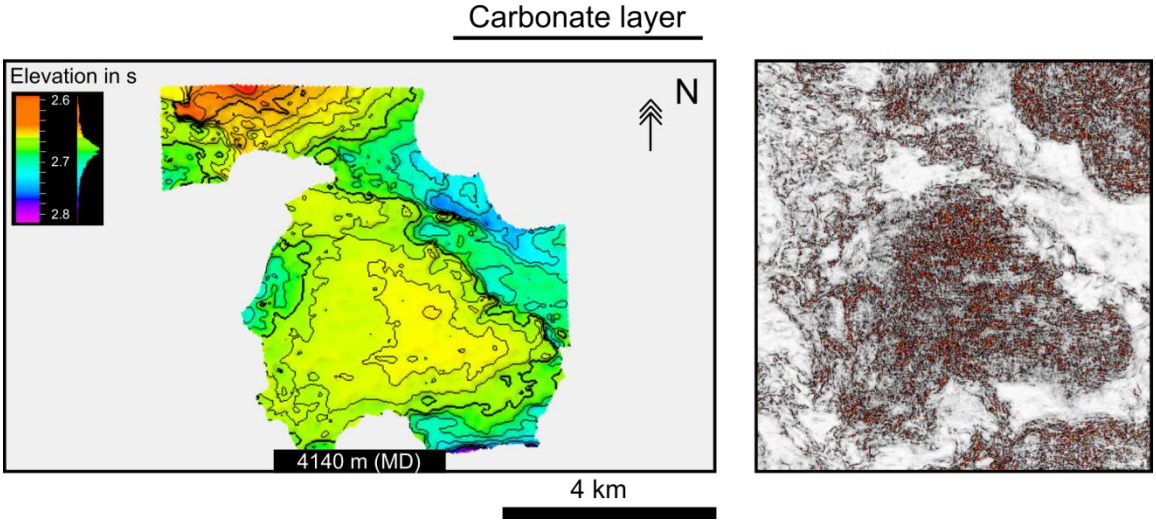

Figure 6.20: 3D interpreted Carbonate layer. The horizon is shown in elevation time at the right, and variance time-slice to the left. Total topographic elevation difference is 0.2 s.

6.4.2 Unit description of seismic between the key horizons

Overlaying the structureless Cretaceous sequence, the sedimentary infill of the mid-Norwegian Margin consists of a set of acoustic formations defined by a more or less layered deposition. Six stratigraphic units (units 1 to 6) have been chosen, due to their seismic characteristics, and main unconformities which are recognisable throughout most of the studied seismic section. These sections can be viewed at the left side of Figure 6.7.

Unit 1(Pliocene to recent)

Unit 1 is observed to display parallel seismic lines, with a low gradient offset towards the NW, in time and depth respectively. Up to four individual sediment packages in the upper part of the unit has been identified. Typical for these structures are the transparent and featureless character corresponding to the thick slide deposits in the basin (more than 1 sec TWT). The top base of the sequence is defined by a high amplitude reflection (see Figure 6.7), which is the topmost boundary "seabed". Smooth well defined and high amplitude reflection defines this level of the data set, and is continuous throughout the whole cube. The bottom of unit one is marked by a strong character reflector, corresponding to the top of the Kai formation.

Unit 2 (Miocene)

Unit 2 is a widespread sequence that exhibits rather variable seismic features throughout the study interval. A strong character high amplitude reflection (Top Brygge) corresponds to the lowermost boundary of the unit. The internal reflection pattern of the sequence consists of chaotic but continuous high amplitude reflectors, originating due to the surface irregularities and diffraction patterns of the underlying lithological unit (Unit 3). The alternating claystone, siltstone and sandstone with interbedded limestone, as interpreted from the well logs are thought responsible for the reflection features internally in the unit. The unit comprises of a widespread sequence throughout the cube, which are overlaying unit 3 and are displaying uniform and continuous deposition against the faulted lowermost unit.

Unit 3 (Eocene to Oligocene)

The uppermost part of unit 3 shows an internal reflection pattern that is characterized by a well-developed system of structural highs, major deep-seated faults and flexures. These structures are seen in the part of the seismic data corresponding to a depth of approximately 2600 meters (3,1s TWT), and downwards to the opal CT transition zone.

The fault patterns are classified as intraformational polygonal faults. The faults exhibit an uncommonly steep displacement gradient just above the Eocene-Oligocene boundary. The lowermost interval of the unit is relatively undisturbed compared to the upper sub unit, although the faulting pattern prograde downward. The reflectors in the lowermost part have a tendency to

lose their character, and transcend into more transparent zones. Lithology recognised at the well is mainly siltstone and sandstone with alternating claystone interbeds.

Unit 4 (Paleocene to Eocene)

Unit 4 defines the transition zone between Eocene and Paleocene. The seismic section can be divided into two sequences displaying variable features across the study area. The lowermost sub unit correspond to structures characterized by discontinuous, low amplitude reflections resembling the chimney/conduit zones of the HTVC's. The overburden and uppermost sub unit contains a stack of high-amplitude events, together with the discontinuous reflectors which terminates upwards at the mounded structures of the HTVC's.

Well data are consistent with the seismic facies observed, and indicate that the unit is made up of by claystones with some thin sandstone stringers. Log-facies analysis indicates a rather significant drop in velocity at the descending sub interval, which correlates to the deduced and interrupted seismicity of the reflectors.

Unit 5 (Paleocene)

The development of the discontinuous and low amplitude reflections at the unit above constitutes the upper most part of this seismic section. Some strong internal reflection patterns within the unit show a high amplitude character, visible at a lateral continuity. These are high impedance structures relative to the surroundings, and are related to the intrusive igneous-provinces in the sedimentary strata. These igneous intrusions produce irregularities and chaotic reflection patterns above and underneath the structure. Sills in this interval have been identified as high-amplitude reflections, with local transgressive segments that tend to pinch out laterally.

There are no main lithological differences between unit 5 and previous unit, and well data show consistent distribution of claystones with some thin sandstone interbeds.

Unit 6 (Upper Cretaceous to Paleocene)

The lowermost unit 6 is characterized by the reservoir horizon defined by a smooth, high amplitude event within the main study area. The reservoir corresponds to the Danian sandstone deposits, penetrated by the well at a depth of approximately 3900 meters. The reservoir forms a well-defined dome, with a four way seal visible in the 3D interpretation (See Figure 6.18). The reservoir unit attains a thickness upwards of 2 seconds (TWT), and amplitude of the dome reflector of 0.1 second. The seismic interpretation done at the reservoir reveals high amplitudes and bright reflectors within the dome, interpreted as a gas-enhanced future (Planke et al., 2007). The post well data suggest that the actual extent is much smaller than the proposed bright-spot amplitude anomaly (Helsem, 2006).

Within the study area, parts of the reservoir reflection are masked by high contrast lavas units to the north, west and east. Some disruptions also occur due to HTVC's and sill reflections to the

west. However, the reservoir horizon can be correlated with fairly good certainty within the 3D cube.

The bottom of the unit is marked by strong character reflectors that correspond to the carbonate horizon. This smooth, high-amplitude event is possible to correlate over the entire study interval, with only a few exceptions where the horizon is masked by the high amplitude regions of the (unit 5) igneous intrusions. The horizon were initially interpreted as the base tertiary unconformity, but well data from drilling show that the horizon represents several thick limestone/chalk layers of a latest Cretaceous age (Planke et al., 2007).

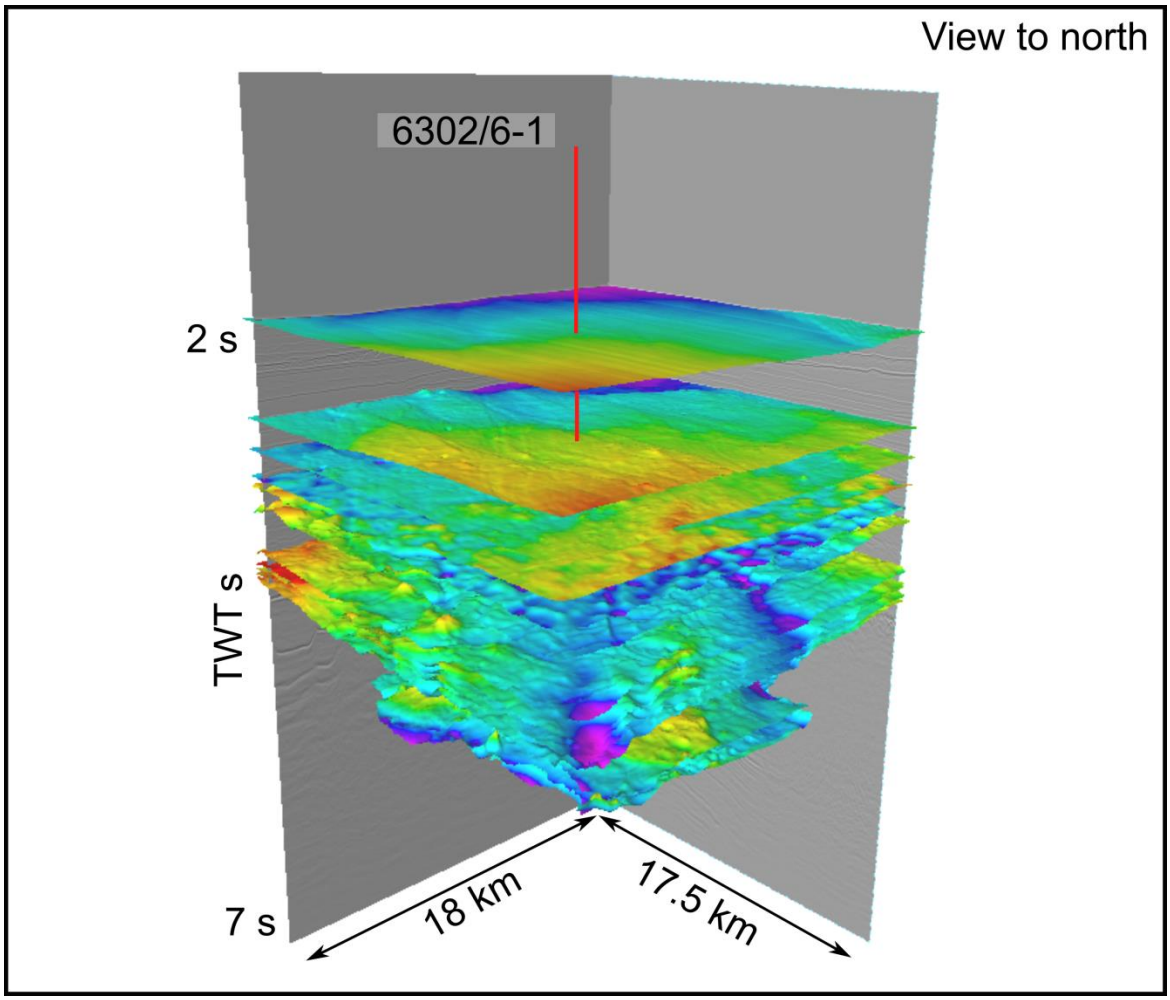

Figure 6.21: Seismic section showing the context and relation of the 14 horizons mapped out in the cropped 3D cube.

6.5 Hydrothermal vent complexes and Seismic Characteristics

In this study, 13 individual hydrothermal vent complexes have been recognized and analysed during the course of seismic interpretation. The structures have been mapped out on key horizons, defined by the Paleocene-Eocene transition interval. 3D horizons, horizons-dip and -amplitude maps together with seismic cross-sections have been produced allowing for detailed morphological studies of the different vent complex structures. The classification of the structures is based on aspect ratio, stratigraphic level of the vent systems, the degree of amplitude anomalies around the structures, and the stratigraphic context. This chapter aims to provide a new understanding of the HTVC based upon the seismic character, morphologies and the underlying conduit zones, together with the relationship of underlying sills and the quantitative size and position of the HTVC.

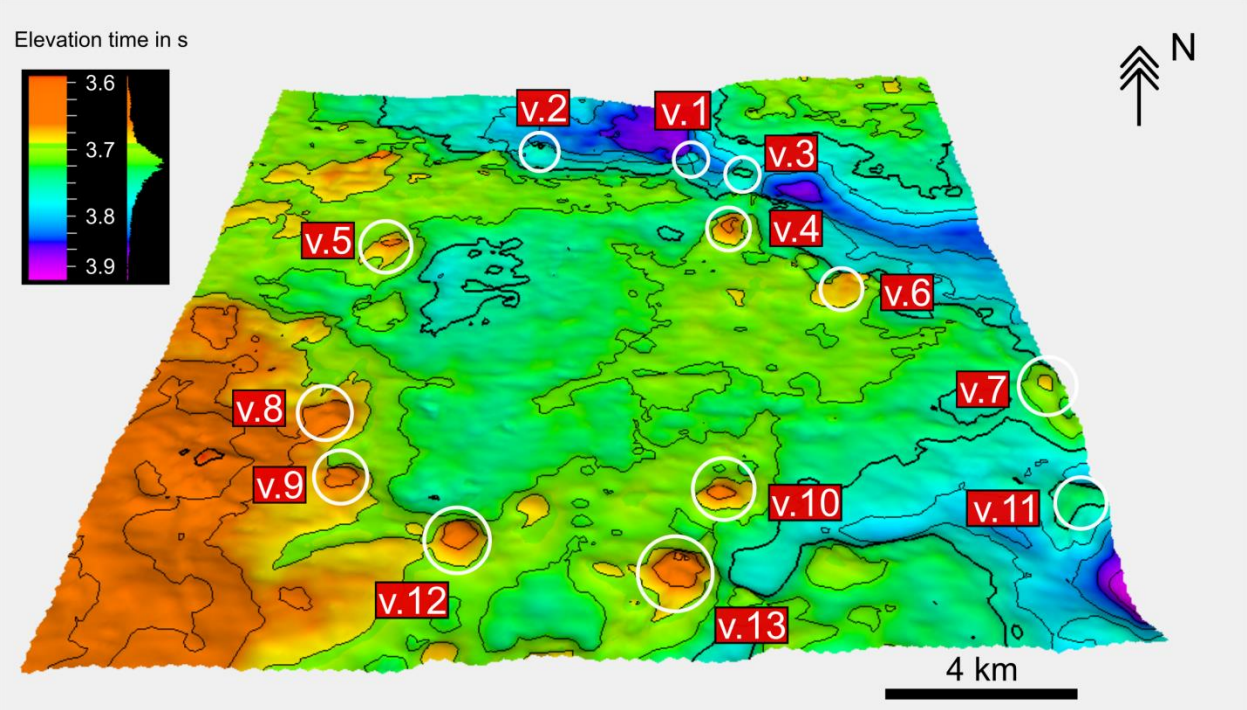

Figure 6.22: Time-structure map of the Top Tare (~ Intra Eocene) horizon. Colour change from purple to orange indicates a difference of 0.2 s (TWT). White circles indicate position of upper part and dome structure of the HTVC, corresponding labelling from v.1 to v.13. All the mapped HTVC's can be viewed in appendix A.1.

6.5.1 Seismic characteristics of the HTVC

HTVC are observed as relatively small mounding features on the Top Tare (~ Intra Eocene) horizon. They typically display sizes ranging from 600-2000 m wide, and 70-120 m height with an elevated aspect ratio of 0.08s (TWT). These structures are exclusively observed in the transition zone of Paleocene-Eocene, and lower part of the intra Eocene reflection interval.

This interval is defined by a relatively abrupt decline in gamma and sonic response from the well 6302/6-1 (See Figure 6.4). In the stratigraphic completion-log the interval is described as claystones with thin sandstone stringers and a variable content of tuff. The values inflicted in this interval could suggest a transition to more under-compacted and homogeneous clay-sandstone composure beneath the Tuff deposits. The reflection patterns at the transition between Paleocene-Eocene and the lowermost Eocene interval, is characterized by partly disrupted sequences at the mounded highs. These mounded high reflectors are often wavy and discontinuous in local places (See Figure 6.23 B). An important observation is that these Top Tare mounded features do not show any observations regarding reflection onlap or truncation from the overlaying sediments. The first 10-70 m of the succession above is more or less undisturbed and uniform in thickness. Above this sequence, onlap and thickness variation of the strata can be observed.

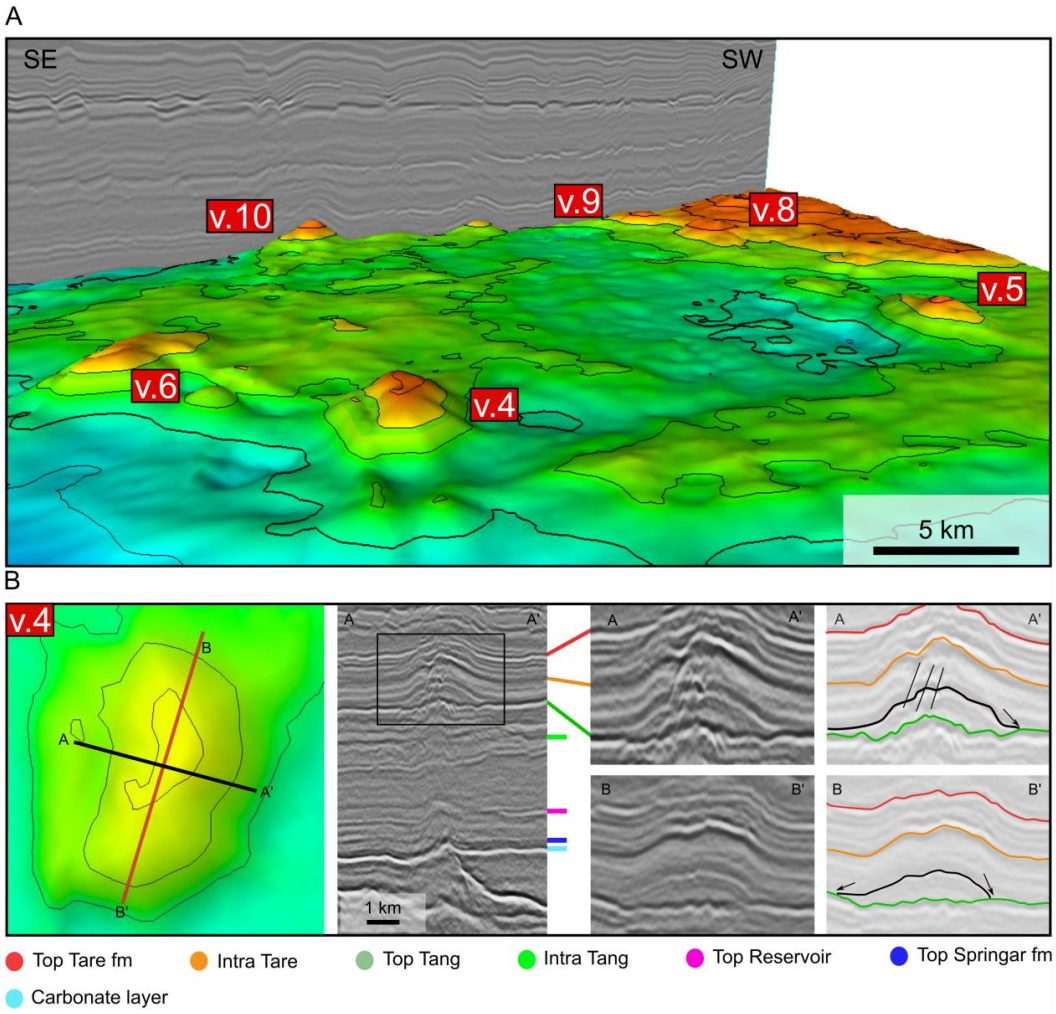

Figure 6.23: A) Perspective view of the intra (lower) Eocene horizon Top Tare, and a seismic crossline-section of the representative mounded structures of the HTVC's. B) Seismic section showing the HTVC v.4. Note that the structure is restricted between the intervals of Paleocene-Eocene (between sill tip at Carbonate layer and mound at Top Tare).

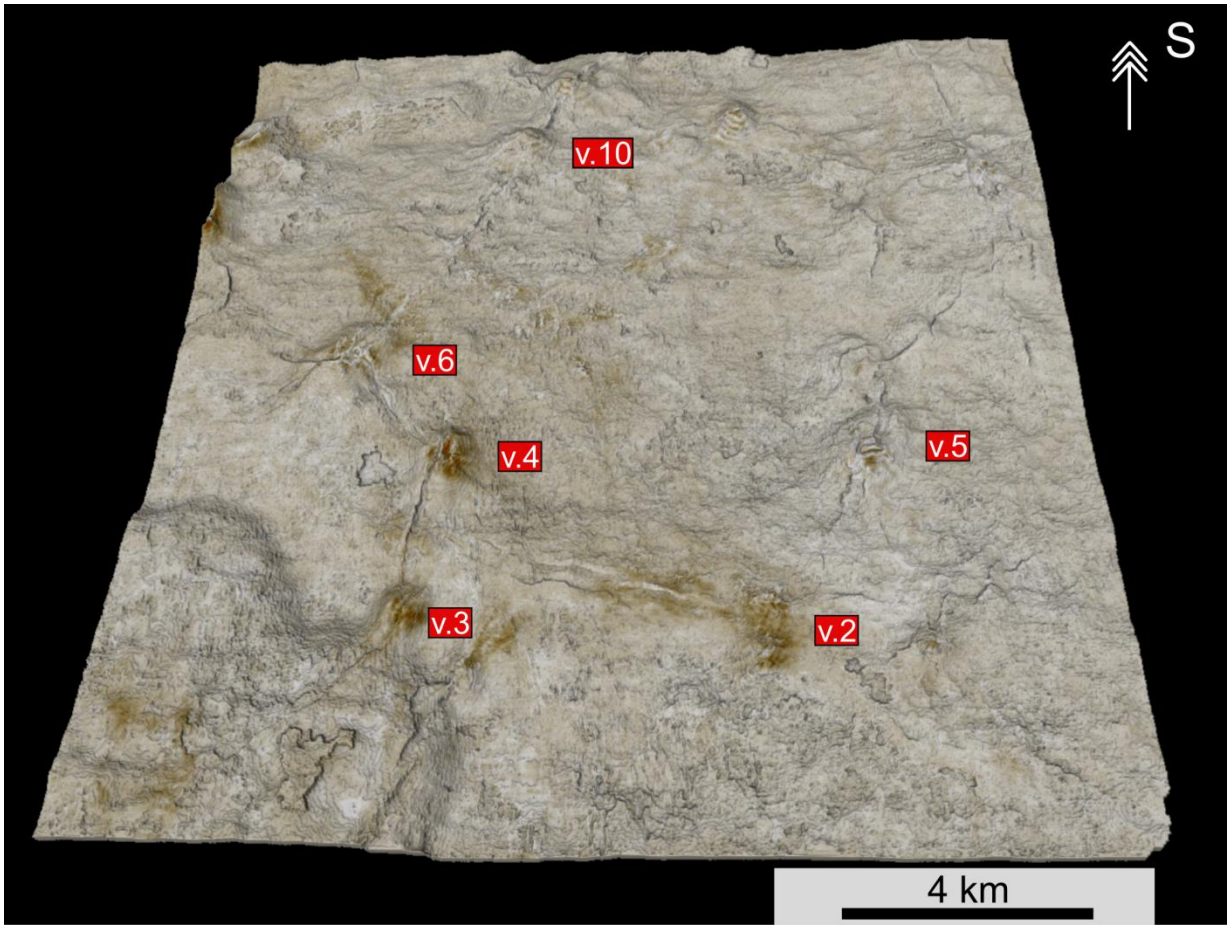

Figure 6.24: Top Tare horizon interpreted using RMS amplitude mixing and coherence attributes. The picture is a good illustration on how radial and interconnected fracture systems can be developed between the HTVC's at certain intervals.

6.5.2 The vent interior

The seismic characteristics of each HTVC are in many cases highly variable. The interior of the vents displays a low reflectivity imaging, and lack of internal structure. Because there are no amplitude anomalies associated with the structures they must be of an acoustically similar material to that of the encasing material (Hansen et al., 2005). To support these observations and provide an understanding of the geological features, it would have been ideally to correlate with well information. However, the well 6302/6-1 did not penetrate any vent systems.

Field observation (Chapter 2.7, HTVC in the field) and well data from other study areas suggest that vents may have a similar composition as the sounding strata (Svensen et al., 2003). Although the HTVC in general display an overall similar acoustic behaviour as the surrounding material, some features are highlighted in terms of seismicity. This change in acoustic impedance may be a result of material alteration due to hydrothermal mineralization of exposed zones, or an alternative composition of magmatic material. However, the later alternative is not likely due to

the presumably higher density and Vp-velocity one would expect, together with a distinct change in acoustic property. The HTVC's in this study is therefore anticipated to be formed as a result of remobilized sediments, and only minor, if any remains of magmatic material.

6.5.3 The Upper part and geometry of dome structures

The upper part of the HTVC is seen in the seismic cross-section as doming features down lapping onto the Top Tang paleosurface (See Figure 6.23B and 6.25). Their geometry and structural context are showing similarities to structures described elsewhere at the Norwegian Margin, but with the distinction of only having the dome shaped morphology at the upper part. Slight depressions are observed at the base of some structures, but the overall feature consists of the down lapping dome, and not the eye-shaped or crater described by for instance (Planke et al., 2005).

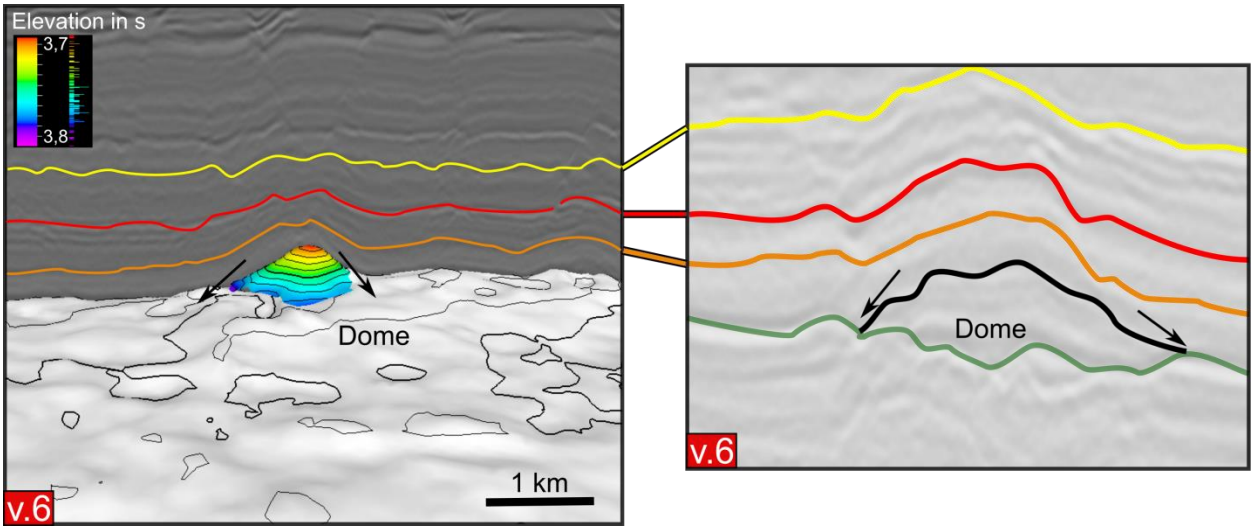

Figure 6.25: 3D/2DSeismic interpretation of the v.6 dome structure, lapping down onto the paleosurface (Top Tang).

Like the Top Tare horizon and the interpretation mounds, the internal dome of the HTVC structures shows no evidence of reflection onlap onto the dome. All of the vent systems mapped in this thesis has some form or shape indicating a dome feature above the stratigraphic surface of Top Tang. Not all the domes can be seen down lapping onto the Top Tang paleosurface, but a sufficient number to state that this is a common behaviour of the HTVC's in this part of the Møre Basin (Appendix A.1 contains detailed mapping of all the HTVC's done in this study). The domes are used as further constraint, to give a qualitative measurement of the upper part of the vent systems. These results will be presented further down this chapter. Figure 6.25 and 6.26 illustrates domes on the Top Tang paleosurface, aspect ratio of the time amplitude structure is about 0.1 s (TWT), corresponding to a height of 80-100 m.

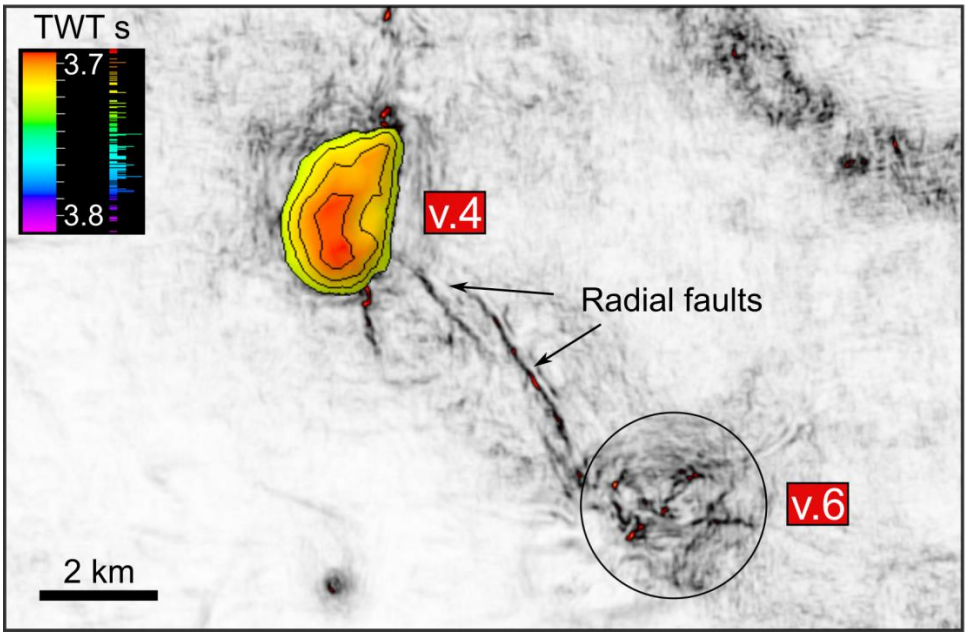

Figure 6.26: "Variance cube"-slice from the Top Tang horizon seen from above. Figure illustrating 3D mapped and time-slice variance representation of dome v. 4 and v. 6. The variance cube highlights lateral discontinuities such as faults. The radial fault pattern away from both vents, suggest development simultaneous as the vents formation.

6.5.4 Vent conduit zone

The vent conduit is regarded as the disrupted, altered or brecciated zones in the host, which fluids can travel from the contact aureole to the paleosurface. Conduit zones in this study are regarded as disruptive reflectors, removing the seismic character of the host strata between the doming structure at the paleosurface and the sill tip. The 3D data exhibits the conduit as vertical zones in the seismic data, where the amplitudes and reflectors are distorted (See Figure 6.27). Prior study of resembling structures (Heggland, 1998), have suggested the conduit chimneys to represent previous and perhaps ongoing migration of gas through this vertical zone.

The conduit zones interpreted show a quite variable morphology, some are conical and becomes thinner towards the sill tip, whiles others are regarded as cylindrical. Not all the conduit zones display a traceable path from the domed structures down to their origin. In cases where the flow pattern is diverted by displaced fault blocks or magmatic bodies, the prediction of the sill and aureole origin is difficult. However, the vent conduits do not appear to follow fault planes in general, and systematically fault cutting is not seen.

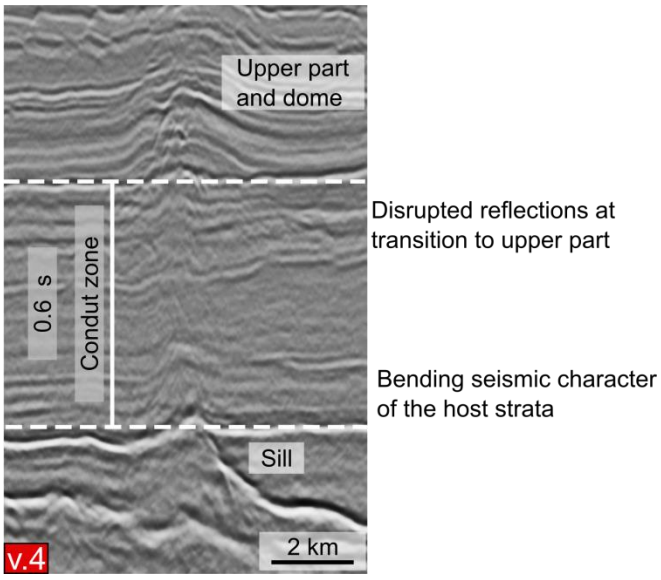

Figure 6.27: Vent conduit zone from a sill located below the Carbonate layer. The zone is continuous from sill-tip to paleosurface at Top Tang. For HTVC locations see Figure 6.22. All conduit zones can be viewed in Appendix A.1.

In the cases where the conduit zone and their nature of origin are uncertain, it might be a result of prohibited seismic resolution and the detection range of too thin seismically zones. The overburden might also play a role in the interpretation. High amplitude reflectors might mask the underlying strata, or create seismic artefacts due to "velocity pull down" which are misinterpreted (Schroot and Schüttenhelm, 2003).

From field-studies in the Karoo Basin no definitive conduit zones were found due to poorly constrained data and lack of outcrops. At the lithological depth one would assume to encounter the conduit zone, some narrow brecciated pipes were mapped (Svensen et al., 2007). These outcrop examples could indicate the escapement structures of fluid flow, but will in many cases be below the seismic resolution range.

6.5.5 Dipping reflectors towards vents and conduit zone

Reflectors in the surrounding host strata are often seen dipping towards the conduit zone and upper part of the HTVC. This feature is best observed in the seismic section associated with the larger HTVC's. Figure 6.28 is highlighting the dipping reflectors observed at the HTVC v.6. To form these dipping reflectors, processes involving material transport and subsidence are required. Fluids expansion which is generated at the sill-tip and at the contact aureole is suggested to pierce the sedimentary strata above. This could indicate that material transported during the same venting process has a potential for volume alteration, and thereby a direct influence on the downward dipping strata at the uppermost part of the HTVC.

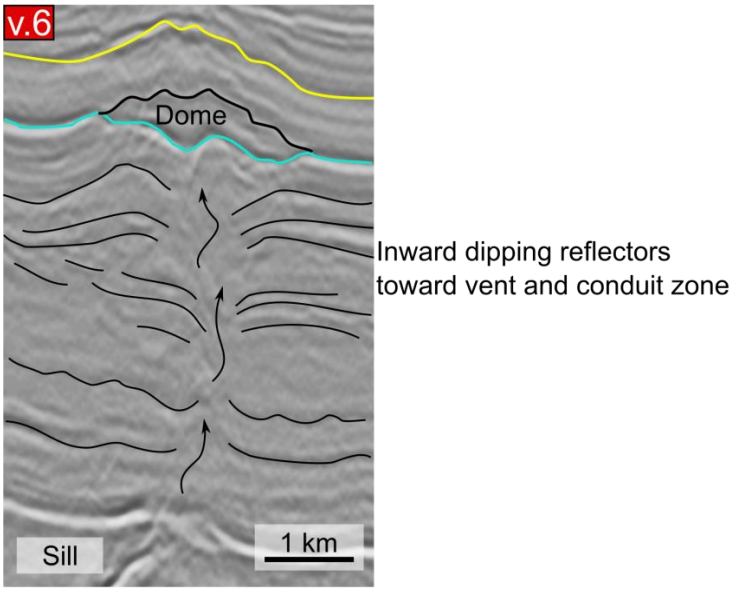

Figure 6.28: Inward dipping reflectors on either side of the HTVC v.6. Arrows in the middle correlates to the disrupted zone of the conduit pipe and indicates fluid and material transport direction.

In many of the studied vent complexes in this thesis, the observations of the dipping reflectors are somewhat hard to interpret. Those interpreted show a distinct incline pattern towards the disrupted zone of the conduit. The lines are rarely seen as continuous over a long distance, and get more disrupted further down in the stratigraphy.

6.5.6 The sill and vent relationship

All the 13 HTVC's mapped out in this study are related to one or more underlying sill complexes. The majority of the vents are associated to the large saucer shaped Tulipan-sill located at the central part of the 3D cube. Because of the sill's distinctive geometry, it is regarded as an important element in explaining the behaviour, position and structural development of the HTVC's.

The extensive sill complex in the Tulipan 3D cube is interpreted based upon the same method as the horizon interpretation. The sills are identified as high amplitude reflections within the sedimentary strata, and are displaying local transgressive segments in the seismic slides (See Figure 6.30). Three sills have been mapped out individually, and picked as separate horizons. The lowermost sill complexes are difficult to map out with confidence, due to the overlaying sills and the acoustic disruption this inflicts on the seismic imaging. The Tulipan sill is regarded as the primary sill in the studied interval. This sill is classified as a saucer-shape intrusion, and is easily recognised in the seismic section. Figure 6.7 and 6.30; show that the underlying Tulipan sill is forcing a dome-shaped morphology of the Carbonate layer, Top Springar and Top reservoir horizons above. The Carbonate and Springar horizons is intersected and pierced by the sill at the flanks, resulting in the most prominent HTVC's imaging in this study.

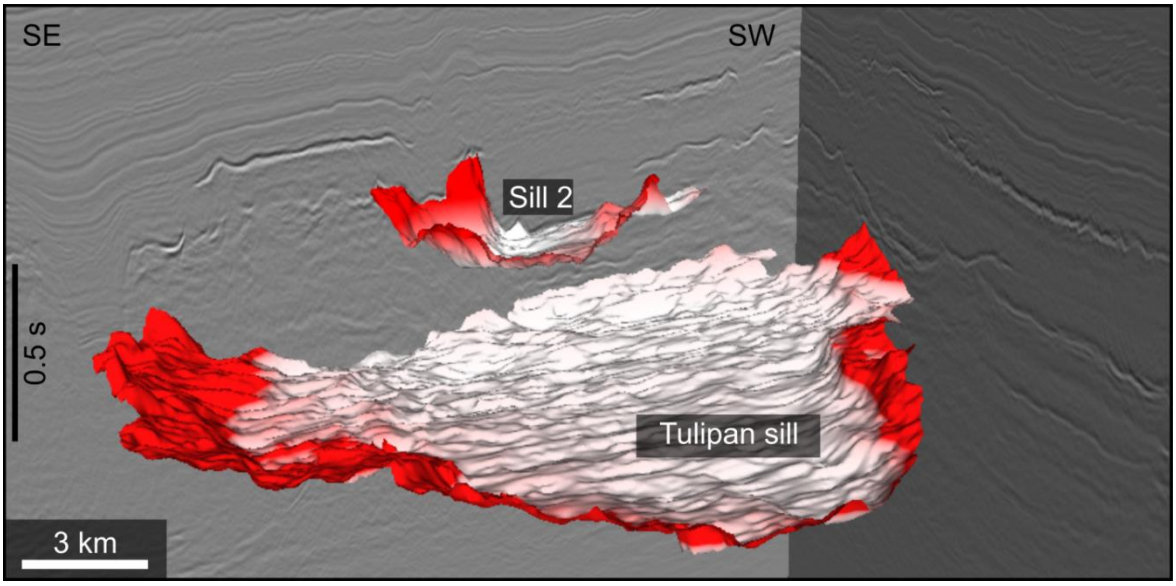

Figure 6.29: Selection of two of the 3D mapped sills in the study area. The sills have individually rather complex geometries, but follow an overall saucer-shaped trend (red colour illustrates the bending of the edges). The image is vertically exaggerated 1:5, to represent the morphological features of the complexes.

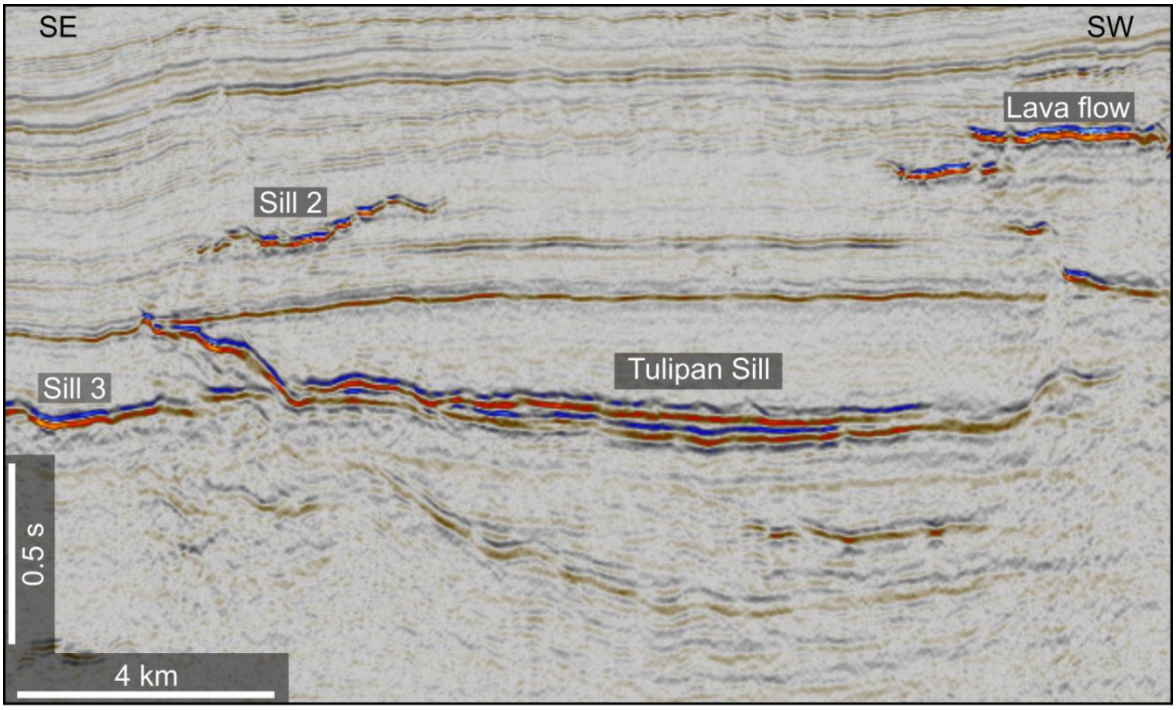

Figure 6.30: Cross-section of sill intrusions and lava flows in the central Møre Basin. Section showing the upper Cretaceous and early Paleocene sedimentary section. Sills representing the Tulipan sill complexes associated with the HTVC occurrence.

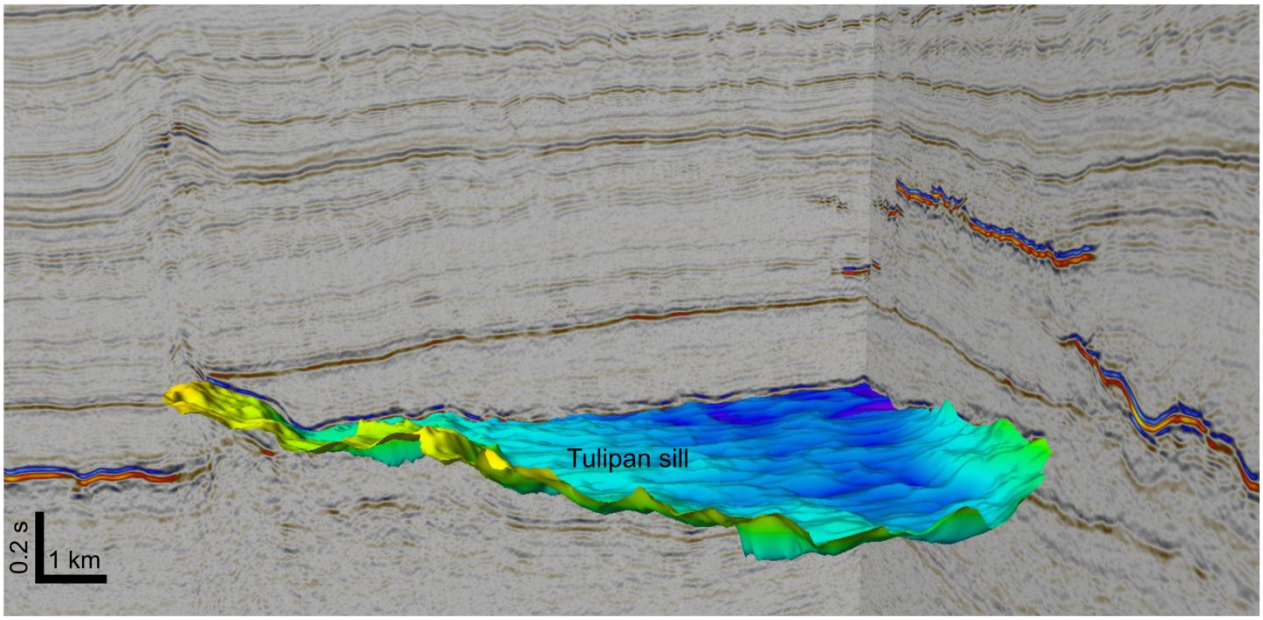

Figure 6.31: Illustration of the HTVC and sill relationship in raw seismic data. The sill complex is 3D mapped for visualization purpose, whiles the vent system is deliberately kept unchanged to illustrate how they look during the interpretation process.

6.5.7 Vent position and the underlying sills

The HTVC's associated with the large Tulipan sill complex are unique and distinguishable in the way they cover the underlying sills. Some of the vents are found above the sill's interior, but the majority is positioned at the edge and rim of the sill margins. There are deviation in the sill-vent position, were some HTVC's occurs at isolated points. However, the most common location is situated above the termination and highest point of the sills.

Because of the number of vents and the extent of the Tulipan sill complex, the relationship can be viewed in more detail then previous studies have undertaken. The excellent imaging of the structures provides opportunity for detailed mapping, which contributes to the overall understanding and context.

Figure 6.32 below shows the relationship between the underlying sill complexes, and the position of the different HTVC. The horizon is the Top Tare paleosurface, in which the doming features of the vents are down-lapping onto. Each of the vents correlates to Figure 6.22 in terms of position and numbering. The spectral decomposition time-slice in Figure 6.32 shows a clear relationship between the geometry of the underlying sills, and the location of the vents. Most of the vents are seen along the outer margins of the major Tulipan sill. The differences in rim-elevation at the sill-margin cause the conduit zones to shallow and deepen, depending on the sill position and elevation. Deeper situated vents are observed where the sill is displaying a gentler angel incline.

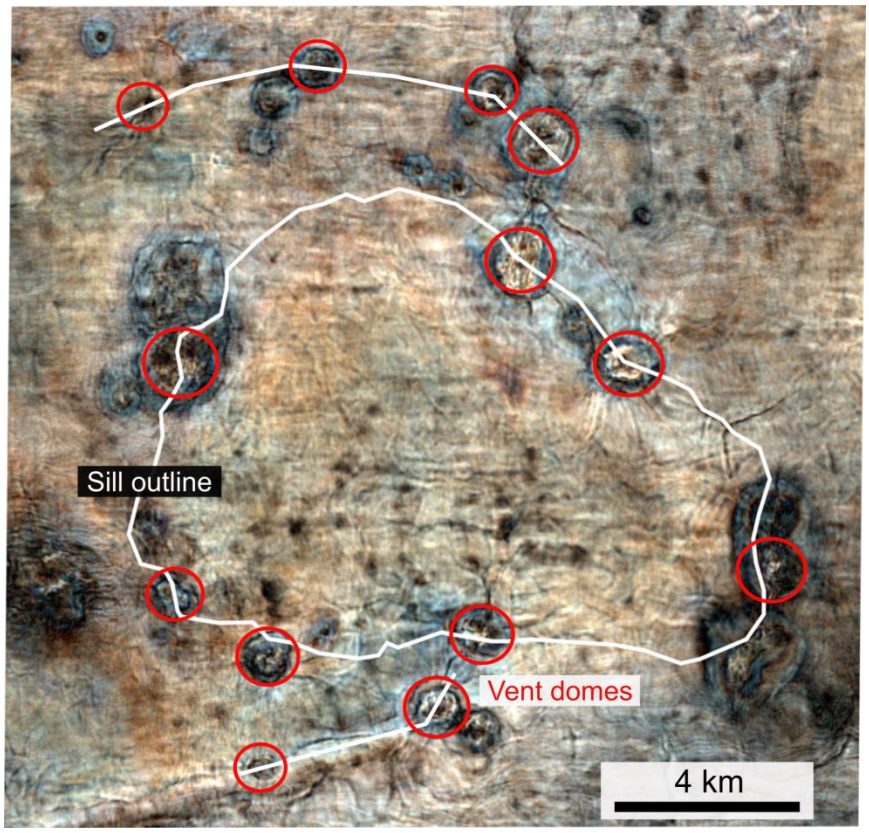

Figure 6.32: Spectral decomposition of the Top Tang paleosurface, Red (22Hz) Green (27Hz) Blue (31Hz). Figure illustrating the relationship between underlying Tulipan sill complex, and the HTVC's seen on the Top Tang surface. Figure is made using the GEO-Teric Software.

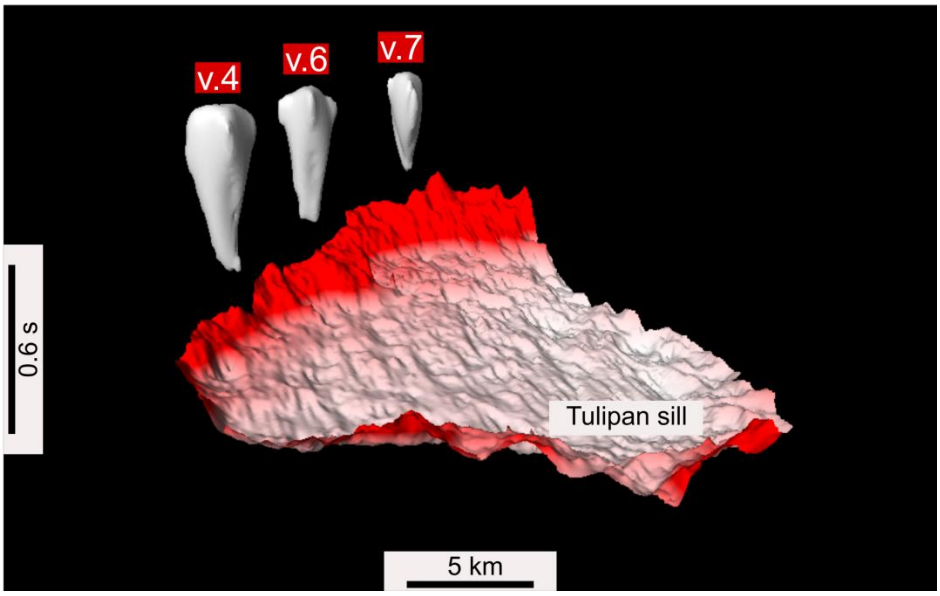

Figure 6.33: 3D representation of v.4, v.6 and v.7 HTVC's in association with the major Tulipan sill. Note the position of the three HTVC's at the sill edge. See Figure 6.22 for map position of individual vent systems.

6.5.8 Vent size and dimensions

The HTVC size is essentially a measurement of the doming structure as a structural relief, made by defining a datum linked to the underlying paleosurface. (Chapter 5, Measurement criteria for HTVC's) describes the method and key features controlling the measurements. The following table will present the sizes of the 13 individual HTVC's mapped in this thesis, with evaluation of the key structural features such as dome diameter, height and conduit proportions.
Something to note is the N/A (Not Available) notification in the table. This indicates that the specific part of the HTVC's could not be measured with confidence and the results thereby would be regarded as false.

To correlate the HTVC's with a pre-defined size arrangement, the data from this study were compared with published data done by Planke et al., (2005). This publication on the Møre and Vøring Basin divided the vents into two categories: Small vents from 0.4 to 2 km and large vents 2 to 5 km in diameter. In this dataset the majority of the vents fall within the small-vent category. Only v.4 and v.5 have a maximal dome-with exceeding the 2 km mark.

Figure 6.34 show a selection of plots regarded as important when comparing the morphological units, and the connection between different unit sizes (e.g. Dome height versus Conduit zone).

Table 6.1: List of the 13 different HTVC's mapped out in this thesis. Figure 6.22 show the location and outline of the individual complexes. The table consists of following headers: vent number ranging from 1 to 13, maximal and minor axis width of the dome structure, dome height from paleosurface and conduit height from sill-tip to paleosurface. See Chapter 5, Figure 5.2 for measurement method and Appendix A.1 for all 13 mapped HTVC's.

Htvc nr.	Maximal width (m)	Minor axis width (m)	Dome heigth (m)	Conduit heigth (m)
1	1400 ± 100	1200 ± 100	100m ± 20	400
2	950 ± 150	600 ± 100	70	200
3	1650 ± 100	1400 ± 100	90	320
4	2100 ± 50	1800 ± 100	100	640
5	2500 ± 100	N/A	120 ± 50	400
6	1850 ± 50	1350 ± 50	80	630
7	1600 ± 100	N/A	100 ± 30	630
8	1200	N/A	N/A	530
9	1200 ± 20	650 ± 20	85	500
10	1570	1150	90	450
11	300 ± 50	N/A	120	400
12	100 ± 30	600 ± 30	80	500
13	1500 ± 50	1350 ± 50	85	650

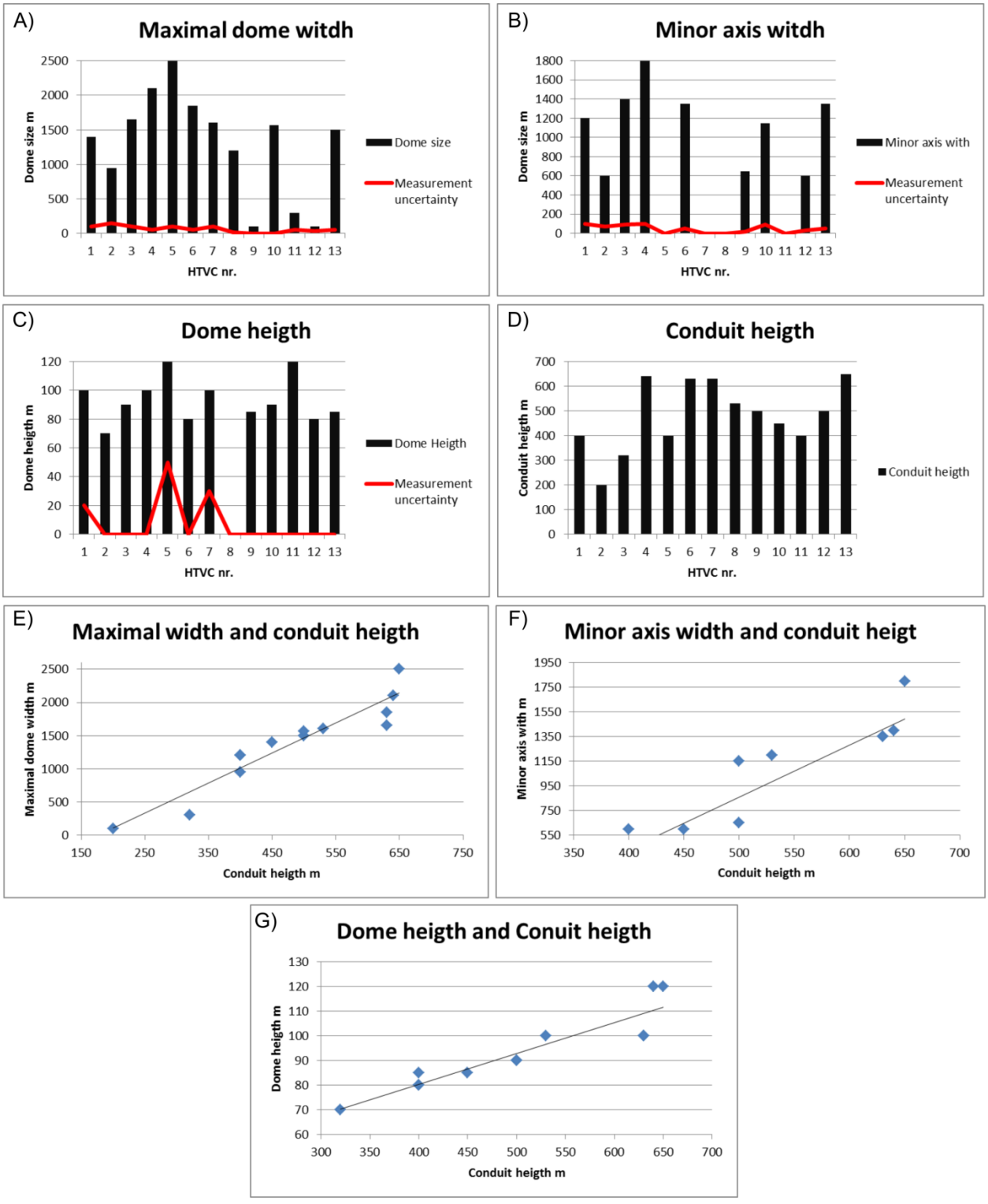

Figure 6.34: A, B, C and D) Column diagram representing unit sizes and corresponding HTVC's from table 6.1. Red line represents measurement uncertainty and possibly deviations during interpretation. E) Maximal width of the dome structure plotted against the conduit height. F) Minor axis width of the dome structure plotted against the conduit height. G) Dome height plotted against conduit height.

7. Modelling results

7.1 Vent modelling

This part presents the results obtained during the sandbox experiment. A total of 12 modelling series were undertaken and implemented width different physical parameters. All experimental parameters are presented in table 7.1.

7.1.1 Experimental results

Each of the experiments started out with a similar condition, in terms of the static granular bedding in the Plexiglas cell, as seen in the Time laps presentation of the experiment in Figure 7.1. The compressed air from the air supply/pressure tank was gradually imposed trough the inlet by manually increasing the air flux using a valve, directly connected to the (constant) supply. The pressure and flux were increased slowly until the predefined supply pressure was reached and the fluid-induced deformation of the matrix material was obtained.

In the experiments with filling exceeding h > 9 cm, a static bobble formed on top of the inlet (Figure 7.1, t2). The bobble did not evolve in size (width or height) trough time, at one given (constant) pressure. This observation together with the observed fluid escape pattern on top of the material infill (Figure 7.1, t2) supports two ideas, one is that the experiment evolves as equilibrium stages and the second is that the unconsolidated material allows fluid escapement through the matrix, and thereby maintains the equilibrium state for that given pressure. The presence of the static bubble also induce lateral compaction of the matrix, together with a moderate uplift resulting in two steeply dipping reverse shear bands on each side of the inlet (Figure 7.1, t2). The dip angle, and diameter of the conical reverse shear bands are influenced by the filling height (h), with increasing values for additional material filling.

When further increasing the inlet pressure beyond the critical equilibrium threshold, full fluidization of the matrix occurred for all the experiments conducted. When manually increasing the imposed velocity, the bubble rapidly moved towards the surface initiating the fluidization. The morphological characteristics of the fluidization deformation, is the rapidly upward transport of the grains together with the ascending bubble (See Figure 7.1, t3 and t4). The transport enables convective movement aligned with the inlet, at the center of the structure. This convective flow generates inward dipping beds exhibited at the lateral sides of the fluidization zone (See fig 6.33, t6). The concentration of fluidized deformation was centralized within the preexisting dipping stress fields generated by the ascending gas bubble. At the rim of the fluidization zone, a distinct crater shape appeared as the material was erupted onto the surface (See fig 6.33, t5 and t6). The angle of the deposited material corresponds to the cohesion strength and the Mohr Coulomb envelope. Picture series of the experiment shows the transition from static bobble to the fluid phase, at 7 frames per second. The total time of experiment, from the

static bobble to the fluidization state is about one second. During the fluidization process the velocity was kept constant.

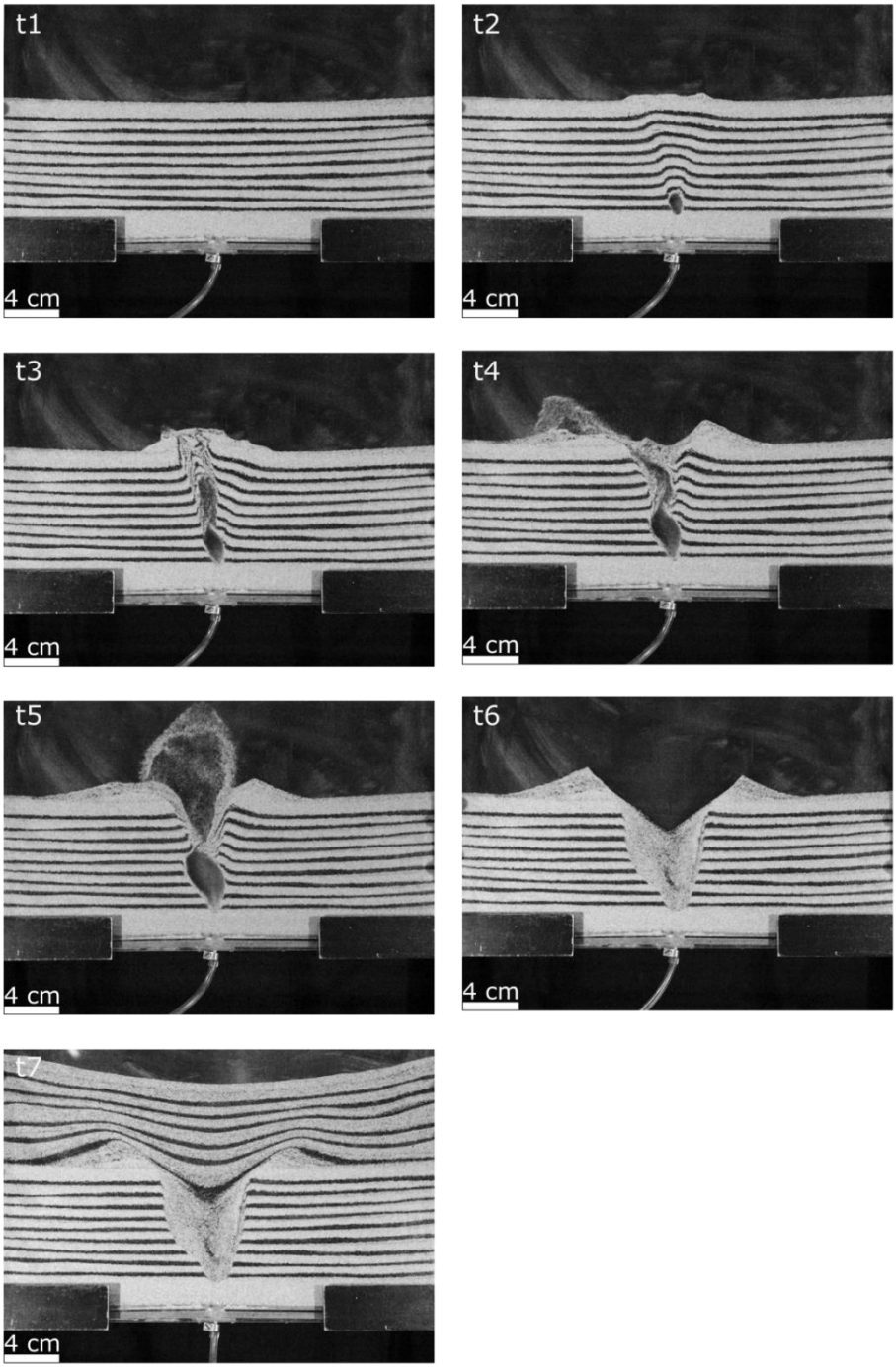

Figure 7.1: Picture of experiment 11, time laps of 7 stages (h = 16 cm (Figure 7.1, t1-t7). (t1): initial configuration of the static bedding. (t2): Static bobble forming at the centred inlet, fluid induced deformation of the matrix. (t3 and t4): Gas bobble grows to the surface, triggering the onset of fluidization. (t5 and t6): Eruption of material at structure rim, and crater shape. (t7): Sedimentation of piercement structure. Picture t1– t6 represents a time step interval of ≈ 0, 17 seconds.

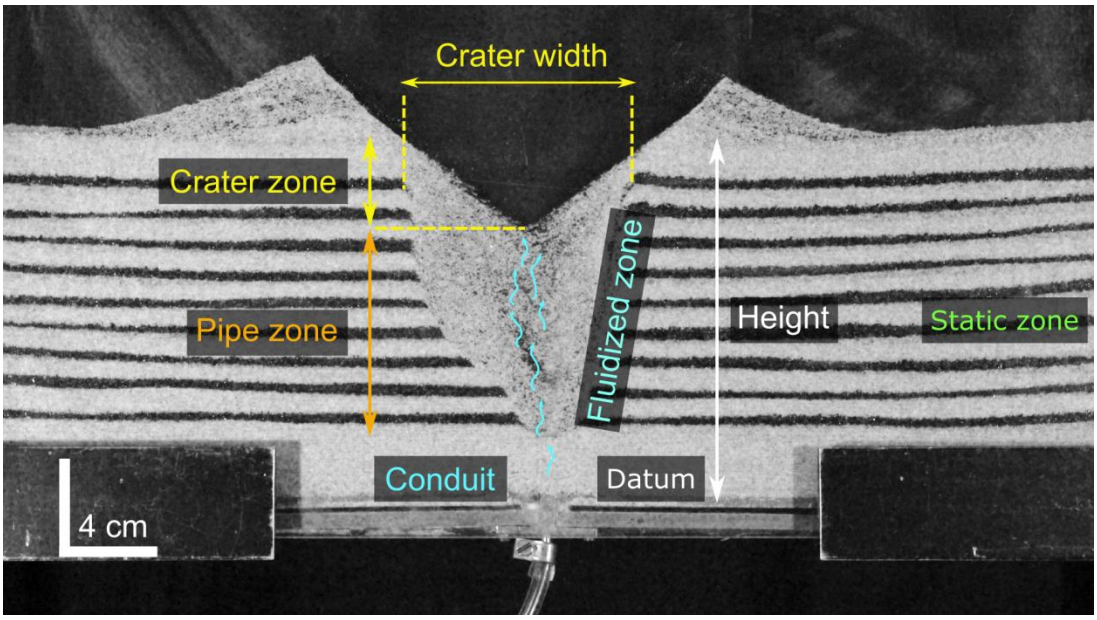

Figure 7.2: Morphological zones defined in the experiment which enables a correlation to the natural occurring HTVC's interpreted in the seismic Tulipan section. Picture corresponds to the t7 frame, of the fluidized phase of the experiment.

Table 7.1: List of the 12 experiments conducted together with the measurements of the piercement structures and the pressure parameters implemented.

Experiment	h (cm)	Pressure (MPa)	Crater (cm)	Pipe (cm)
1	11	0.15	8.6	5.2
2	9	0.15	10.2	2.8
3	12	0.2	9.6	3.2
4	21	0.5	12	11
5	14.5	0.25	8	8.8
6	14.5	0.2	9.6	8
7	17.6	0.25	12.8	10.5
8	18.5	0.3	10.5	11
9	9.5	0.15	8.5	5.5
10	19	0.2	13	11
11	16	0.25	11	8.5
12	13	0.25	13	7

7.1.2 Geometrical measurements

Several measurements were performed on the geometry of the piercement structures. These measurements may provide interesting and useful information regarding geological structures such as the HTVC. Figure 7.2 gives an overview of the morphological details obtained during the experimental procedure. Development and behaviour of key features whit alternating parameters can be viewed in the plots below.

The length of the pipe (conduit) zone is measured from the datum and inlet position to the top of the fluidized zone. The crater width is measured as the maximal horizontal distance of the fluidized zone. Both these values are dependent on the filling height (h), and will increase with increasing height. From the plots one can observe the linear trend of the structures and the dependence on filling height regarding the size distribution.

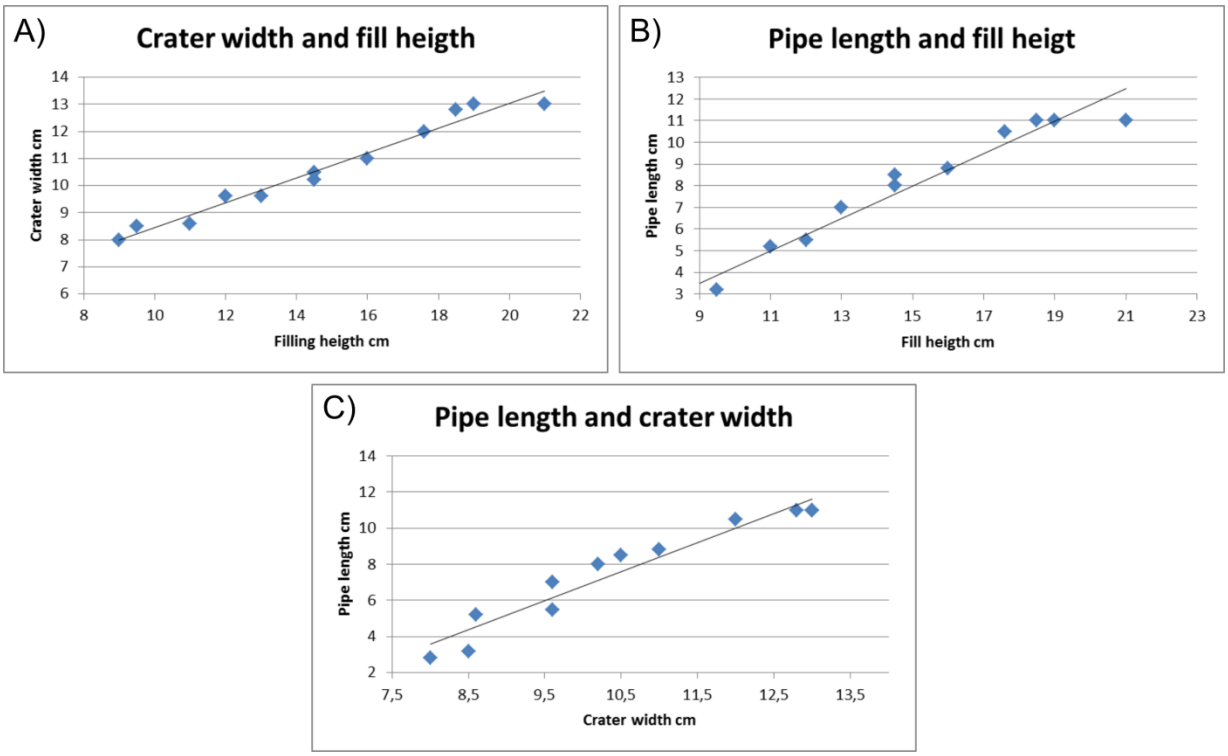

Figure 7.3 A) Crater width plotted against the fill height. B) Pipe length plotted against filling height. C) Pipe Length plotted against the crater width. Linear trends are observed in all plots, and dependent on the filling height h in the experiments.

7.2 Synthetic modelling

This chapter contains the result of the synthetic modelling preformed on the most representative picture from the sandbox experiment described in the previous chapter. The sandbox model was assigned with elastic properties corresponding to the well log data provided in this thesis.

The model was placed at a depth comparable to that of the actual HTVC interval in the Møre Basin. Frequency wavelet ranges from 10-30 Hz together with increasing velocities at depth. The illumination vectors described in Chapter 5.6 provide essential information regarding the resolution and the seismic illumination.

There are two primary goals of this chapter in terms of the synthetic modelling results. One is to obtain synthetic images of the sandbox experiment, and then provide a link between what is seen in situ and the structures made in the laboratories. The other is to give estimation on how the ray paths of the seismic signals alter the resolution details and illumination of the seismic structures.

7.2.1 The predefined model

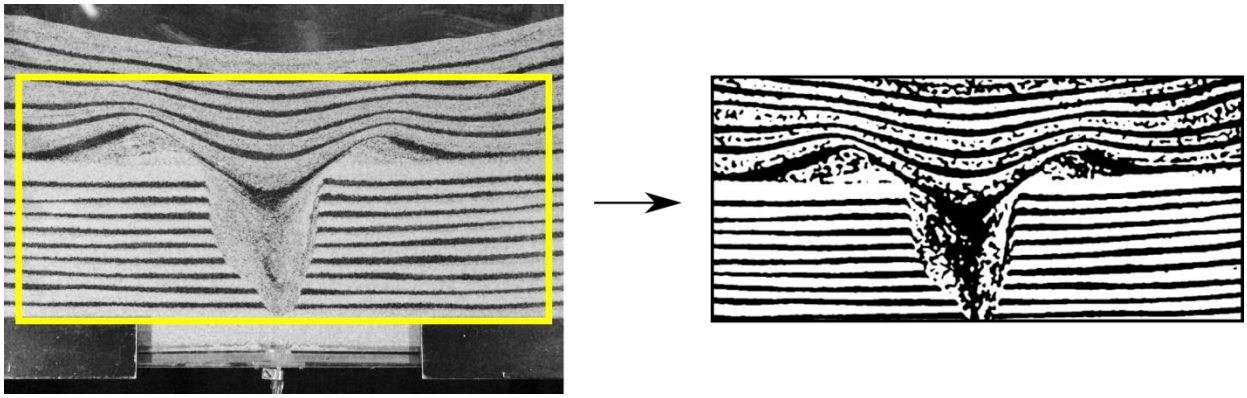

Figure 7.4: The alternating light and dark coloured sand used in the sandbox experiment makes up the basic geometry and the polygon boundaries in the synthetic background model. 15 different layers are specified to relate the sedimentary sequences and coherent change in elastic values (Vp- and Vs- velocities) in the model.

Figure 7.4 shows how the experimental succession is subdivided into a number of separated units and implemented with black and white zones. These zones are assigned different synthetic properties from the borehole data, representative to the depth of the HTVC interval in the Møre Basin. The black and white domains represent reflectivity and impedance boundaries, enabling elastic wave propagation at different intervals in the subsurface. The model is defined as a 2D layered model, which implies that property variations only takes place in one direction (vertical/depth). Seismic properties and interval depth is presented in table 7.2.

Table 7.2: Synthetic properties provided from the borehole data (Well: 6302/6-1) at the depth of the HTVC interval in the Møre Basin. Core depth and formations are set between the first appearance of the conduit zone (at sill interaction), and the upper mounded structures at the Top Tare horizon.

Formation/Group	Core depth	Density (g/cm^3)	Velocity Vp	Velocity Vs	Vp/Vs
Top Tare	3220	2.0	2.50	1.10	2.3
Intra Tare	3260	2.2	2.70	1.20	2.3
Top Tang	3335	2.1	2.80	1.80	1.55
Intra Tang	3410	2.2	2.70	1.50	1.80
Top Reservoir	3870	2.4	2.80	1.3	2.20
Top Springar	4050	2.45	3.0	1.5	2.0

7.2.2 Synthetic modelling and qualitative seismic comparison

Comparison between the original and the synthetic seismic was performed to establish a connection between the two. Although the synthetic seismic does not match the actual data in a perfect manner, they are seen to shear many common morphological features both at large and small scale. The major reflections generated in the synthetic model appear at the same intervals, and the amplitude pattern between the reflections seems to be within a reasonable range.

The reflection pattern of the post sediment overburden above the piercement structure show large areas of seemingly structureless sequences. These can to some degree be correlated to the depositional structures of the upper vent. Bending of the overlaying strata and the seismic response of the reflectors resembles the mounded structures which are characteristic to the HTVC's observed in the Møre Basin.

The most prominent features are found at the conduit zone. In both the sandbox experiment and the synthetic image, the features of the downward dipping reflectors towards the structureless center are clearly observed. This supports the assumption that hydrothermal derived fluids are reworking and redistributing material in the conduit zone. The conduit itself shows the typical conical aspect ratio, defined by thinning of the zone towards the origin.

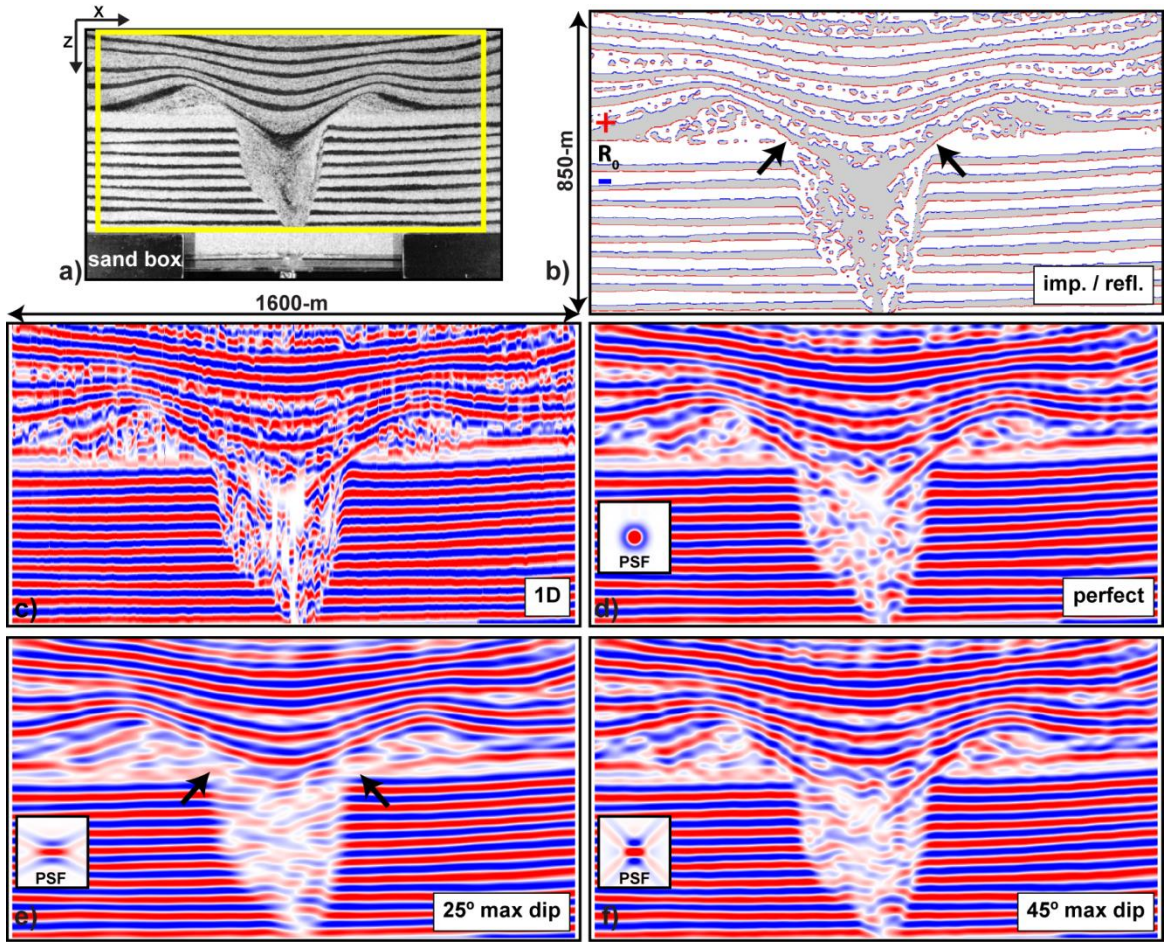

Figure 7.5: Synthetic modelling of the sandbox experiment: a) Sandbox photo. b) Impedance model from the predefined background photo (High impedance-white, Low impedance -grey), elastic properties from well 6302/6-1 in the Tulipan prospect. c) 1D convolution. d) Perfect angle, perpendicular relative to horizontal plane. e) 25° max dip relative to the horizontal plane. f) 45° max dip relative to the horizontal plane. Arrows in figure b and c) highlights how different angles affect the seismic imaging retrieved.

7.2.3 Synthetic modelling, ray pats and resolution

One of the primary goals of this chapter is to give estimation on how the structures alter depending on the ray path, offset and stacking of the seismic data. The results are based upon the 2D convolution operators, called Point-Spread-Function (PSF) explained in Chapter 5.6.2.

For decades the most used seismic modelling tool for subsurface targets have been the1D convolution model. This approach combines stacking of multiple traces perpendicular to the horizontal plane and then creating the seismic image. However, the 1D convolution method is in many cases too simplistic and does not reflect the geological structures in a satisfying way. In Figure 7.5, c) the 1D convolution imaging of the piercement structure is displayed. Especially the more disrupted interior and the deposited upper part of the structure have poor resolution details and makes interpretation of some key features difficult. To overcome these obstacles the predefined model has undergone state-of-the -art seismic modelling by completing a PSF-build.

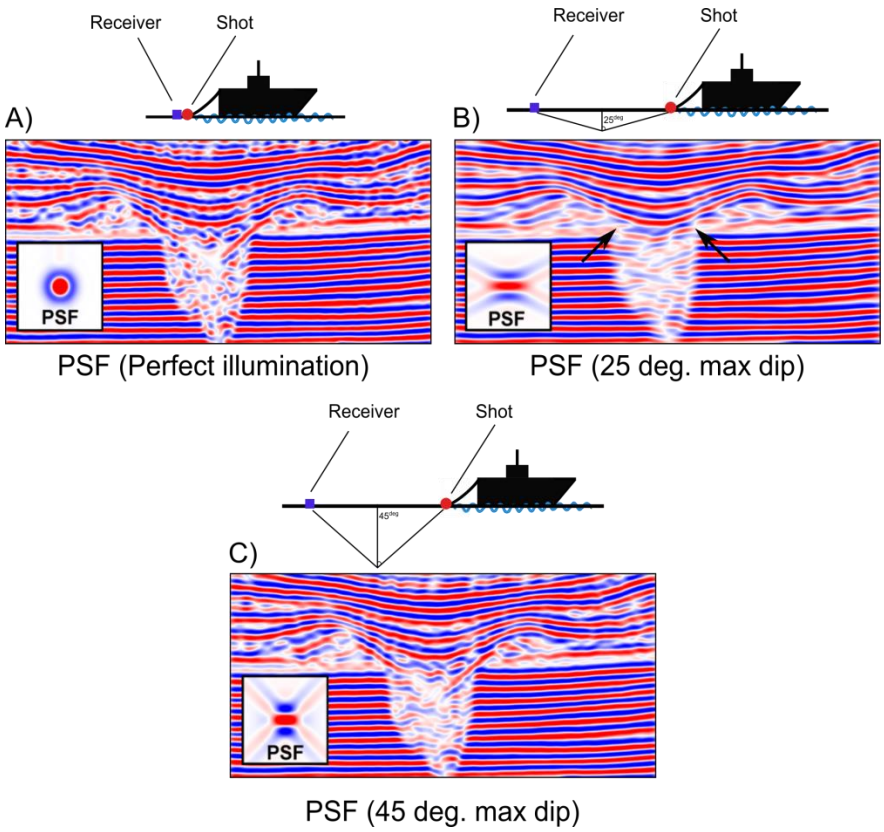

Figure 7.6: A) Figure showing Perfect angle, perpendicular relative to horizontal plane. No offset between shot and receiver. B) 25° max dip relative to the horizontal plane. Structures with reflection angles exceeding the 25° will not be captured by the receiver. C) 45° max dip relative to the horizontal plane. Same as previous figure, Structures with angles exceeding the 45° mark will not be recorded.

Figure 7.6 A) illustrates the modelling result from a zero offset and perfect illumination. One thing to note is the lateral resolution in the PSF modelling compared to the 1D convolution in Figure 7.5 c). At especially the lateral reflectors, seismic signals in the perfect illumination emerge as more continuous in the seismogram. Also the conduit zone stands out in terms of resolution of the dipping reflectors. Figure 7.6 B) illustrates the modelling result from a 25° max dip on the offset angle. This result in features exceeding the 25° incline angle will disappear in the images. The arrows highlight how some of the otherwise well-defined reflectors are missing and are creating misleading seismic artefacts. The effect of resolution and survey offset is something that has to be considered when interpreting the actual in situ structures. Additionally, the disrupted conduit zone appears as blurry and weak in the seismogram compared to the others. This implies that longer offset angles create better coverage of the target zone, but sacrifices the resolution. Figure 7.6 C) corresponds to symmetrical illumination of the PSF modelling. Angles exceeding 45° max dip is not recorded in the seismogram. One direct result to note in this seismogram is the steeper dipping reflectors in the conduit zone seems to have a more lateral and

continuous extension. Also the apparent thinning of the overburden layers is wrongly induced by 1D convolution in comparison to 45° illumination. If comparing the conduit interior between the 45° and the perfect illumination, the latter it is slightly improved in regards to reflection strength.

8. Discussions

The HTVC's described in this thesis provide evidences for focused fluid and gas migration in this part of the Møre Basin during the Paleocene-Eocene time period. A number of questions arise from the recognition and study of these structures, including (1) the HTVC geometries and deformation patterns in seismic (2) nature and source for mobilizing the HTVC's, (3) the initiation depth of the HTVC's, as well as (4) the timing of fluid migration and age of the HTVC's. The HTVC's is interesting also when looking at the system in a broader perspective. Taking into account the diverse distribution of the HTVC's argues for a widespread fluid and gas migration in this basin. The processes of vertical fluid flow to these complexes in relatively unconsolidated sediments are not widely discussed prior to this thesis. The evidences presented here might thus widen the consideration and understanding of these types of fluid migration structures.

The key to many of these questions can be partly constrained by examination of the seismic and stratigraphic data, the timing of fluid mobilization and the implementation of experimental and synthetic modelling. The discussion below focuses on the HTVC's as one complete system, but will be discussed in parts covering morphology, formation mechanisms and age correlations.

8.1 Seismic

The HTVC's in the Møre Basin are interpreted as fluid migration paths that were fracturing and piercing the Top Tang paleosurface at the Paleocene-Eocene transition. The interpretation in this thesis is based on the recognition of the intrusive geometry in the seismic sections, utilizing similar interpretations methods as described by Planke et al., (2005), Knopf (2002) and Hovland et al., (1998).

The HTVC's exhibits a clear relationship with the deeper situated sill intrusions, suggesting an origin for fluid ascent through the fluidized and seismic disrupted conduit zones. These chaotic reflection patterns are interpreted to be remanence of gas and fluid chimneys, similar to those described by Heggland (1998) and Svensen et al., (2006). The conduit zones are recognized on seismic data from their character as conical or cylindrical zones of disrupted or even collapsed stratal reflections. They are generally observed to emerge from the incline lateral part of sill edges (e.g., in saucer shaped sills). The conduit zones exhibits a considerable range in dimensions, with diameters from c. 100 m to 2 km, and elevation heights from 200 m to 650 m. From the sandbox experiment (Chapter 7), one can observe a linear trend and dependency between the zone length and the diameter/width (Figure 7.3). The v-shaped or inward dipping reflectors seen at the uppermost part of the conduit zone suggest either refraction of fluid/gas migration, or material collapse of the near-surface sediments as proposed by Løseth et al., (2003) (Figure 6.28). These dipping structures are also encounter in the sandbox experiment as a result of 'convective' currents and collapse at the edges of the piercement structure. Similar results during analogue piercement experiments are seen (e.g., Walters et al., 2006; Nermoen et al.,

2010), where material moves up at the source inlet, and other material may collapse downwards at the edge in a circular convection motion.

The shape of the upper part of the HTVC's can in some cases be seen as craters or eye shaped structures at the seafloor (Figure 2.6 and appendix A.1). However, internal reflections and interpretation of individual HTVC's show that the majority of the upper part geometry consists of domes. These dome structures are characterized as a down-lapping feature on the Top Tang horizon (See figure 6.25). The reflectors are interpreted as local high-amplitude events terminating at this stratigraphic level. The differences in acoustic properties from the surrounding strata are probably caused by the presence of gas or local differences in the material diagenesis (Barrington and Kerr, 1961; Hovland and Judd, 1988). The lack of onlapping reflections on to the crest of these domes together with the homogeneous thickness of the sediment layer above, is taken as an indication of structural modification taking place after the initial formation (will be discussed in the chapter 'Dome shape and differential compaction model'). The doming features show a variable range of sizes, the minimum and maximum diameters vary from 100 m to 2500 m respectively (See Table 6.1), and the total relief (from Top Tang horizon as datum) varies from 70 m to 120 m. The HTVC Statistics from this thesis are comparable to those done by Planke et al., (2005). They mapped out 20 HTVC's terminating at the upper Paleocene sequence in the Møre Basin. Geometrical characteristics from that study concluded with mainly upward doming events at the upper part, and size distribution similar to those presented in this study.

Based on the vertical position of the amplitude anomalies and the interval termination of the HTVC's, the fluid/gas migration can be correlated to one specific stratigraphic interval at the Tang formation for all the HTVC's in this thesis study (Figure 6.7). This interval is the shallowest occurrence observed regarding these anomalies, and suggests that the development resulted in hydrothermal derived material and fluid expulsions at the seabed in the late Paleocene, early Eocene period.

All interpretations done of the HTVC's in seismic data, needs to take into account the possibilities of seismic artefacts. For example, high amplitude sill events above the study interval may cause velocity pull-down, reflection multiples or alter the original seismic image (Schroot and Schüttenhelm, 2003). To account for this a study of synthetic seismic is undertaken, in the aim of validating the interpretation and to view how well the seismic data are able to reproduce the structural features.

8.2 Synthetic seismic

Synthetic imaging of geological structures can lead to better interpretation and understanding of limitations and potential pit-falls in seismic data. Synthetic modelling can give a higher level of confidence when interpreting different geological features in the subsurface. The main task here is to present the use of synthetic methodology to study the impact and geometry of piercement structures in sedimentary basins. The evolution of the piercement structure is based on the sandbox experiment described in Chapter 7. Seismic imaging requires an input of elastic

properties (Vp and Vs velocities). These properties were retrieved from the well data at the interval of the HTVC's in the Møre Basin. The depth of the model is approximately 3200 meters, and regarded as fairly deep in conventional seismic. Changing the illumination direction by manipulating the ray-path and offset angle can contribute to retrieve and highlight internal structures in the specific model (I_{SR} illumination vector, Figure 5.5, B) (Lecomte et al., 2015). These parameters are therefore tested during the seismic modelling procedure with a span of 25°-90°. The synthetic model was able to capture complex features of the piercement structure and produce realistic geometries and deformation fields.

The synthetic modelling emphasizes on the impact of internal structure in terms of seismic amplitude anomalies and offset angles (Figure 7.5 shows comparison between the different modelling results). Even though the different seismic images produced are similar, there are clear differences between them. One of the most prominent characteristic when comparing the 25° to 45° max dip, is how the reflectors in the images are displayed (Figure 8.1). By increasing the distance between source and receiver, a greater coverage could be obtained. But this also leads to restriction on the inbound angle of which the receiver can detect the ray signals. If the reflected energy from dipping rock-layers leads to more spread in wave energy and longer traveling distance, it might surpass the receiver and fail to appear on the seismogram (Drottning et al., 2009).

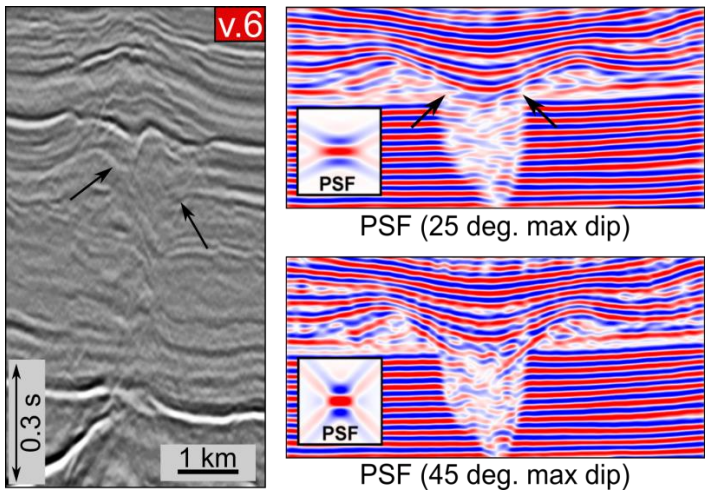

Figure 8.1: To the right: HTVC (v.6) seismic section, illustrating how the dipping reflectors in the conduit zone are displayed in the data (See also Figure 6.28). Black arrows indicate steeply dipping reflectors within the disrupted conduit. To the left: 45° and 25° max dip illumination in the seismogram. The two figures illustrate how offsets angles can restrict dipping reflectors. Black arrows indicate structural differences between the two angel dependent models.

From both the seismic and the synthetic section the near horizontal reflectors are displayed properly (Figure 8.1), but this is not the case regarding the dipping reflectors. The combination of offset angle and layer dip makes for two different structural interpretations of the seismograms. When comparing these results to the actual seismic section of the HTVC's, one can see that the dipping reflectors in the conduit zone usually do not exceeding c. 45°- 50°. This could imply that

the processed data is unable to properly visualize reflections above this angle. A reasonable maximum illuminated dip is taken to be about 45°. A direct implication of this is that strongly dipping structural features within the HTVC's can be overlooked or that interpretation within certain intervals is incorrect. The synthetic modelling thereby provides a method for more confident interpretations of geological features, plus the ability to validate seismic attributes and artefacts to avoid pit-falls and misinterpretations.

8.3 HTVC composition and Well-tie

Similar structures as the HTVC's described at the mid-Norwegian Margin by Hansen et al., (2005) and Hjelstuen et al., (1997) are known to have origin in sedimentary units. These are characterised by extremely low density and high porosity in the ooze layers at the Tare and Brygge formation. In this study, the interval of the HTVC's is characterized by a relatively low gamma-ray response suggesting a homogeneous clay and sandstone composition within the Tang Formation (Figure 8.2). Determining the exact composition of the HTVC's in the Møre Basin is difficult since no vents or conduits have been drilled through in this part. The interpretation of material-composition is therefore based on the completion logs together with seismic amplitudes.

Some materials, although they have completely different composition, can display somewhat similar seismic property (Rollet et al., 2012). This makes it difficult to distinguish between them, and opens up for misinterpretation. Igneous or magmatic compositions are expected to reflect waves in a more significant manner then the host rock. However, hydrothermal alternated material and/or gas pockets may also display highly reflective boundaries and bright spots (Judd and Hovland, 1992, 2007)

During exploration drilling, a few HTVC have been sampled. One example is the well 6607/12-1, drilled in 1986 in the Vøring Basin (Svensen et al., 2003). This provides a unique opportunity to study the geological framework and the structural development of the HTVC. The upper part of one HTVC was penetrated, revealing material from remobilized sediments together with remanence of mafic fragments interpreted to have been broken off the sill and transported to the surface. No direct evidence of large scale material transport or deposition on the paleosurface has been established with the well parameters at the Møre Basin. However, the same remobilization mechanism of sediments in the conduit is believed to have occurred.

Care has been taken during the interpretation to ensure stratigraphic control of the depth by check-shot implementation. This correlation is important when mapping out key horizons such as the Top Tang paleosurface and the Top Tare Mound horizon. The well data and check-shot measurements conclude that all HTVC's mapped out in this study terminates at on constant stratigraphic interval. Velocity from well data has been implemented at transitions zones between main lithological formations (Figure 6.4 and 8.2).

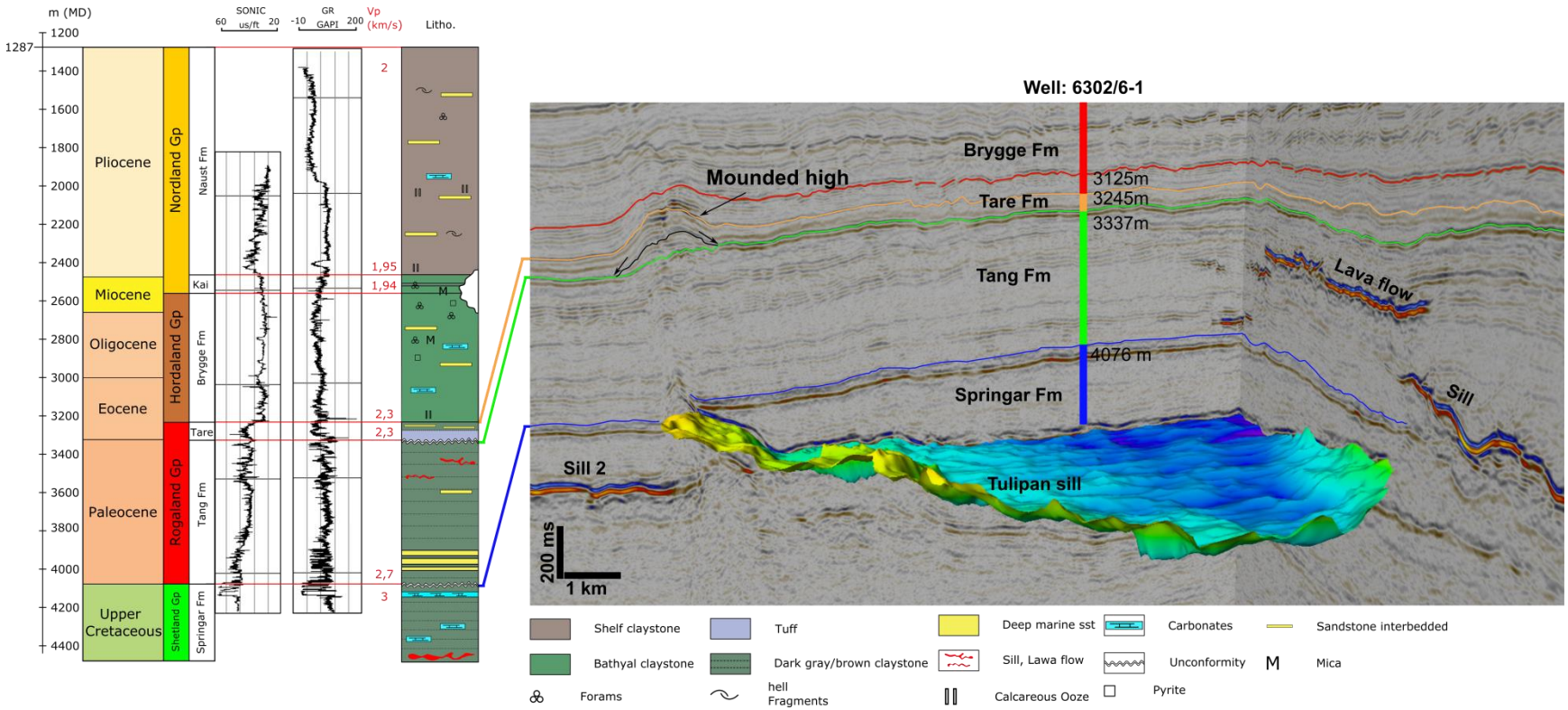

Figure 8.2: Figure summarizing different methods implemented to resolve the key questions regarding the HTVC's in the Møre Basin. The investigation has focus on (1) the vent complex geometries, (2) the induced surface deformation patterns, (3) the intrusions (heat source) relation, as well as (4) the emplacement depth and age of the hydrothermal vent complexes.

8.4 HTVC formation

The formation of HTVC's requires that fluid pressure at the contact aureole overcomes the equilibrium threshold from the opposing hydrostatic pressure. Instantaneous overpressure release can only occur if the pressure build-up is faster than the pressure release and seepage in the host-rock. Jamtveit et al., (2004) proposed a model in which they discuss the condition of overpressure generated at the sill-sediment interface in nature. Their presentation suggests that venting mechanism is based on boiling of pore water as the cause for pressure build-up at the contact aureole around the sill intrusion (Figure 2.7). Lithological results from well 6302/6-1 show that the host rock consists of primarily mudstone, claystone and sandstone at the conduit interval. Because of this composition, water is expected to have been generated due to breakdown of hydrous minerals, as the sill intruded (e.g., Aarnes et al., 2010). The amount of fluids generated are expected to be related to the overall thickness of the aureole, which again depends on the initial temperature of the host, as well as the thickness and temperatures of the intruding sills (Aarnes et al., 2010). From the seismic interpretation the intruding sills are easily recognised due to their impedance contrast. This is not the case for the affected contact aureoles. In this study, no clear evidence of material alteration around the sills has been proven.

Fluids generated at the contact aureoles will have greater buoyancy compared to the water trapped in the sediments, and of the solid component at the host due to thermal expansion and alteration. Presence of lighter components such as methane may enter the fluids, as breakdown of organic rich matter in the sedimentary rocks during thermal maturation (Svensen and Jamtveit, 2010; Wang and Manga, 2015). The amount these light components depends on the total amount of organic carbon of the host.

As a result, the confined high pressure fluids tend to rise through the sedimentary strata reaching the paleosurface. The same effect can be seen in the seismic study-interval of the HTVC. The fracturing of pore space or instant opening of pre-existing cracks under pressure build-up can be seen as vertical conduit pathways.

HTVC's and similar piercement structures (e.g., mud volcanos and kimberlite pipes) are common in nature. Similar for all these structures are the development due to abrupt release of pressurized fluids, forced through sediments and rocks (Nermoen et al., 2010). Under circumstances where the flux rate of fluids is low, the discharge rate through the medium will follow Darcy's Law. This imply that the instantaneous release is dependent on the permeability of the host rock, together with the viscosity of the fluid over a given distance (Whitaker, 1986). If the fluids generated are greater than the flux, a critical state is reach and venting can occur.

8.5 HTVC formation and the sandbox experiment

In this section, discussion on similarities between the HTVC's seen in seismic data compared to structures gathered during the sandbox experiment is presented. It is clear from the previous section that HTVC's are dependent on focused flow to generate the structural features seen in the seismic imaging. When comparing seismic cross-sections of HTVC's against the sandbox

experiments, similarities can be observed (Figure 6.23 and 7.2). When fluid pressure increases beyond the equilibrium threshold, subsequent fracturing and brecciating above the source will develop. The fluidized zone in the sandbox experiment will act in the same way as the conduit zone in the natural setting, a path way for fluids to reach the surface. The fluidized zone in the sandbox experiment develops two well-defined sections, the first consisting of a narrow lower pipe/conduit zone and the other consisting of an upper crater zone (Figure 7.2). These two morphological features can be correlated to the upper and lower part of the HTVC's (e.g., Jamtveit et al., 2004; Planke et al., 2005).

Field data show that the HTVC's contains brecciated elements with lithological differences compared to the surrounding strata (Jamtveit et al., 2004; Svensen et al., 2006). This is also seen in the fluidized pipe/conduit zone of the sandbox experiment. Observations in field, seismic and experiment show inward dipping strata above the source/inlet and the center of the structure (e.g., Planke et al., 2003; Svensen et al., 2003). The experiment time-lapse presentation in Figure 7.1 suggests convective flow during material transport, resulting in volume reduction that causes the upper sediments to collapse downwards creating the inward dipping beds.

Size comparison has been undertaken between the sandbox results and the seismic results. Although HTVC's are symmetrical structures formed in a 3 dimensional setting and the sandbox experiment consists of a planar 2 dimensional structure in a confined cell, correlation of basic parameters such as sizes and width/height ratios can be performed.

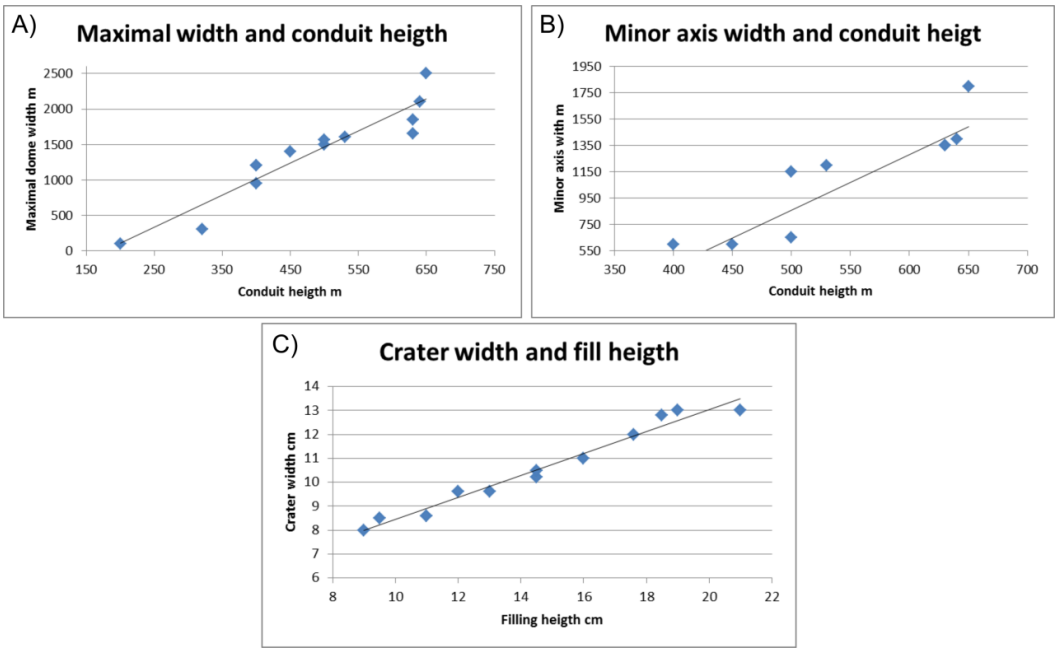

Figure 8.3: Comparison-plot between HTVC's and piercement structures in the sandbox experiment: A) Maximal with of the dome structure plotted against the conduit. B) Minor axis with of the dome structure plotted against the conduit height. C) Pipe/conduit length plotted against the crater width (in sandbox experiment). See table 6.1 for vent statistics, and table 7.1for experimental statistics.

Figure 8.3 shows similarities between at the upper part of the HTVC's compared to the upper part of the sandbox structures. The plots show that crater/dome structures scales approximately linearly with the conduit/filling height ratio. This is a trend also seen in the seismic data, where the longer conduit zones develop larger surface patterns. Although the linearity may not represent the best fit in terms of the actual HTVC's, the height/width dependency is clearly visible.

8.6 Dome shape and differential compaction model

From the sandbox experiment one can clearly see the crater morphology above the fluidized conduit zone (Figure 7.2). The opposite is found regarding the HTVC's interpreted in this thesis. The formation of HTVC's at the Top Tang horizon shows few direct indications of crater shapes (See appendix A.1 for detailed mapping), instead the characteristic down lapping dome structure on paleosurface define the upper part geometry (Figure 6.25). To correlate the doming structures to the observation of piercement structures in the sandbox experiment, one model related to differential compaction is proposed.

Differential compaction develops in for instance inhomogeneous sedimentary deposits, where the material properties vary (e.g., Miles and Cartwright, 2010; Jackson, 2012; Zhao et al., 2014). All materials that are undergoing additional load will compact due to gravitational stresses. Variation in how the different materials behave during this process is dependent on their composition. The result can be seen as local areas compacting more than others, and that geological structures may be affected geometrically during compaction stresses. This process have previously been described in terms of the upper vent geometry by Skogseid et al., (1992) and Planke et al., (2005), where it was considered as a possibility for the vent-fill to compact less than the surrounding strata, thus causing the characteristic dome morphology.

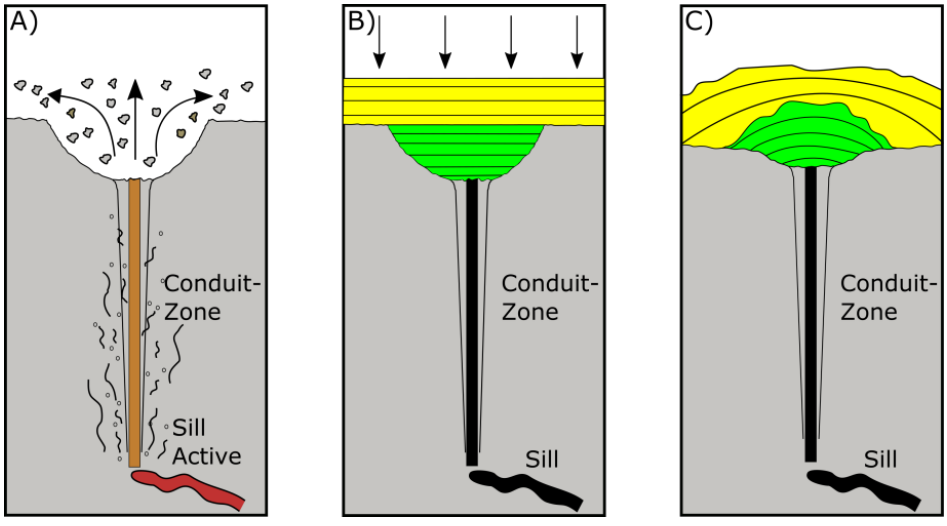

Figure 8.4: The differential compaction model: A) The model starts out as a crater or depression at the paleosurface caused by underlying expulsion and collapse of the affected strata. B) Sedimentation on the seafloor illustrated by the yellow layer and overburden stress illustrated by black arrows. The green area illustrates the hydrothermal

altered material. D) Sediment load compact surrounding strata more than the hardened vent material. Dome feature arise after sufficiently thick sediment loads is deposited on top of it.

Reflections traced above the upper vent and dome is interpreted as stratal reflections (i.e., related to bedding). These reflections show little variation in thickness and no onlap on the dome itself. Based on these observations, the tree dimensional dome is thought unlikely to form due to conventional sediment deposition, or due to compression from the vent sides. Instead, the most probable explanation regarding doming is the differential compaction model.

8.7 Timing and age of the Møre Basin vent complexes

Age determination of the HTVC's in this thesis is based upon the results obtained during seismic interpretation, well-tie correlations and the palynological reports focusing on the sediment layers at the HTVC interval. The Top Tang paleosurface is defined as the time-horizon of emplacement regarding the HTVC's. The intrusive nature of the conduit zone below and the observation of down-lapping domes onto the paleosurface argue for formation at this interval. From the well data and check-shots logs, the measured depth of the Top Tang horizon is correlated to 3335 m (figure 6.7 and 8.2). This stratigraphic interval has been linked to the presence of the palynomorphs *Apectodinium augustum*. This is a species that is now considered to be diagnostic of the Paleocene-Eocene time period (Schmitz et al., 2004; Sluijs et al., 2006). The palynological investigation confirms that this depth contains the last natural occurrence of *A. augustum*, and makes this a key taxa with high resolution at this interval (Planke et al., 2007). Some other taxa have also been recorded (e.g., first appearance of Phelodinium, and last occurrence of *Cerodinium dartmoorium*), and may be used to refine the age of the sediments with greater confidence.

The suggested age and timing of the HTVC's in the Møre Basin is estimated to be within the earliest Paleocene-Eocene transition period at 54.9-55.8 Ma.

8.8 Basin evolution and Implications

8.8.1 Paleocene-Eocene thermal maximum (PETM)

In the previous section a correlation between timing and age of HTVC's was established. The age determined coincide with one of the most extreme transient shifts in the Cenozoic time. The Paleocene-Eocene Thermal Maximum (PETM) occurred at ~55 Ma and lasted between 100-200 kyr (e.g., Norris and Röhl, 1999; Röhl et al., 2000; Röhl et al., 2007) (Figure 8.5). This event is associated with a significant temperature rise of the oceans and the atmosphere, together with changes in ocean chemistry and extinction of benthic foraminiferal species traceable in the biostratigraphical record (e.g., Bice and Marotzke, 2002; Kennett and Stott, 1991; Röhl et al., 2000; Röhl et al., 2007).

The PETM is coeval with the initial opening of the NE Atlantic Ocean, which has been linked to magma intruding the Møre Basin (e.g., Faleide et al., 2008). These sill intrusives are recognised in the seismic section as the heat source thought to have initiated the HTVC's. Although no direct evidence for contact aureoles have been established during the seismic interpretation, the relation between contact metamorphism and sill intrusions are known to provide a link between the release of carbon gasses, such as CH_4 and CO_2 into the oceans or atmosphere (e.g., Aarnes et al., 2015; Brekke, 2000). The observations of vertical conduit zones together with the observed mechanisms of venting in the sandbox experiment, suggest an efficient pathway for fluid and gasses stored in the sedimentary basins. Vent complex statistics from both the Møre and Vøring basins done by Planke et al., (2005) could indicate that the supposedly thousands of individual HTVC's formed within this timespan, may have acted as one of the main triggers for concentrated carbon-gas levels. Sedimentary basins influenced by LIP's and coherent HTVC's, can thus provide a setting for rapid carbon-gas emissions of otherwise steady seeping reservoirs.

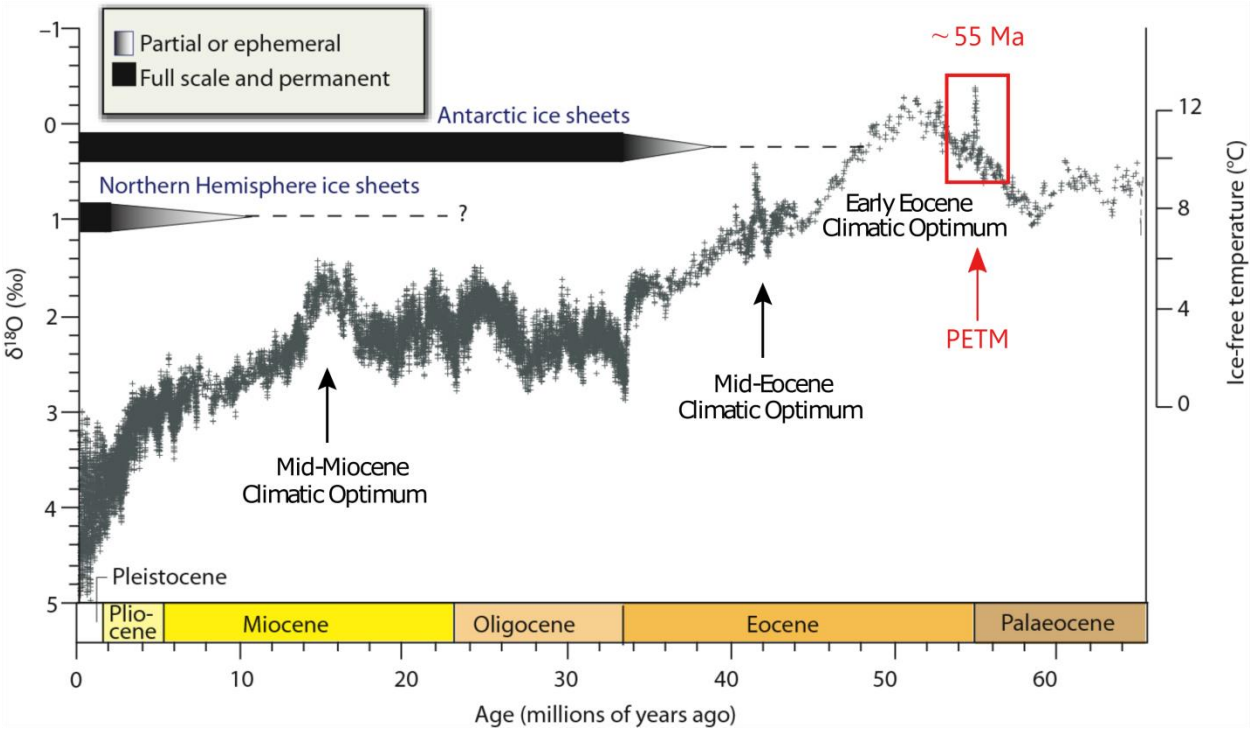

Figure 8.5: Slightly modified Cenozoic climate curve taken from Zachos et al., (2008). The curve is a stacked deep-sea benthic foraminifera oxygen-isotope curve based on the Ocean Drilling Program (OPD) and Deep Sea Drilling Project (DSDP) sites (Zachos et al., 2001; Zachos et al., 2008). The red rectangle is highlighting the PETM peek of the climate curve, coinciding with the HTVC timing and age in the Møre Basin.

8.8.2 Petroleum migration

The presence of HTVC's in sedimentary basins can provide new potential for petroleum generation, accumulation and trapping. The upper part of the HTVC can function as a seal system, utilizing the conduit zone for petroleum migration between potential reservoir units (Planke et al., 2007). At the Møre Basin the HTVC interval is defined by the organic rich clay stone at the Tang Formation. The maturity of the kerogen could be greatly affected by the release of heat from the igneous intrusions (Aarnes et al., 2015). Additionally the Danian sandstone reservoir is seen affected by both sills and the vertical conduit zones. Materials inside the HTVC's and especially the domed upper part have the potential to form stratigraphic reservoir traps, if the material diagenesis provide sufficient seals (Hansen et al., 2005). Some observations of bright-spots at the uppermost part of the dome structure could suggest trapping of gas-pockets (See appendix A.1, V4 section A-A').

9. Conclusions and further suggested studies

The regional seismic mapping in the Møre Basin off mid Norway has documented an extensive hydrothermal vent complex assemblage at the Paleocene-Eocene interval. 13 individual vent complexes have been mapped out within the main study area measuring approximately 310 km^2. All the venting structures observed are located above sill intrusions, and are therefore assumed to develop as a direct consequence of igneous intrusive events. The complex architecture associated with the HTVC's represents sediment mobilization structures, caused by injection of fluid and gas along vertical deep-seated conduit pathways. The HTVC's were formed primarily during explosive eruption of gasses, liquids and sediments, resulting in depressions and craters at the seafloor. The upper parts of the HTVC's in this study are dominated by domes and mounded features measuring upwards to 2.5 km in diameter and 120 meters in height. This upper geometry is thought to be a result of structural basin modification described in Figure 8.4. The upper part of the vent complexes are terminating at one consistent interval at the transition Paleocene-Eocene at the Tang Formation. By implementing well-tie correlations and biostratigraphical analysis the age of these structures have been determined to lie within the range of 54.9-55.8 Ma. This period is characterized by the intrusive events during the initial volcanism phase at the mid-Norwegian Margin, corresponding to the NE Atlantic break-up. Timing of the HTVC's coincides with one of the most extreme climatic shifts in the Cenozoic time called the Paleocene-Eocene Thermal Maximum. Due to the HTVC's architecture a link between the release of carbon gasses stored in the basins into the oceans and atmosphere can be established.

This thesis has used state-of-the-art methods to produce unique 3D images of seismic reflection-data together with simulated modelling to map out the HTVC's within the Møre Basin. The methods utilized, demonstrate how the final analyses can provide new images of sediment deformation and fluid/gas migration patterns using 3D seismic and modelling procedures. Combining this, makes it possible to recognize geometry with considerable confidence, and furthermore mapping out important relationships between fluid-flow pathways and structural behaviour with precision.

For this study only regional investigation of the Tulipan prospect and correlation to nearby basins have been done. Further investigation should focus on establishing a depth and age comparison on especially basins associated with Paleocene-Eocene rifting and continental break-up in the NE Atlantic. This would ensure a better understanding of the implications these venting systems have on previous climatic changes, fluid migrations patterns and overall basin development. Additionally, the modelling undertaken could in the future include more detailed property implementation, such as additional overburden, information between geo-mechanical modelling and lateral property variations in the layers.

References

Aarnes, I., Planke, S., Trulsvik, M., and Svensen, H., 2015, Contact metamorphism and thermogenic gas generation in the Vøring and Møre basins, offshore Norway, during the Paleocene–Eocene thermal maximum: Journal of the Geological Society, v. 172, no. 5, p. 588-598.

Aarnes, I., Svensen, H., Connolly, J. A., and Podladchikov, Y. Y., 2010, How contact metamorphism can trigger global climate changes: Modeling gas generation around igneous sills in sedimentary basins: Geochimica et Cosmochimica Acta, v. 74, no. 24, p. 7179-7195.

Barrington, J., and Kerr, P. F., 1961, Breccia pipe near Cameron, Arizona: Geological Society of America Bulletin, v. 72, no. 11, p. 1661-1674.

Bell, B., and Butcher, H., 2002, On the emplacement of sill complexes: evidence from the Faroe-Shetland Basin: Geological Society, London, Special Publications, v. 197, no. 1, p. 307-329.

Bice, K. L., and Marotzke, J., 2002, Could changing ocean circulation have destabilized methane hydrate at the Paleocene/Eocene boundary?: Paleoceanography, v. 17, no. 2.

Botter, C., Cardozo, N., Hardy, S., Lecomte, I., and Escalona, A., 2014, From mechanical modeling to seismic imaging of faults: A synthetic workflow to study the impact of faults on seismic: Marine and Petroleum Geology, v. 57, p. 187-207.

Brekke, H., 2000, The tectonic evolution of the Norwegian Sea continental margin, with emphasis on the Voring and More basins, Special Publication-Geological Society of London, Volume 167, p. 327-378.

Buckley, S. J., Kurz, T. H., Howell, J. A., and Schneider, D., 2013, Terrestrial lidar and hyperspectral data fusion products for geological outcrop analysis: Computers & Geosciences, v. 54, p. 249-258.

Cartwright, J. A., 1994, Episodic basin-wide fluid expulsion from geopressured shale sequences in the North Sea basin: Geology, v. 22, no. 5, p. 447-450.

Chevallier, L., and Woodford, A., 1999, Morpho-tectonics and mechanism of emplacement of the dolerite rings and sills of the western Karoo, South Africa: South African Journal of Geology, v. 102, no. 1, p. 43-54.

Cicchino, A., Sargent, C., Goulty, N., and Ramdhan, A., 2015, Regional variation in Cretaceous mudstone compaction trends across Haltenbanken, offshore mid-Norway: Petroleum Geoscience, v. 21, no. 1, p. 17-34.

Dalland, A., Worsley, D., and Ofstad, K., 1988, A Lithostratigraphic Scheme for the Mesozoic and Cenozoic and Succession Offshore Mid-and Northern Norway, Oljedirektoratet.

Deagan, C., and Scull, B., 1977, A proposed standard lithostratigraphic nomenclature for the Central and Northern Sea: Rep. Inst. Geol. Sci., n. 77/25: Bulletin NPD, no. 1.

Dickens, G. R., O'Neil, J. R., Rea, D. K., and Owen, R. M., 1995, Dissociation of oceanic methane hydrate as a cause of the carbon isotope excursion at the end of the Paleocene: Paleoceanography, v. 10, no. 6, p. 965-971.

Dorn, G. A., 1999, Method and system for horizon interpretation of seismic surveys using surface draping, Google Patents.

Drottning, A., Branston, M., and Lecomte, I., 2009, Value of illumination-consistent modelling in time-lapse seismic analysis: First break, v. 27, no. 10.

Du Toit, A., 1920, The Karoo dolerites of South Africa: a study in hypabyssal injection: Transactions of the Geological Society of South Africa, v. 23, p. 1-42.

Duncan, R. A., Hooper, P., Rehacek, J., Marsh, J., and Duncan, A., 1997, The timing and duration of the Karoo igneous event, southern Gondwana.

Faleide, J. I., Tsikalas, F., Breivik, A. J., Mjelde, R., Ritzmann, O., Engen, O., Wilson, J., and Eldholm, O., 2008, Structure and evolution of the continental margin off Norway and the Barents Sea: Episodes, v. 31, no. 1, p. 82-91.

Falkowski, P., Scholes, R., Boyle, E., Canadell, J., Canfield, D., Elser, J., Gruber, N., Hibbard, K., Högberg, P., and Linder, S., 2000, The global carbon cycle: a test of our knowledge of earth as a system: science, v. 290, no. 5490, p. 291-296.

Galland, O., Gisler, G. R., and Haug, Ø. T., 2014, Morphology and dynamics of explosive vents through cohesive rock formations: Journal of Geophysical Research: Solid Earth, v. 119, no. 6, p. 4708-4728.

Gibb, F., and Kanaris-Sotiriou, R., 1988, The geochemistry and origin of the Faeroe-Shetland sill complex: Geological Society, London, Special Publications, v. 39, no. 1, p. 241-252.

Grapes, R., Reid, D., and McPherson, J., 1974, Shallow dolerite intrusion and phreatic eruption in the Allan Hills region, Antarctica: New Zealand journal of geology and geophysics, v. 17, no. 3, p. 563-577.

Hansen, J., Cartwright, J., Huuse, M., and Clausen, O. R., 2005, 3D seismic expression of fluid migration and mud remobilization on the Gjallar Ridge, offshore mid-Norway: Basin Research, v. 17, no. 1, p. 123-139.

Haug, Ø. T., Galland, O., and Gisler, G. R., 2013, Experimental modelling of fragmentation applied to volcanic explosions: Earth and Planetary Science Letters, v. 384, p. 188-197.

Heggland, R., 1998, Gas seepage as an indicator of deeper prospective reservoirs. A study based on exploration 3D seismic data: Marine and Petroleum Geology, v. 15, no. 1, p. 1-9.

Helsem, A., 2006, 6302/6-1 (Tulipan) discovery report, Statoil reportp. 51 pp.

Hjelstuen, B. O., Eldholm, O., and Skogseid, J., 1997, Vøring Plateau diapir fields and their structural and depositional settings: Marine Geology, v. 144, no. 1, p. 33-57.

Hovland, M., and Judd, A., 1988, Seabed pockmarks and seepages: Impact on geology, biology and the marine environment: London: Graham and Trotman, v. 293.

Jackson, C. A.-L., 2012, Seismic reflection imaging and controls on the preservation of ancient sill-fed magmatic vents: Journal of the Geological Society, v. 169, no. 5, p. 503-506.

Jamtveit, B., Svensen, H., Podladchikov, Y. Y., and Planke, S., 2004, Hydrothermal vent complexes associated with sill intrusions in sedimentary basins: Physical geology of high-level magmatic systems, v. 234, p. 233-241.

Johnson, M., Van Vuuren, C., Visser, J., Cole, D., Wickens, H. d. V., Christie, A., and Roberts, D., 1997, The foreland Karoo Basin, South Africa: African basins. Sedimentary basins of the World, v. 3, p. 269-317.

Jolley, d. w., 2006, Westerly sourced palynofloras in the eocene – paleocene sediments.

Judd, A., and Hovland, M., 2007, Seabed fluid flow—the impact on geology: Biology and the Marine Environment.

Judd, A., and Hovland, M., 1992, The evidence of shallow gas in marine sediments: Continental Shelf Research, v. 12, no. 10, p. 1081-1095.

Kennett, J., and Stott, L., 1991, Abrupt deep-sea warming, palaeoceanographic changes and benthic extinctions at the end: Nature, v. 353, p. 19.

Kopf, A. J., 2002, Significance of mud volcanism: Reviews of Geophysics, v. 40, no. 2.

Krynauw, J., Hunter, D., and Wilson, A., 1988, Emplacement of sills into wet sediments at Grunehogna, western Dronning Maud Land, Antarctica: Journal of the Geological Society, v. 145, no. 6, p. 1019-1032.

Lecomte, I., Gjøystdal, H., and Drottning, Å., Simulated Prestack Local Imaging: a robust and efficient interpretation tool to control illumination, resolution, and time-lapse properties of reservoirs, *in* Proceedings 2003 SEG Annual Meeting2003, Society of Exploration Geophysicists.

Lecomte, I., and Kaschwich, T., Closer to real earth in reservoir characterization: a 3D isotropic/anisotropic PSDM simulator, *in* Proceedings 2008 SEG Annual Meeting2008, Society of Exploration Geophysicists.

Lecomte, I., Lavadera, P. L., Anell, I., Buckley, S. J., Schmid, D. W., and Heeremans, M., 2015, Ray-based seismic modeling of geologic models: Understanding and analyzing seismic images efficiently: Interpretation, v. 3, no. 4, p. SAC71-SAC89.

Lecomte, I., Lavadera, P. L., Kjoberg, S., Botter, C., Anell, I., Buckley, S. J., Eide, C. H., Grippa, A., Mascolo, V., and 2016, 2(3)D convolution modelling of complex
geological targets beyond 1D convolution: fb special topic, no. first break volume 34, May 2016, p. 64-72.

Løseth, H., Wensaas, L., Arntsen, B., and Hovland, M., 2003, Gas and fluid injection triggering shallow mud mobilization in the Hordaland Group, North Sea: Geological Society, London, Special Publications, v. 216, no. 1, p. 139-157.

Mahdi, S., and Ayress, M., 2006, A Biostratigraphical Evaluationof the Pleistocene to Late Cretaceous interval in well 6302/6-1,Tulipan Prospect, NOCS.

Miles, A., and Cartwright, J., 2010, Hybrid flow sills: a new mode of igneous sheet intrusion: Geology, v. 38, no. 4, p. 343-346.

Nermoen, A., Galland, O., Jettestuen, E., Fristad, K., Podladchikov, Y., Svensen, H., and Malthe-Sørenssen, A., 2010, Experimental and analytic modeling of piercement structures: Journal of Geophysical Research: Solid Earth, v. 115, no. B10.

Norris, R. D., and Röhl, U., 1999, Carbon cycling and chronology of climate warming during the Palaeocene/Eocene transition: Nature, v. 401, no. 6755, p. 775-778.

Npd.no (2016) "Well 6302/6-1". Available at: http://factpages.npd.no (Accessed: 18.03.2016)

Planke, S., Rasmussen, T., Rey, S., and Myklebust, R., Seismic characteristics and distribution of volcanic intrusions and hydrothermal vent complexes in the Vøring and Møre basins, *in* Proceedings Geological Society, London, Petroleum Geology Conference series 2005, Volume 6, Geological Society of London, p. 833-844.

Planke, S., Svensen, H., Hovland, M., Banks, D., and Jamtveit, B., 2003, Mud and fluid migration in active mud volcanoes in Azerbaijan: Geo-Marine Letters, v. 23, no. 3-4, p. 258-268.

Planke, S., Svensen, H., Malthe-Sørensen, A., Planke, E., and Polteau, S., 2007, Tulipan Peteroleum System and Paleogene Volcanism.

Planke, S., Svensen, H., Myklebust, R., Bannister, S., Manton, B., and Lorenz, L., 2014, Geophysics and Remote Sensing.

Rogers, A. W., Du Toit, A. L., and Broom, R., 1905, An introduction to the geology of Cape Colony, Longmans, Green and co.

Rollet, N., McGiveron, S., Hashimoto, T., Hackney, R., Petkovic, P., Higgins, K., Grosjean, E., and Logan, G. A., 2012, Seafloor features and fluid migration in the Capel and Faust basins, offshore eastern Australia: Marine and Petroleum Geology, v. 35, no. 1, p. 269-291.

Ross, J. A., Peakall, J., and Keevil, G. M., 2011, An integrated model of extrusive sand injectites in cohesionless sediments: Sedimentology, v. 58, no. 7, p. 1693-1715.

Rowsell, D., and De Swardt, A., 1976, Diagenesis in Cape and Karoo sediments, South Africa, and its bearing on their hydrocarbon potential: Transactions of the Geological Society of South Africa, v. 79, no. 1, p. 81-145.

Röhl, U., Bralower, T., Norris, R., and Wefer, G., 2000, New chronology for the late Paleocene thermal maximum and its environmental implications: Geology, v. 28, no. 10, p. 927-930.

Röhl, U., Westerhold, T., Bralower, T. J., and Zachos, J. C., 2007, On the duration of the Paleocene-Eocene thermal maximum (PETM): Geochemistry, Geophysics, Geosystems, v. 8, no. 12.

Saunders, A., Fitton, J., Kerr, A. C., Norry, M., and Kent, R., 1997, The north Atlantic igneous province: Large igneous provinces: Continental, oceanic, and planetary flood volcanism, p. 45-93.

Schmitz, B., Peucker-Ehrenbrink, B., Heilmann-Clausen, C., Åberg, G., Asaro, F., and Lee, C.-T. A., 2004, Basaltic explosive volcanism, but no comet impact, at the Paleocene–Eocene boundary: high-resolution chemical and isotopic records from Egypt, Spain and Denmark: Earth and Planetary Science Letters, v. 225, no. 1, p. 1-17.

Schroot, B. M., and Schüttenhelm, R. T., 2003, Shallow gas and gas seepage: expressions on seismic and otheracoustic data from the Netherlands North Sea: Journal of Geochemical Exploration, v. 78, p. 305-309.

Skogseid, J., Pedersen, T., Eldholm, O., and Larsen, B. T., 1992, Tectonism and magmatism during NE Atlantic continental break-up: the Vøring Margin: Geological Society, London, Special Publications, v. 68, no. 1, p. 305-320.

Sluijs, A., Schouten, S., Pagani, M., Woltering, M., Brinkhuis, H., Damsté, J. S. S., Dickens, G. R., Huber, M., Reichart, G.-J., and Stein, R., 2006, Subtropical Arctic Ocean temperatures during the Palaeocene/Eocene thermal maximum: Nature, v. 441, no. 7093, p. 610-613.

STOSE, G. W., and LEWIS, J. V., 1916, Triassic igneous rocks in the vicinity of Gettysburg, Pennsylvania: Geological Society of America Bulletin, v. 27, no. 1, p. 623-644.

Svensen, H., and Jamtveit, B., 2010, Metamorphic fluids and global environmental changes: Elements, v. 6, no. 3, p. 179-182.

Svensen, H., Jamtveit, B., Planke, S., and Chevallier, L., 2006, Structure and evolution of hydrothermal vent complexes in the Karoo Basin, South Africa: Journal of the Geological Society, v. 163, no. 4, p. 671-682.

Svensen, H., Planke, S., Chevallier, L., Malthe-Sørenssen, A., Corfu, F., and Jamtveit, B., 2007, Hydrothermal venting of greenhouse gases triggering Early Jurassic global warming: Earth and Planetary Science Letters, v. 256, no. 3, p. 554-566.

Svensen, H., Planke, S., and Corfu, F., 2010, Zircon dating ties NE Atlantic sill emplacement to initial Eocene global warming: Journal of the Geological Society, v. 167, no. 3, p. 433-436.

Svensen, H., Planke, S., Jamtveit, B., and Pedersen, T., 2003, Seep carbonate formation controlled by hydrothermal vent complexes: a case study from the Vøring Basin, the Norwegian Sea: Geo-Marine Letters, v. 23, no. 3-4, p. 351-358.

Svensen, H., Planke, S., Malthe-Sørenssen, A., Jamtveit, B., Myklebust, R., Eidem, T. R., and Rey, S. S., 2004, Release of methane from a volcanic basin as a mechanism for initial Eocene global warming: Nature, v. 429, no. 6991, p. 542-545.

Svensen, H., Planke, S., Polozov, A. G., Schmidbauer, N., Corfu, F., Podladchikov, Y. Y., and Jamtveit, B., 2009, Siberian gas venting and the end-Permian environmental crisis: Earth and Planetary Science Letters, v. 277, no. 3, p. 490-500.

Svensen, H. H., Polteau, S., Cawthorn, G., and Planke, S., 2015, Sub-volcanic intrusions in the Karoo basin, South Africa.

Walker, G. P., 1993, Basaltic-volcano systems: Geological Society, London, Special Publications, v. 76, no. 1, p. 3-38.

Walters, A., Phillips, J., Brown, R., Field, M., Gernon, T., Stripp, G., and Sparks, R., 2006, The role of fluidisation in the formation of volcaniclastic kimberlite: grain size observations and experimental investigation: Journal of Volcanology and Geothermal Research, v. 155, no. 1, p. 119-137.

Wang, D., and Manga, M., 2015, Organic matter maturation in the contact aureole of an igneous sill as a tracer of hydrothermal convection: Journal of Geophysical Research: Solid Earth, v. 120, no. 6, p. 4102-4112.

Whitaker, S., 1986, Flow in porous media I: A theoretical derivation of Darcy's law: Transport in porous media, v. 1, no. 1, p. 3-25.

Zachos, J., Pagani, M., Sloan, L., Thomas, E., and Billups, K., 2001, Trends, rhythms, and aberrations in global climate 65 Ma to present: Science, v. 292, no. 5517, p. 686-693.

Zachos, J. C., Dickens, G. R., and Zeebe, R. E., 2008, An early Cenozoic perspective on greenhouse warming and carbon-cycle dynamics: Nature, v. 451, no. 7176, p. 279-283.

Zhao, F., Wu, S., Sun, Q., Huuse, M., Li, W., and Wang, Z., 2014, Submarine volcanic mounds in the Pearl River Mouth Basin, northern South China Sea: Marine Geology, v. 355, p. 162-172.

A. Appendix

A.1 Mapping and projection of HTVC's

NS UTM [m]: 705261
EW UTM [m]: 488611
UTM zone: 31

Vent Complex (V1) Central Norwegian margin;

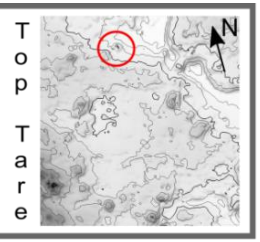

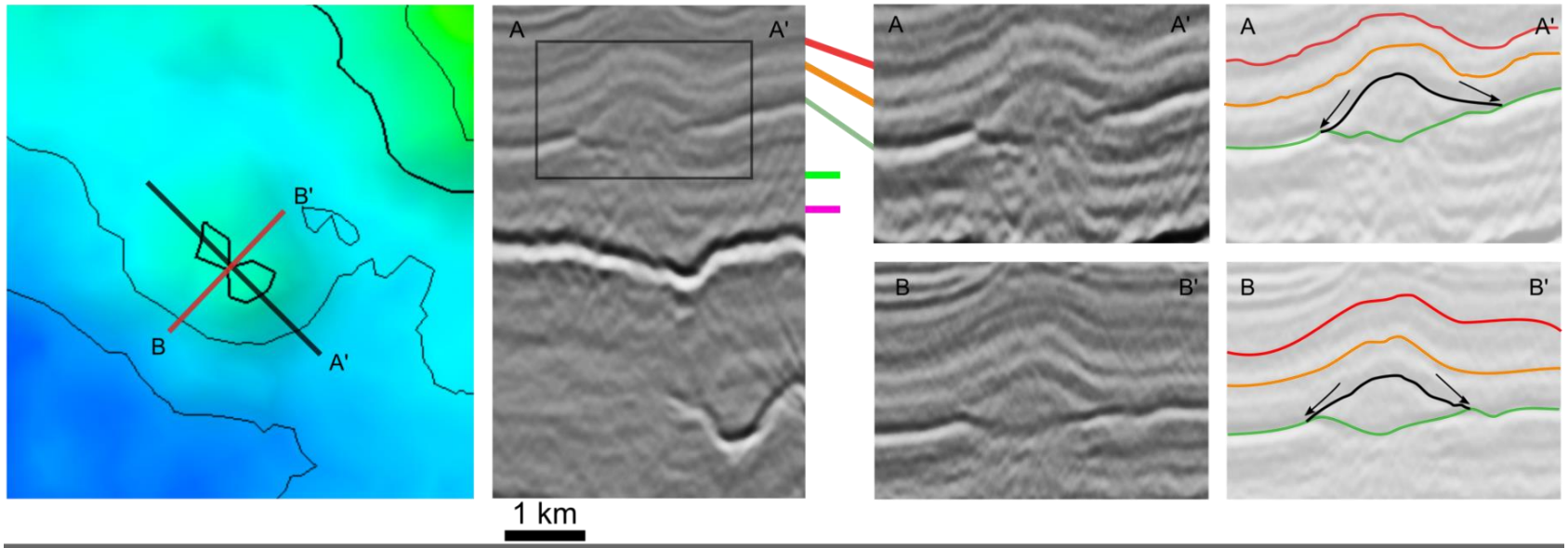

V1:
Measurements:
(See chapter 5 for measurement criteria)

Maximal with: 1400m ± 50m
Minor axis with: 1200m ± 50m
Height: 100m ± 20m

Mapping and description of the (**V1**) HTVC are restricted to the areas between the Top Tare (early Eocene) and the Top Tang (late Palaeocene) reflections.
Structures define as upper part is seen as mounded features on the top Tare horizon.
Dome terminating/down lapping onto the Top Tang paleosurface.
Deeper section (conduit zone) is measured to (approximately **400 m**), from sill intersection to upper part (Top Tang paleosurface).

- Top Tare fm
- Intra Tare
- Top Tang fm
- Intra Tang
- Top Reservoir

NS UTM [m]: 7052506
EW UTM [m]: 488628
UTM zone: 31

Vent Complex (V2) Central Norwegian margin;

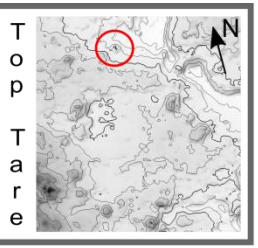

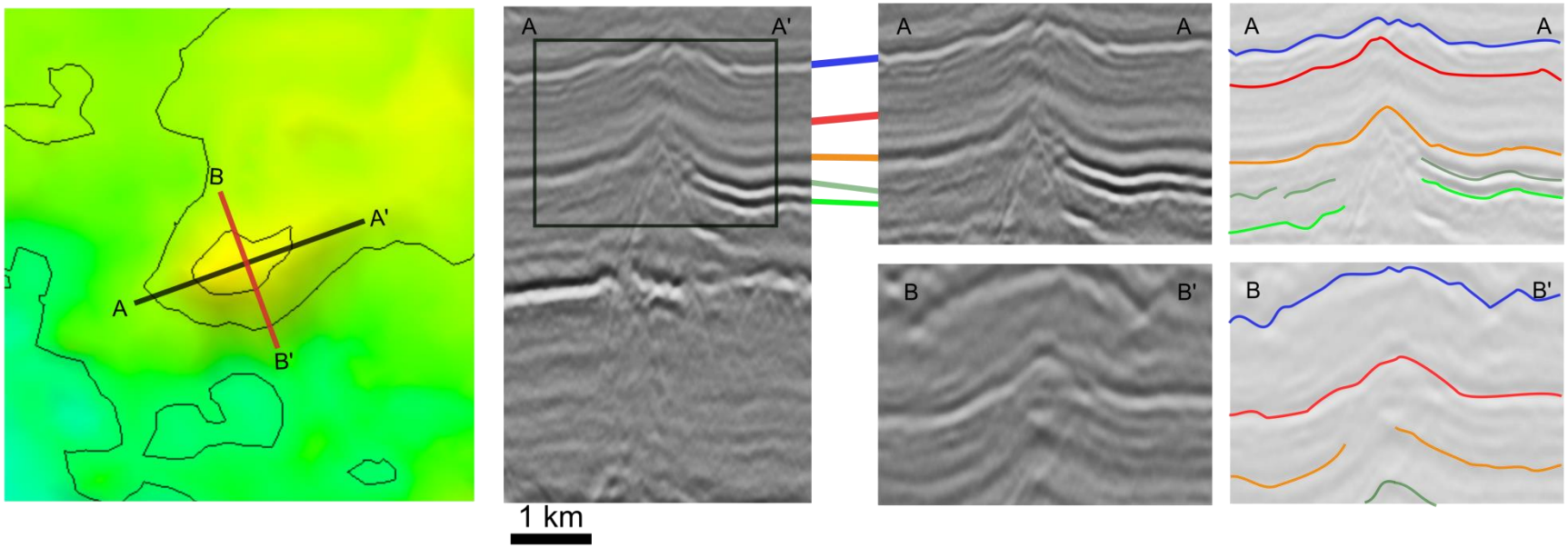

V2:
Measurements:
(See chapter 5: for measurement criteria)

Maximal with: 950m ± 150
Minor axis with: 600m ± 100
Height: 70m

Mapping and description of the (**V2**) HTVC are restricted to the areas between the Top Tare (early Eocene) and the Top Tang (late Palaeocene) reflections.
Structures define as upper part is seen as mounded features on the top Tare horizon.
No down-lapping onto the Top Tang paleosurface observed.
Deeper section (conduit zone) is measured to (approximately **200 m**), from sill intersection to upper part (Top Tang paleosurface)

- Intra Brygge 2
- Top Tare fm
- Intra Tare
- Top Tang fm
- Intra Tang

NS UTM [m]: 7048841
EW UTM [m]: 492436
UTM zone: 31

Vent Complex (V3) Central Norwegian margin;

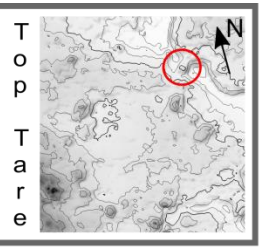

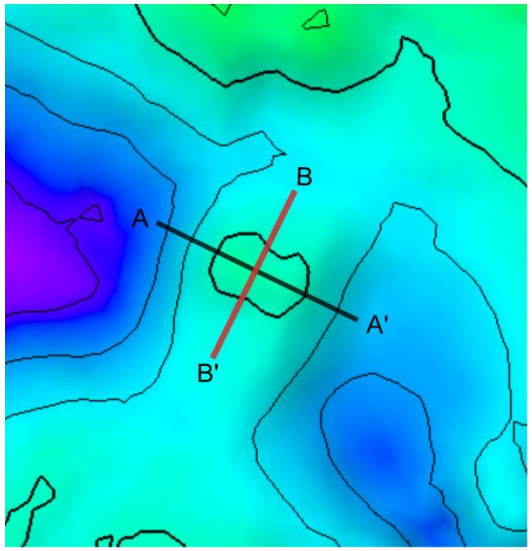

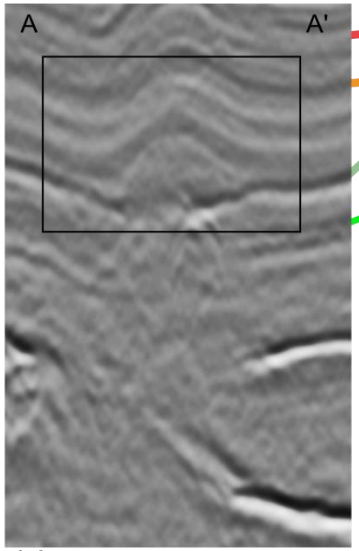

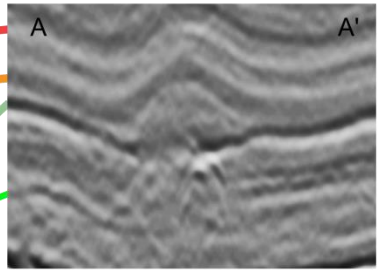

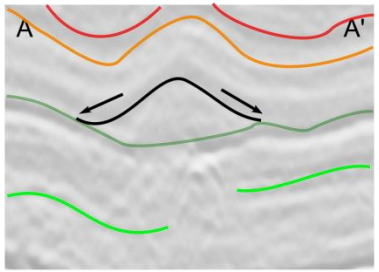

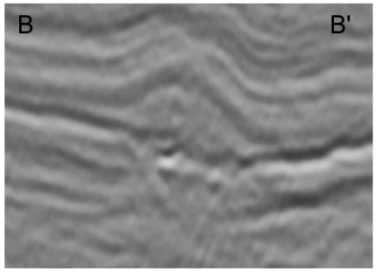

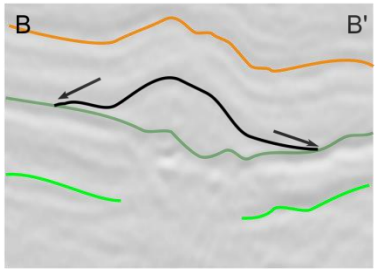

1 km

V3:
Measurements:
(See chapter 5: for measurement criteria)

Maximal with: 1650m ± 100
Minor axis with: 1400m ± 100
Height: 90m

Mapping and description of the (**V3**) HTVC are restricted to the areas between the Top Tare (early Eocene) and the Top Tang (late Palaeocene) reflections.
Structures define as upper part is seen as mounded features on the top Tare horizon.
Dome terminating/down lapping onto the Top Tang paleosurface.
Deeper section (conduit zone) is measured to (approximately **320 m**), from sill intersection to upper part (Top Tang paleosurface)

- Top Tare fm
- Intra Tare
- Top Tang fm
- Intra Tang

NS UTM [m]: 7047062
EW UTM [m]: 490037
UTM zone: 31

Vent Complex (V4) Central Norwegian margin;

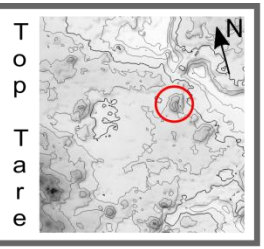

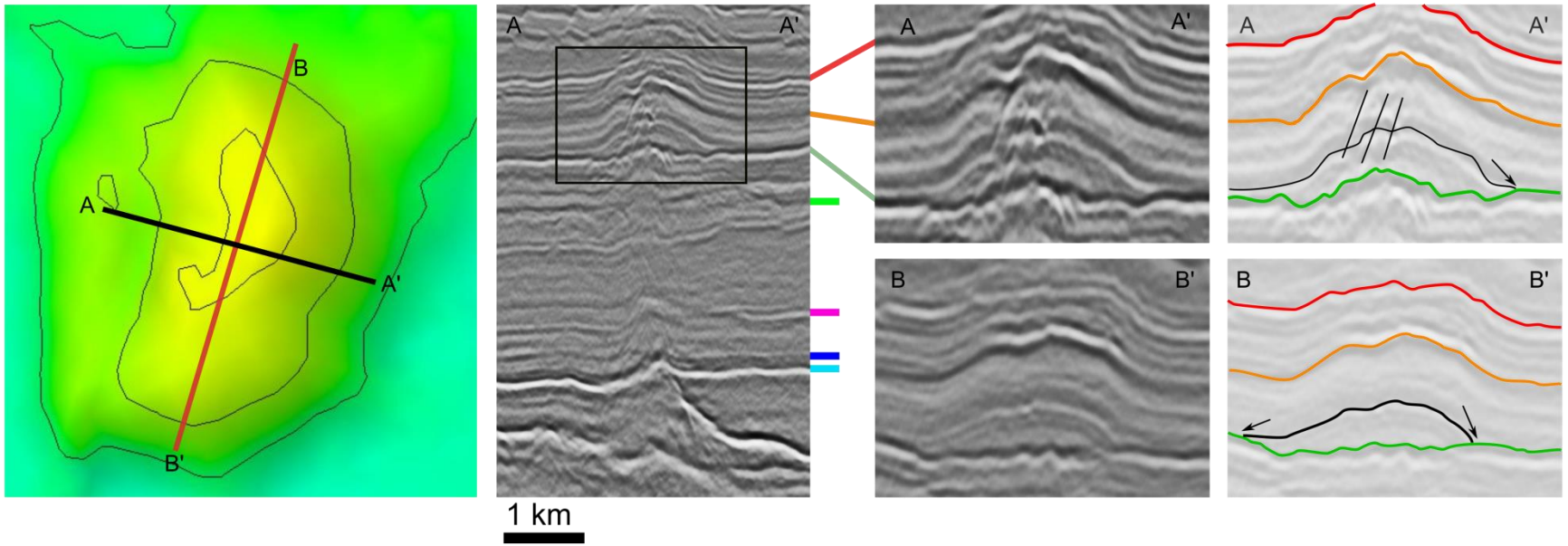

V4:
Measurements:
(See chapter 5: for measurement criteria)

Maximal with: 2100m ± 50
Minor axis with: 1800m ± 100
Height: 100m

Mapping and description of the (**V4**) HTVC are restricted to the areas between the Top Tare (early Eocene) and the Top Tang (late Palaeocene) reflections.
Structures define as upper part is seen as mounded features on the top Tare horizon.
Dome partly terminating/down lapping onto the Top Tang paleosurface.
Deeper section (conduit zone) is measured to (approximately **640 m**), from sill intersection to upper part (Top Tang paleosurface)

- Top Tare fm
- Intra Tare
- Top Tang fm
- Intra Tang
- Top Reservoir
- Top Springar fm
- Carbonate layer

NS UTM [m]: 7049614
EW UTM [m]: 483777
UTM zone: 31

Vent Complex (V5) Central Norwegian margin;

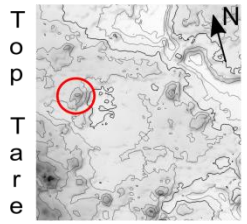

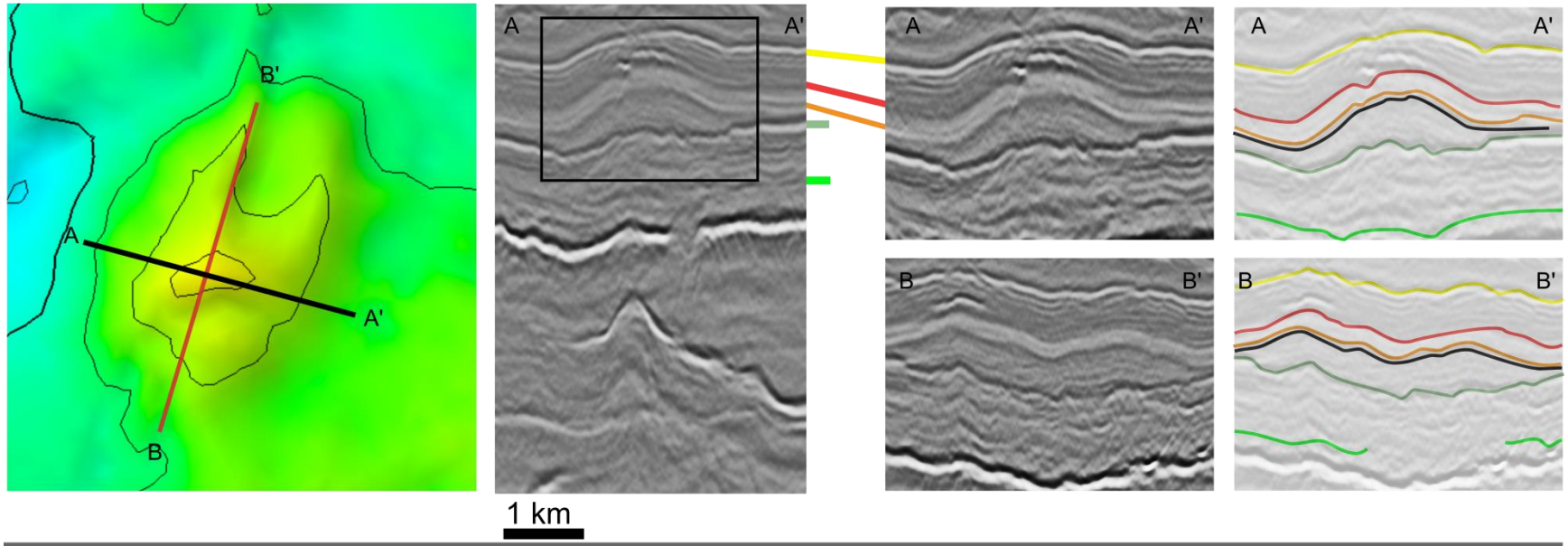

V5:
Measurements:
(See chapter 5: for measurement criteria)

Maximal with: 2500m ± 100
Minor axis with: N/A
Height: 120m ± 50

Mapping and description of the (**V5**) HTVC are restricted to the areas between the Top Tare (early Eocene) and the Top Tang (late Palaeocene) reflections.
Structures define as upper part is seen as mounded features on the top Tare horizon.
Dome partly terminating/down lapping onto the Top Tang paleosurface.
Deeper section (conduit zone) is measured to (approximately **400 m**), from sill intersection to upper part (Top Tang paleosurface)

- Intra Brygge 2
- Top Tare fm
- Intra Tare
- Top Tang fm
- Intra Tang

NS UTM [m]: 7043460
EW UTM [m]: 491769
UTM zone: 31

Vent Complex (V6) Central Norwegian margin;

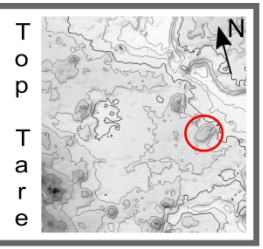

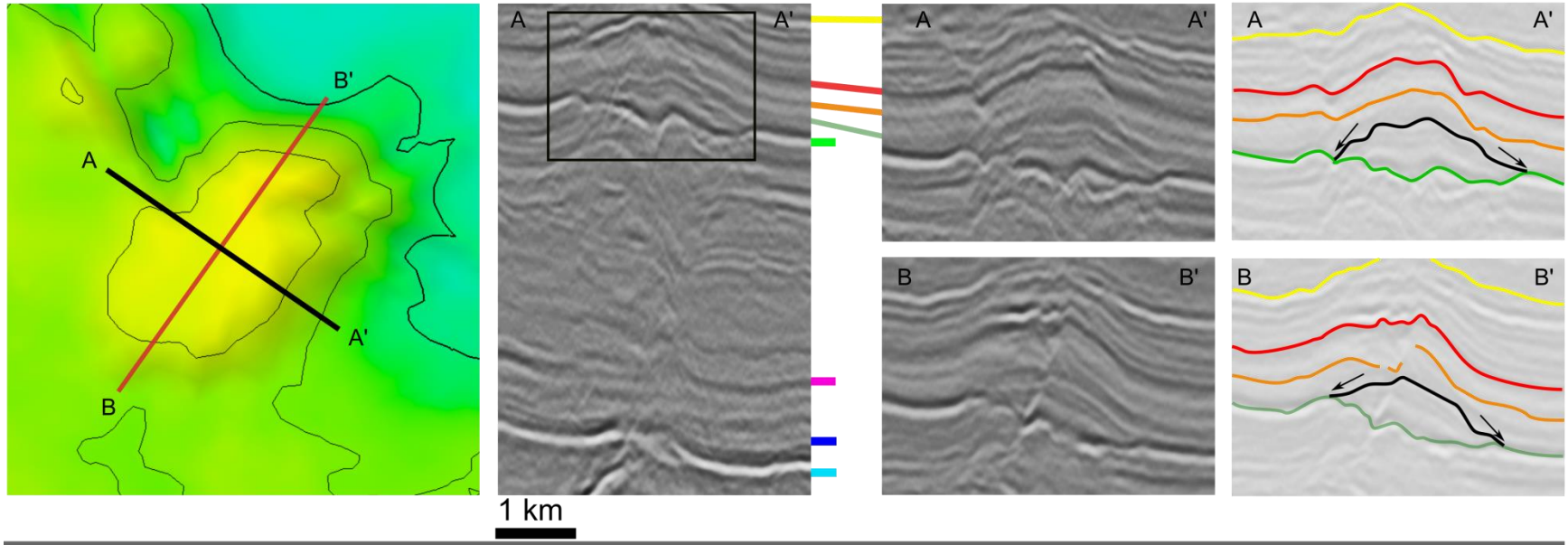

V6:
Measurements:
(See chapter 5: for measurement criteria)

Maximal with: 1850m ± 50
Minor axis with: 1350m ± 50
Height: 80m

Mapping and description of the (**V6**) HTVC are restricted to the areas between the Top Tare (early Eocene) and the Top Tang (late Palaeocene) reflections.
Structures define as upper part is seen as mounded features on the top Tare horizon.
Dome terminating/down lapping onto the Top Tang paleosurface.
Deeper section (conduit zone) is measured to (approximately **630 m**), from sill intersection to upper part (Top Tang paleosurface)

- Intra Brygge 2
- Top Tare fm
- Intra Tare
- Top Tang fm
- Intra Tang
- Top Reservoir
- Top Springar fm
- Carbonate layer

NS UTM [m]: 7038444
EW UTM [m]: 493175
UTM zone: 31

Vent Complex (V7) Central Norwegian margin;

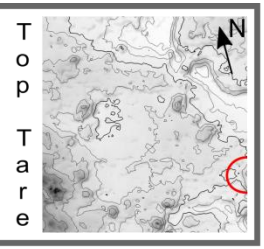

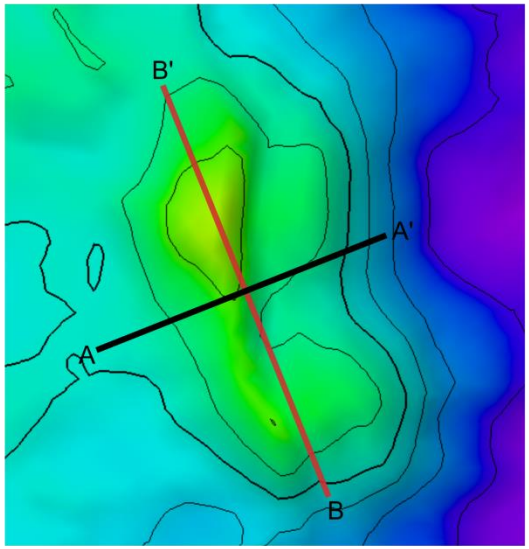

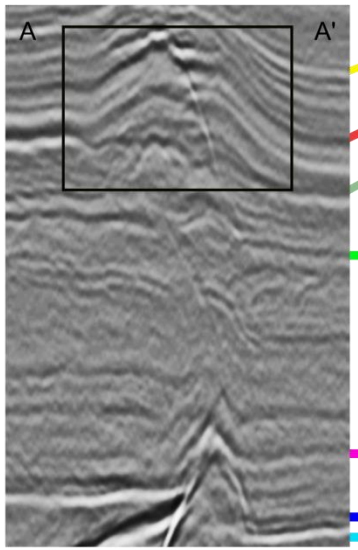

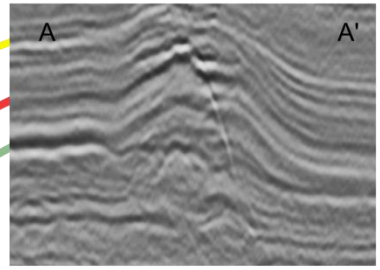

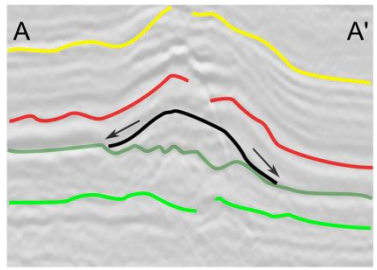

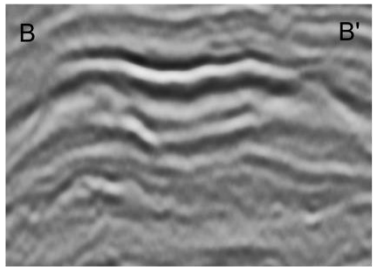

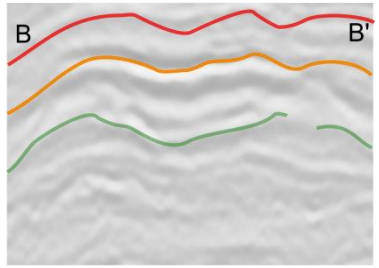

1 km

V7:
Measurements:
(See chapter 5: for measurement criteria)

Maximal with: 1600m ± 100
Minor axis with: N/A
Height: 100m ± 30

Mapping and description of the (**V7**) HTVC are restricted to the areas between the Top Tare (early Eocene) and the Top Tang (late Palaeocene) reflections.
Structures define as upper part is seen as mounded features on the top Tare horizon.
Dome partly terminating/down lapping onto the Top Tang paleosurface.
Deeper section (conduit zone) is measured to (approximately **630m**), from sill intersection to upper part (Top Tang paleosurface)

- Intra Brygge 2
- Top Tare fm
- Intra Tare
- Top Tang fm
- Intra Tang
- Top Reservoir
- Top Springar fm
- Carbonate layer

NS UTM [m]: 7044707
EW UTM [m]: 480978
UTM zone: 31

Vent Complex (V8) Central Norwegian margin;

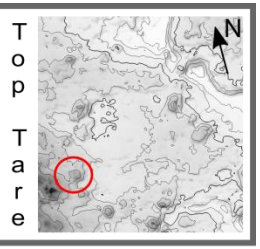

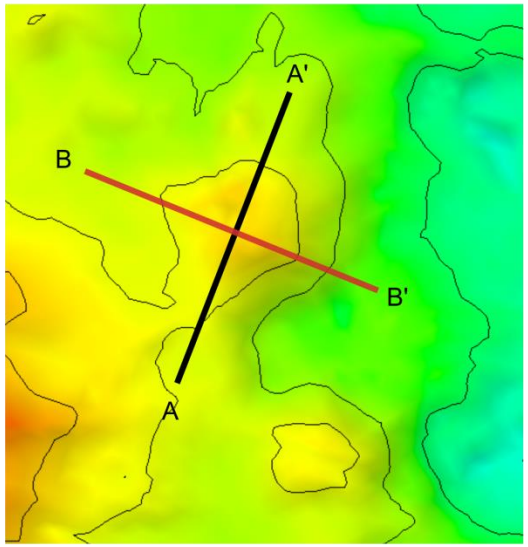

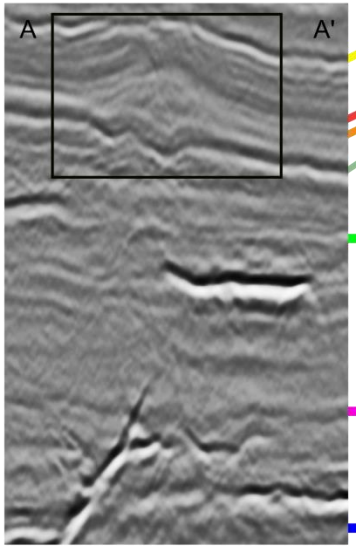

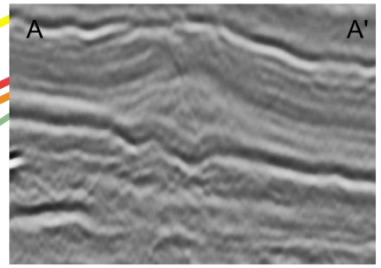

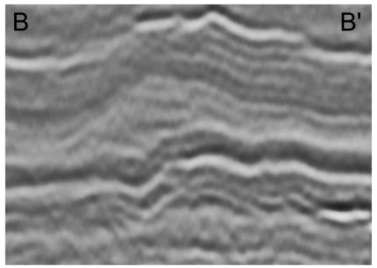

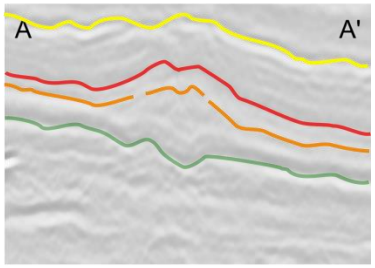

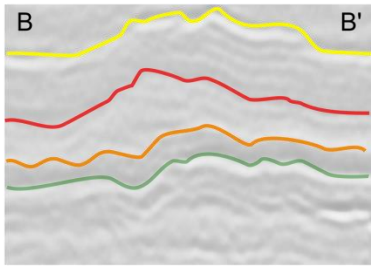

1 km

V8:
Measurements:
(See chapter 5: for measurement criteria)

Maximal with: 1200m
Minor axis with: N/A
Height: N/A

Mapping and description of the (**V8**) HTVC are restricted to the areas between the Top Tare (early Eocene) and the Top Tang (late Palaeocene) reflections.
Structures define as upper part is seen as mounded features on the top Tare horizon.
No down-lapping onto the Top Tang paleosurface.
Deeper section (conduit zone) is measured to (approximately **530 m**), from sill intersection to upper part (Top Tang paleosurface)

- Intra Brygge 2
- Top Tare fm
- Intra Tare
- Top Tang fm
- Intra Tang
- Top Reservoir
- Top Springar fm
- Carbonate layer

NS UTM [m]: 7043460
EW UTM [m]: 491769
UTM zone: 31

Vent Complex (V9) Central Norwegian margin;

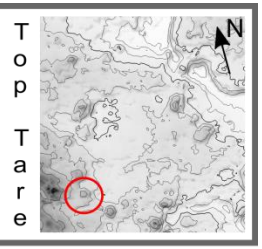

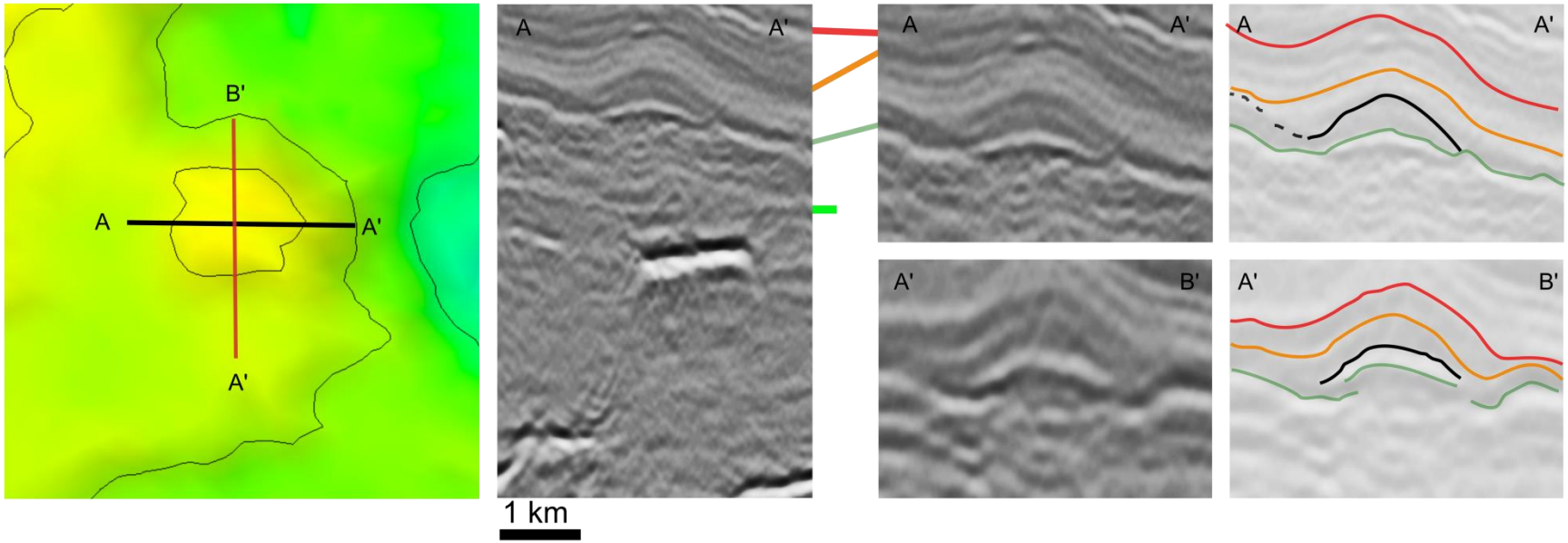

V9:
Measurements:
(See chapter 5: for measurement criteria)

Maximal with: 1200 ± 20
Minor axis with: 650 ± 20
Height: 85

Mapping and description of the (**V9**) HTVC are restricted to the areas between the Top Tare (early Eocene) and the Top Tang (late Palaeocene) reflections.
Structures define as upper part is seen as mounded features on the top Tare horizon.
No down-lapping onto the Top Tang paleosurface.
Deeper section (conduit zone) is measured to (approximately **500 m**), from sill intersection to upper part (Top Tang paleosurface)

- Intra Brygge 2
- Top Tare fm
- Intra Tare
- Top Tang fm
- Intra Tang

NS UTM [m]: 7039592
EW UTM [m]: 486333
UTM zone: 31

Vent Complex (V10) Central Norwegian margin;

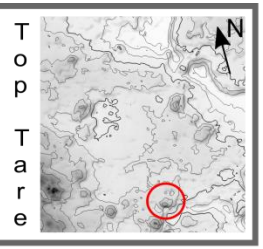

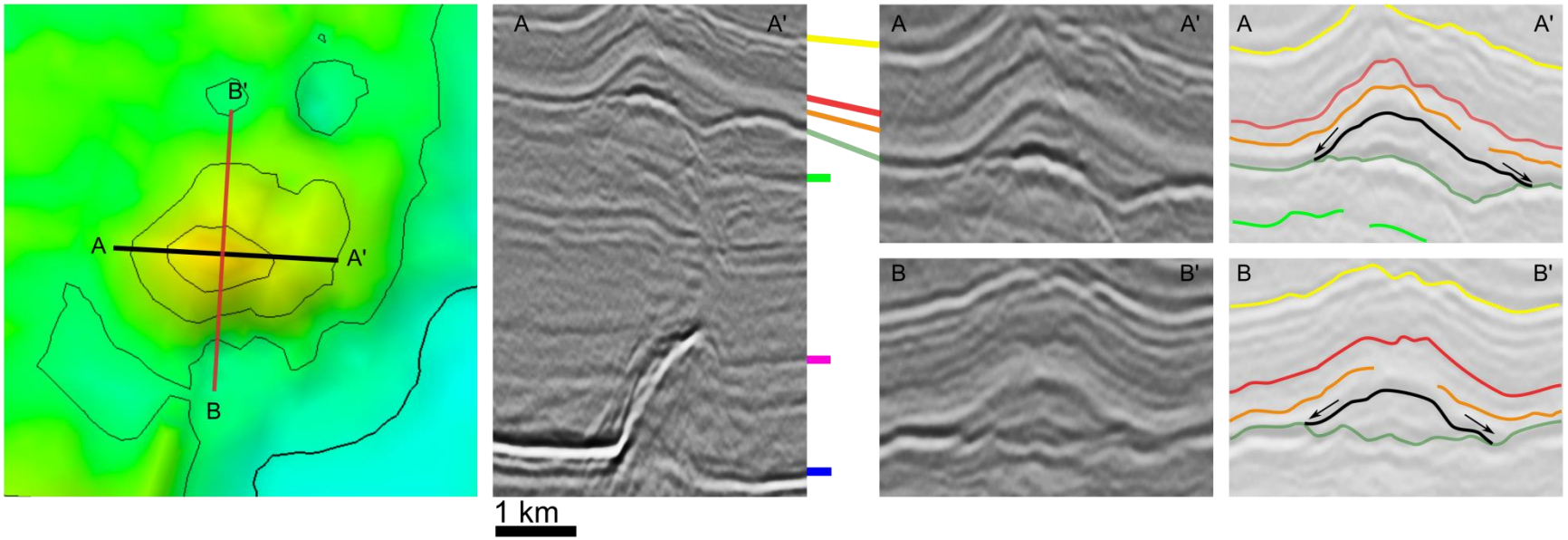

V10:
Measurements:
(See chapter 5: for measurement criteria)

Maximal with: 1570
Minor axis with: 1150
Height: 90

Mapping and description of the (**V10**) HTVC are restricted to the areas between the Top Tare (early Eocene) and the Top Tang (late Palaeocene) reflections.
Structures define as upper part is seen as mounded features on the top Tare horizon.
Dome terminating/down lapping onto the Top Tang paleosurface.
Deeper section (conduit zone) is measured to (approximately **450 m**), from sill intersection to upper part (Top Tang paleosurface)

- Intra Brygge 2
- Top Tare fm
- Intra Tare
- Top Tang fm
- Intra Tang
- Top Reservoir
- Top Springar fm
- Carbonate layer

NS UTM [m]: 7036731
EW UTM [m]: 491858
UTM zone: 31

Vent Complex (V11) Central Norwegian margin;

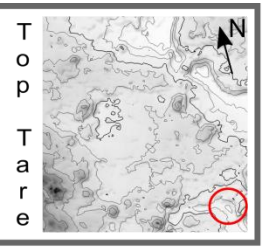

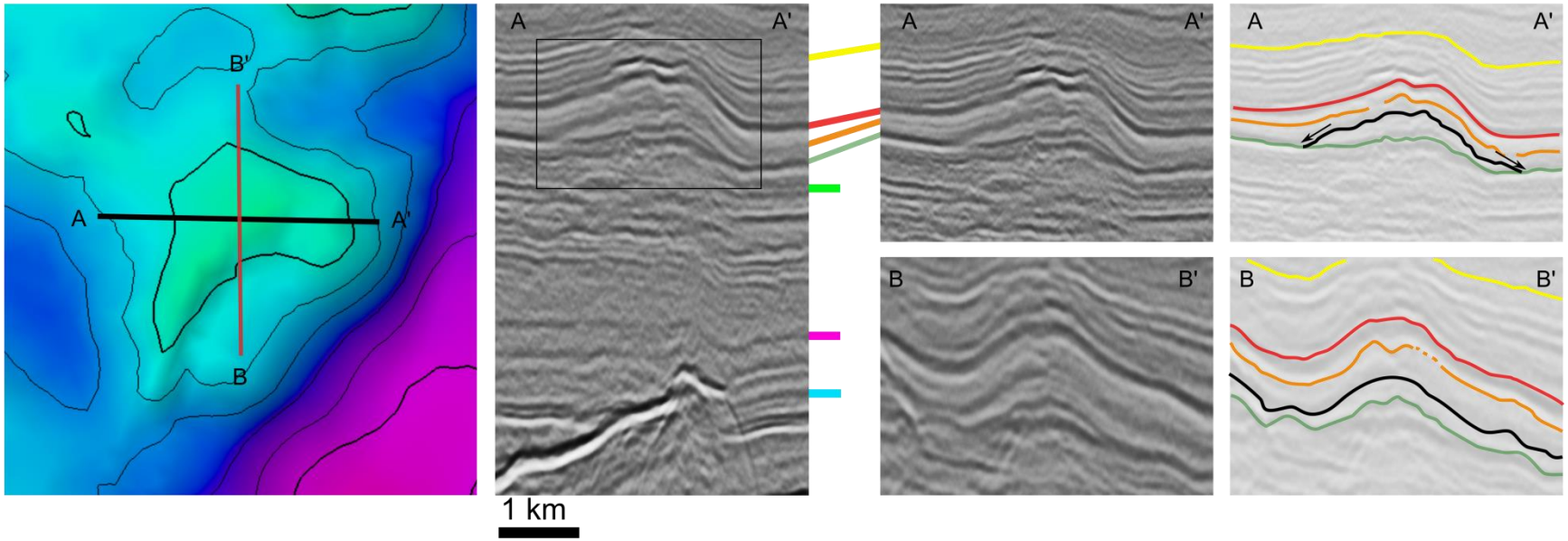

V11:
Measurements:
(See chapter 5: for measurement criteria)

Maximal with: 3000 ± 50
Minor axis with: N/A
Height: 120

Mapping and description of the (**V11**) HTVC are restricted to the areas between the Top Tare (early Eocene) and the Top Tang (late Palaeocene) reflections.
Structures define as upper part is seen as mounded features on the top Tare horizon.
Dome partly terminating/down lapping onto the Top Tang paleosurface.
Deeper section (conduit zone) is measured to (approximately **400 m**), from sill intersection to upper part (Top Tang paleosurface)

- Intra Brygge 2
- Top Tare fm
- Intra Tare
- Top Tang fm
- Intra Tang
- Top Reservoir
- Top Springar fm
- Carbonate layer

NS UTM [m]: 7040894
EW UTM [m]: 481953
UTM zone: 31

Vent Complex (V12) Central Norwegian margin;

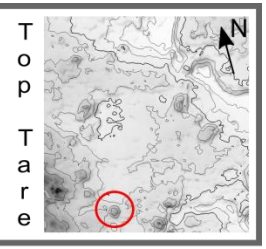

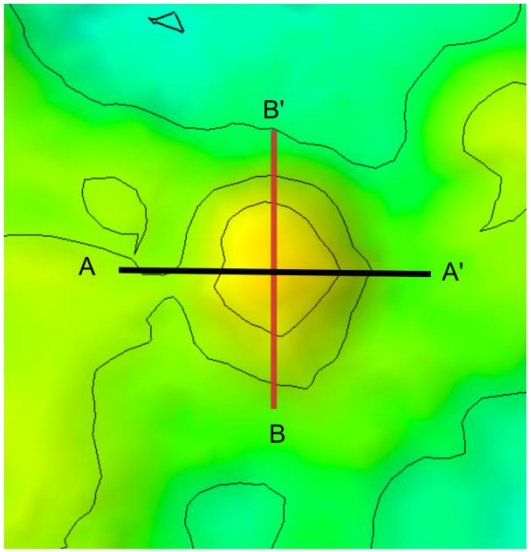

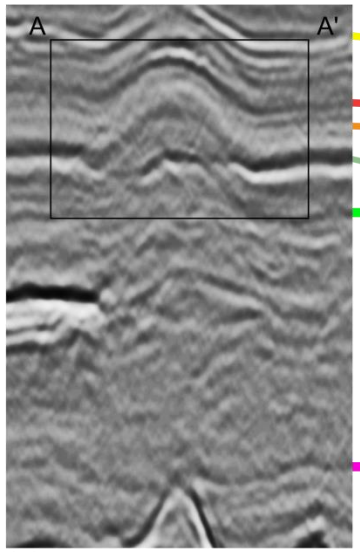

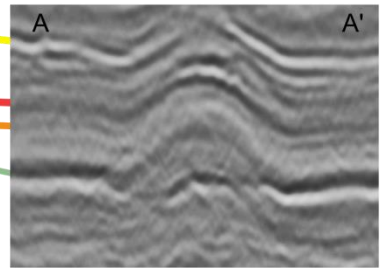

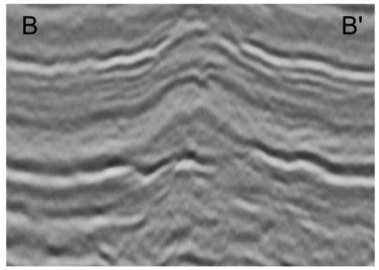

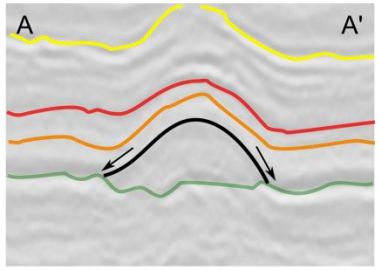

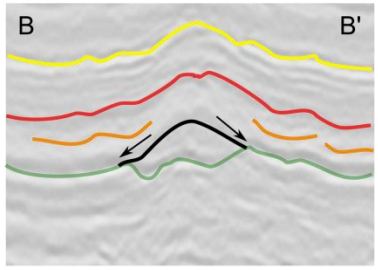

1 km

V12:
Measurements:
(See chapter 5: for measurement criteria)

Maximal with: 1000 ± 30
Minor axis with: 600 ± 30
Height: 80

Mapping and description of the (**V12**) HTVC are restricted to the areas between the Top Tare (early Eocene) and the Top Tang (late Palaeocene) reflections.
Structures define as upper part is seen as mounded features on the top Tare horizon.
Dome terminating/down lapping onto the Top Tang paleosurface.
Deeper section (conduit zone) is measured to (approximately **500 m**), from sill intersection to upper part (Top Tang paleosurface)

- Intra Brygge 2
- Top Tare fm
- Intra Tare
- Top Tang fm
- Intra Tang
- Top Reservoir

NS UTM [m]: 7038525
EW UTM [m]: 484813
UTM zone: 31

Vent Complex (V13) Central Norwegian margin;

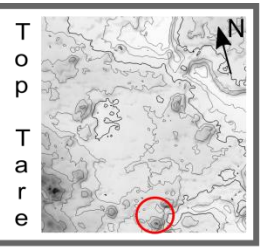

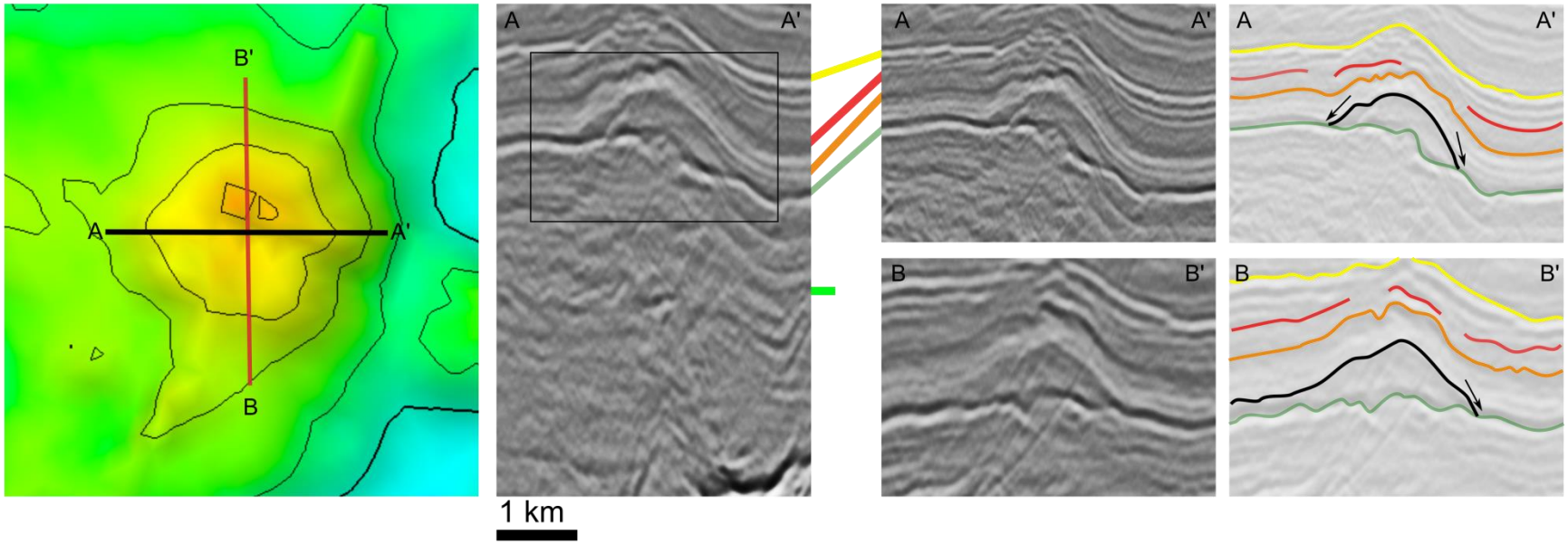

V13:
Measurements:
(See chapter 5: for measurement criteria)

Maximal with: 1500m ± 50
Minor axis with: 1350m ± 50
Height: 85m

Mapping and description of the (**V13**) HTVC are restricted to the areas between the Top Tare (early Eocene) and the Top Tang (late Palaeocene) reflections.
Structures define as upper part is seen as mounded features on the top Tare horizon.
Dome partly terminating/down lapping onto the Top Tang paleosurface.
Deeper section (conduit zone) is measured to (approximately **650 m**), from sill intersection to upper part (Top Tang paleosurface)

- Intra Brygge 2
- Top Tare fm
- Intra Tare
- Top Tang fm
- Intra Tang

A.2 Poster submitted and presented at the EGU conference in Austria, Vienna 2016

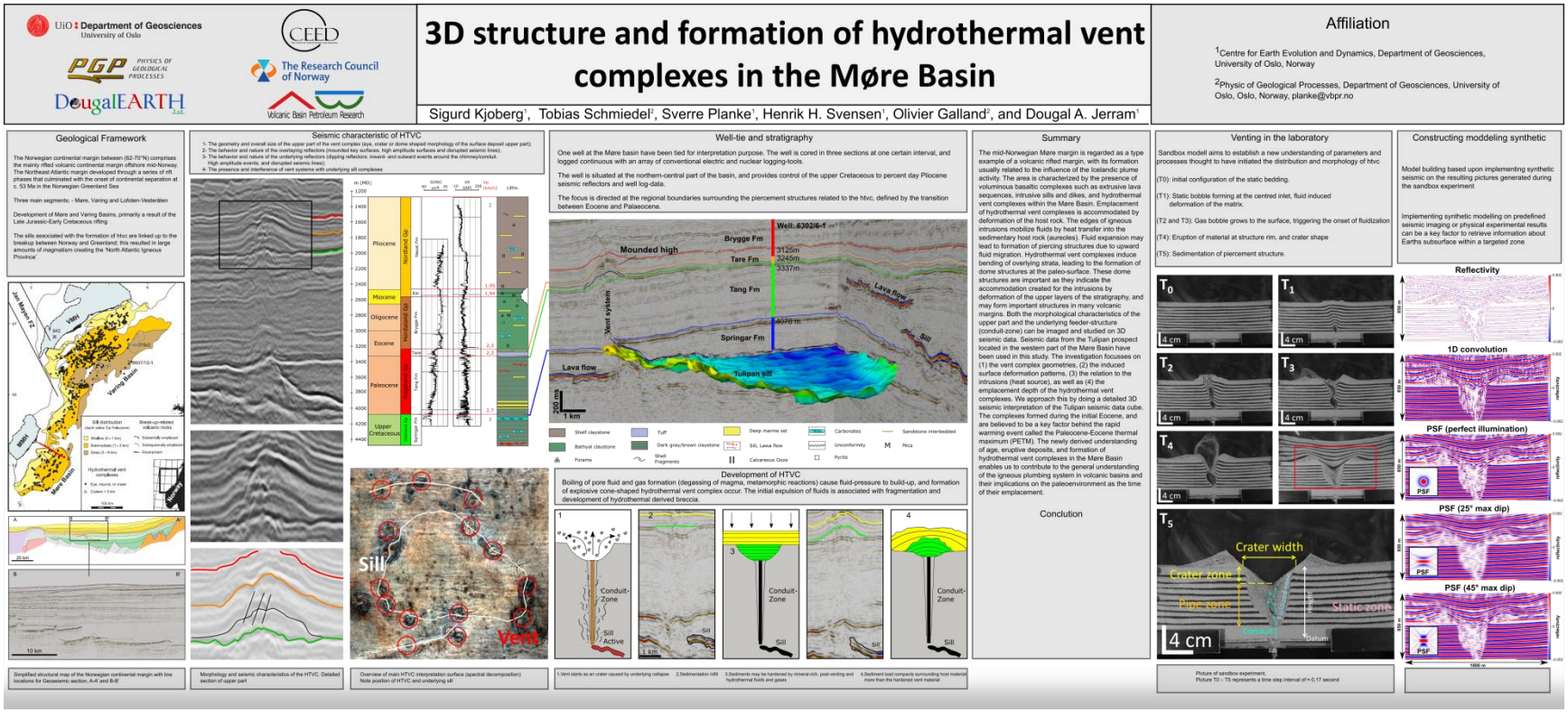

A.3 Biostratigraphical charts

MA	de Grac. et al.	HAQ/ PGS	STAGE		Plank for z	Palyno-zones		TOPS	MAXIMA OR ACMES	BASES
25.38	Ch3	TA1.2-1.3/ Pg260-270	Late Oligo	Chatt.	P 22	Tp11	b	D. phosphoritica (c), C. dispersum/partispinum reg	P. lophophorum, Pyxidiniopsis sp.	
27.49	Ch2						a	M. aspinatum (c), T. pelagica (r), Pentadinium lophophorm		
					P 21	Tp10	d	A. semicirculata (s)		
28.5	Ch1	1.1/250					c	Wetzeliella symmetrica, P. amoenum	Svalb. inflata/granulata/rotunda	S. inflata/granulata/rotunda
29.4	Ru3	TA4.5/ Pg240	Lower Oligocene	Rupelian				A. semicirculata LRO, Wetzeliella gochtii, D. phosphoritica LCO		
					P20/ 19		a	R. draco E. peniculata, P. comatum (r),		A. semicirculata
32.00	Ru2									
		TA4.4 220			P18	Tp9	e	D. ellipticum(s-LRO),S. chlamydophora, T. pelagica (c-LRO),		
		TA4.4 210					d2	S. cooksoniae, K. coeleothrypta Cenosphaera LCCO/LAO		
33.7	Pr4/Ru1						d1	Spiniferites sp. 1Manum, Areosp.pectiniformae ?LO, P. comatum,	S. sp.1, D. phosphoritica	S. sp. 1, S. cooksoniae (acme)
34.65	Pr3	4.1-.3 /180-200	Lt. Eoc	Priab	P 17	Tp 9	c	A. diktyoplocus, T. fenestrata,	P. comatum, D. phosphoritica A. pectiniforme, bisaccate pollen,	
36.00	Pr2				P 16		b	C. cf funiculatum, C. incompositum,		C. cantharellum
37.10	Pr1/Ba2				P 15		a	Spiniferites verrucatus, A. michoudii, W. articulata (s.l.), ?H. porosa		T. fenestrata, S. cooksoniae?FA
39.07	Ba1	TA3.5-3.6/Pg 160-70	Middle Eocene	Bart	P 14	Tp8	c	Heteraulacacysta porosa, R. porosum, R. borussica (s)	Xenicodinium verrucosm	?T. fenestrata
41.30	Lu4				P 13		b	W. ovalis, D. rhomboideum		Glaphyrocysta semitecta
				Lutetian	P12		a	D. colligerum (s), P. distinctum, P. powellii,	Cenosphaera spp.	
		TA3.3-.4 Pg150			P11	Tp7	d	T.delicata (reg), D. pseudoficusoides,	P. clithrydium/regale	H. porosa , R. draco
43.95	Lu3				P10		c	D. ficusoides LO,		
46.09	Lu2						b	D. ficusoides(reg) , W. art. "pentagonalis", H. clauseni		
48.14	Lu1	3.2/140					a2	D. pachydermum LRO, E. ursulae LO	D. ficusoides	
49.00	Yp10	TA3.1/ Pg130					a1	E. ursulae LRO/COM	D. pachdermum	A. diktyoplokus (reg)
50.02			Lower Eocene	Ypresian	P9	Tp6	d2	Azolla spores, C amplectens	E. ursulae ACME, Azolla spores	
							d1	C. collumna	W. art. pentagonalis	
		TA2.7-2.9/ Pg 110-120			P8		c	D. varielongitudum	A. cf medusettiformis	A. diktyoplokus ?FAD, C. collumna
50.29	Yp9				P7		b	D. politum, D. condylos D. simile, S linaperta	D. varielongitudum	D. varielongitudum,
	Yp8						a2	D. oebisfeldensis, LO, D. solidum, Alisocysta sp 2, , D. solidum	I. hiatus LAO	
51.05	Yp8									
		TA2.6/Pg100			P6c		a1		S. linapperta/pat H. tubiferum,	
51.50	Yp6(-7)									
53.15	Yp5	2.5				Tp5	b4		D. oebisfeldensis, H. tubiferum	Coscinodiscis sp 1

Biostratigraphical table of the early Paleocene to late Oligocene, provided by Planke et al., (2007).

MA	deGrac. et al.	HAQ/ PGS	STAGE		Pl fmz	Palyno-zones		TOPS	MAXIMA OR ACMES	BASES
53.61	Yp4		earliest or L.Pal-E.Eo	Ypresian	P 6B	Tp5	b4	Coscinodiscus sp. 1, C. sp 2	D. oebisfeldensis, Taxod./Caryapollenites spp.	
54.60	Yp3						b3	Kallosphaeridium spinosa, C. cf dartmoorium , C wardenense	K. spinosa/	
		TA2.4					b2		C. wardenensis	
54.80	Yp2	/ Pg90					b1	Cerodinium dartmoorium		
54.90	Yp1/Th7	2.3/80			P6A		b0	Phelodinium sp OCC	Leiospaereres/prasinophycids	
55.40	Th6/Yp0	TA2.2	Late Paleocene	Thanetian	P5		a	Apectodinium augustum LO (LCO variable)	A. augustum, A. spp.	Cerodinium dartmoorium
55.80	Th5	/ Pg70								A. augustum FO Tax./Car. FAO
							c	Palaeoperidinium pyrophorum (s), Alisocysta margarita (s), Trudopollis/ Alnipollis spp., Aggluts: S. spectabilis, Rz. minima, Ret. paupera etc		
56.42	Th4	Pg60				Tp4	b	A. margarita (LRO) Areoligera "gippingense"		
56.75	Th3				P4		a2	Spiniferites "multispinula", Xenic. "baculatum" Trochammina ruthvenmurrayi	S. hyalinus, A. margarita, A. gippingensis	
57.40	Th2						a1	S. "hyalinus"		
57.90						Tp3	b3	Glapyrocysta oligacantha	G oligacantha	
58.53	Se2/Th1	TA2.1 Pg50		Seland.			b 1-2	Palaeocystodinium bulliforme (rare), Cerodinium striata	P. pyrophorum COM P. pyrophorim MAX	
		4 0					a2	Isabelidinium viborgense, F. annetorpense	Radiolaria	A margarita (reg) I viborgense
60.7Se		TA1.4			P3B				P. bulliforme	
60.9Stg	Se 1	/ Pg30			P3A		a1	Sub pseudopbulloides LO	Areoligera spp	A. margarita (s)
	Da4=61.4		E Pal	Danian	P2	Tp2	b	Subbotina trivialis, Sub. pseudobulloides LRO Alisocysta reticulata, Hystrichosphaeridium sp. 2 (LRO), S. magnifica		
62.84	Da3	TA1.3 / Pg20			P1C		a	Trithyrodinium evittii/fragile , Cerodinium diebeli (ss, reg-s) Xenicodinium spp.(rare) S. inornata LO/rare	S. magnifica,	A. reticulata
64.08	Da2	TA1.2			P1B	Tp1	a2	Senoniasphaera inornata consistent, Danea spp., Glob. daubjergensis	C. diebeli(c), Xenicodinium spp	
64.75	Da1	/ Pg10			*		a1	Spongodinium delitiense (LO, rare)		Senoniasphaera inornata
65.00		TA1.1	C	M				P. grallator(c), Aquilapollenites spp. (s-c), Trithyrodinium evittii (c)		

Biostratigraphical table of the early Paleocene to late Oligocene, provided by Planke et al., (2007).